

UCLA

UCLA Electronic Theses and Dissertations

Title

Synthesizing New Dielectric Elastomers for Actuation

Permalink

<https://escholarship.org/uc/item/7853f6g4>

Author

Hu, Wei

Publication Date

2015

Peer reviewed|Thesis/dissertation

UNIVERSITY OF CALIFORNIA

Los Angeles

Synthesizing New Dielectric Elastomers for Actuation

A dissertation submitted in partial satisfaction of the
requirements for the degree Doctor of Philosophy in
Materials Science and Engineering

By

Wei Hu

2015

© Copyright by

Wei Hu

2015

ABSTRACT OF THE DISSERTATION

Synthesizing New Dielectric Elastomers for Actuation

by

Wei Hu

Doctor of Philosophy in Materials Science and Engineering

University of California, Los Angeles, 2015

Professor Qibing Pei, Chair

Dielectric elastomers can be actuated under electric field responding to electrostatic force. Compared with other electrical actuation technologies, the advantages of dielectric elastomer actuators include: light weight, good compliancy, large actuation strain, high energy density, quiet operation and low cost. As the active part of an actuator device, the dielectric elastomer material plays a central role. However, most popular elastomers used for dielectric actuation are commercial products designed for other applications. And their confidential formulations also make it difficult to understand the mechanism and further improve the actuation performances. Therefore, the development of new dielectric elastomers from molecular level is of great importance.

One subject in this dissertation is the synthesis of a group new dielectric elastomers from molecular level which demonstrate high actuation strains. These dielectric elastomers are polyacrylate

formulations with n-butyl acrylates as the based monomer and formed through ultra-violet polymerization. The influences of acrylic acid in the formulation on the mechanical and dielectric properties are investigated. The optimal formulation demonstrates an area actuation strain of 186 %, a dielectric strength of 222 MV/m and an energy density as high as 1.4 MJ/m³.

As the dielectric constant of a dielectric elastomer plays a significant role in its actuation performances, one focus of this dissertation is to improve the dielectric constant by utilizing nanocomposites. Aluminum nanoparticles with a self-passivated oxide shell are used as the conductive fillers to increase the dielectric constant of a polyacrylate elastomer while retaining a high dielectric strength. With the addition of 4 vol% Al nanoparticles, the nanocomposite has a dielectric constant as high as 8.4 with a maximum actuation strain of 56 %, a dielectric strength of 140 MV/m and a maximum actuation pressure of 1.5 MPa.

Another focus of this dissertation is the innovation of a dielectric elastomer with tunable stiffness. This novel elastomer contains furan-maleimide Diels-Alder adduct moieties as the dynamic bonding. The moduli of these elastomers can be tuned reversibly and incrementally through modulating their crosslinking densities via thermal treatments at moderate temperatures. Capacitive sensors and actuators which can work in multiple modes were fabricated using the new materials.

The dissertation of Wei Hu is approved.

Yong Chen

Yunfeng Lu

Qibing Pei, Committee Chair

University of California, Los Angeles

2015

To

My always supportive parents,

Ling Wei and Falin Hu

and my brilliant boyfriend

Dr. Jiechen Wu

for their encouragement to make this dissertation possible.

Table of Contents

List of Figures.....	ix
List of Tables	xiv
Acknowledgements	xv
Vita	xvii
Publications	xvii
1. Introduction	1
1.1. Background	1
1.1.1. Mechanisms of dielectric elastomer	1
1.1.2. Study of dielectric elastomer	2
1.1.3. Optimization of dielectric elastomers – Design guidelines for dielectric elastomers ...	8
<i>1.1.3.1. Dielectric properties</i>	<i>8</i>
<i>1.1.3.2. Mechanical properties</i>	<i>13</i>
<i>1.1.3.3. Environmental effects.....</i>	<i>15</i>
<i>1.1.3.4. Fabrication of DE films</i>	<i>18</i>
1.1.4. Applications of dielectric elastomers	19
<i>1.1.4.1. Actuators with various configuration</i>	<i>19</i>
<i>1.1.4.2. Products and prototypes</i>	<i>20</i>
1.2. Motivation of this thesis	21
1.3. Scope and layout of the dissertation.....	21
2. Dielectric Elastomers with High Actuation Strain	23
2.1. Background of this study	23
2.2. Experimental design.....	24
2.2.1. Materials	24
2.2.2. Film preparation	24
2.2.3. Tensile test.....	25
2.2.4. Actuation characterization.....	25
2.2.5. Actuation blocking force measurement.....	25
2.2.6. Actuation lifetime measurement.....	26
<i>2.2.6.1. Actuation lifetime at a static voltage</i>	<i>26</i>

2.2.6.2. Actuation cycle lifetime.....	27
2.3. Results and discussion.....	27
2.3.1. Mechanical properties.....	27
2.3.2. Measurement of dielectric constant.....	28
2.3.3. Actuation performance	30
2.3.3.1. Actuation of all elastomers with 300% by 300% prestrain	30
2.3.3.2. Actuation of AA-13 elastomer at various prestrain ratios.....	30
2.3.3.3. Actuation lifetime at a static voltage	32
2.3.3.4. Actuation cycle lifetime.....	34
2.3.4. Effect of acrylic acid.....	35
2.3.5. Effect of pre-strain.....	37
2.4. Conclusions	38
3. Enhancing Dielectric Constant Using Nanocomposite.....	39
3.1. Background of this study	39
3.1.1. The need of high dielectric constant.....	39
3.1.2. Approaches to enhance dielectric constant.....	39
3.1.1.1. Incorporation of ceramic fillers with high dielectric constants.....	40
3.1.1.2. Incorporation of metallic fillers.....	44
3.1.1.3. Introduction of covalently bonded polarizable organic groups	45
3.2. Experimental design.....	46
3.2.1. Materials	46
3.2.2. Surface modification of Al nanoparticles	46
3.2.3. Nanocomposite film preparation	47
3.2.4. Tensile test.....	48
3.2.5. Dielectric constant measurement.....	48
3.2.6. Resistivity measurement.....	49
3.2.7. Actuation performance characterization.....	49
3.3. Results and discussion.....	49
3.3.1. Bonding nanoparticle to polymer matrix.....	49
3.3.2. Film preparation	53
3.3.1. Mechanical properties.....	56
3.3.2. Measurement of dielectric constant.....	58

3.3.3. Measurement of leakage current.....	60
3.3.4. Actuation performance	62
3.4. Conclusions	65
4. Dielectric Elastomers with Tunable Moduli	66
4.1. Background of this study	66
4.2. Experimental design.....	68
4.2.1. Synthesis of FM-A.....	68
4.2.1.1. <i>Materials</i>	68
4.2.1.2. <i>Synthesis of FM-A</i>	68
4.2.2. Preparation of PADA elastomer films.....	70
4.2.3. TGA of PADA elastomers.....	70
4.2.4. Stiffness change via reversible DA reaction.....	71
4.2.5. Other characterizations	72
4.2.6. Application as capacitive Sensors	72
4.2.7. Application as actuators.....	73
4.3. Results and discussion.....	73
4.3.1. Synthesis of FM-A.....	73
4.3.2. Preparation of DA elastomer films	74
4.3.3. Stiffness change via reversible DA reaction.....	77
4.3.4. Achieving multiple states by controlling crosslinking density.....	81
4.3.5. Applications as sensors and actuators	85
4.3.5.1. <i>Capacitive sensing</i>	85
4.3.5.2. <i>Actuation</i>	87
4.4. Conclusion.....	89
5. Summary and Future Researches	90
5.1. Summary of the dissertation.....	90
5.2. Future researches.....	91
References	93

List of Figures

Figure 1-1. A schematic illustration of a dielectric elastomer actuator.	1
Figure 1-2. Chemical structures of representative DE materials.	3
Figure 1-3. Dielectric behavior over frequency. (<i>adopted from [24]</i>).....	10
Figure 1-4. Characteristic stress of a DE film as a function of mechanical strain or electric field (constant voltage condition). The chart with origin at O are for a non-prestrained film at O' for the prestrained film. The cross (×) indicates dielectric breakdown and the bar (-) indicates stable actuation strain. Small o and large O represent the apparent breakdown field and actual breakdown strength respectively. (<i>adopted from [3]</i>).....	12
Figure 1-5. A 3M TM VHB TM actuator's performance as a function of time. The actuation voltage is applied at 0.05 s and removed at 1.05 s. (<i>adopted from [15]</i>)	14
Figure 1-6. 3M TM VHB TM 's (a) Storage and loss moduli as a function of temperature at a frequency of 0.1 Hz; and (b) dielectric constants of different temperatures as a function of frequency. (<i>adopted from [30]</i>)	16
Figure 1-7. Performance of actuators of 3M TM VHB TM and a silicone as a function of temperature. (<i>adopted from [15]</i>)	17
Figure 1-8. Effect of relative humidity on actuation cycles to failure of 3M TM VHB TM acrylate actuators at room temperature. (<i>adopted from [15]</i>)	17
Figure 1-9. Lotz's process for fabricating multilayer DEAs. (<i>adopted from [31]</i>).....	19
Figure 2-1. An actuator for blocking force test.....	26
Figure 2-2. Stress-stain curves of AA-0, AA-6, AA-13 and AA-20.	28

Figure 2-3. Blocking force test of AA-0, AA-6, AA-13 and AA-20. 3M™ VHB™ 4905 was tested as a reference..... 29

Figure 2-4. Actuation performances of AA-0, AA-6, AA-13 and AA-20 elastomers. All elastomers were pre-stretched 300% by 300% biaxially. 30

Figure 2-5. Actuation performances of AA-13 with various prestrain ratios. 31

Figure 2-6. Lifetime measurement of an actuator with self-clearing electrodes. The leakage current of the actuator was monitored while constant actuation voltage was maintained to keep the actuation strain at ~ 150 % area strain. 33

Figure 2-7. Lifetime measurement of an actuator with carbon-grease electrodes. The leakage current of the actuator was monitored while constant actuation voltage was maintained to keep the actuation strain at ~ 150 % area strain. 34

Figure 2-8. Cycle lifetime measurement at 0.5 Hz. AC voltage was applied to achieve a peak actuation area strain of ~ 110 %. Actuation strain at **(a)** initial 50 sec (25 cycles) and **(b)** until failure of the actuator. 35

Figure 2-9. **(a)** Dielectric constant and energy density and **(b)** actuation performances change with different weight parts of acrylic acid. 36

Figure 2-10. Actuation performances of AA-13 with different prestrain ratios. 38

Figure 3-1. **(a)** Schematic representation of the composite structure and chemical properties of the particle surface. **(b)** Optical micrograph of composite with 15 vol% uncoated TiO₂; and **(c)** SEM of cryo-fracture surface of composite with silicone coated TiO₂. (*adopted from [41]*)..... 43

Figure 3-2. Synthesized dipole, enabling the subsequent grafting reaction to silicone. (*adopted from [46]*)..... 45

Figure 3-3. (a) An example of preparation of a dipole crosslinker; (b) a fluorescent microscopy image of a film with dipole crosslinker. (<i>adopted from [47]</i>)	46
Figure 3-4. TEM images of as-received nanoparticles. (Scale bar: 40 nm).....	50
Figure 3-5. Surface modification of Aluminum nanoparticles.	50
Figure 3-6. FT-IR spectrum of surface-modified Al nanoparticles.	51
Figure 3-7. The TGA curve of surface-modified Al nanoparticles.....	51
Figure 3-8. TGA curves of as-received and as-modified Al nanoparticles at 80 °C in air atmosphere for one hour.	52
Figure 3-9. Solubility of surface-modified Al nanoparticles. The dispersions of as-received Al (a) and as-modified Al nanoparticles (c) were dropped on the top of DI-water. The dispersions of (b) as-received Al and (d) as-modified Al nanoparticles on water after 30 mins.	53
Figure 3-10. (a) Optical photographs of samples A-00 and A-15; SEM images of cross sections of (b) A-00, (c) control sample using unmodified nanoparticles, (d) A-05, (e) A-10 and (f) A-15.	55
Figure 3-11. Tensile test of aluminum nanocomposites.	58
Figure 3-12. (a) Dielectric constants and (b) dielectric losses of A-00, A-05, A-10 and A-15 from 100 Hz to 100 kHz.	59
Figure 3-13. Dielectric constants at various loadings measured at 200 V AC and 400 Hz.	60
Figure 3-14. Measured leakage current density of nanocomposite samples with electric field. The electrode area and thickness of the samples were 11.4 cm ² and ~50 μm (after pre-stretching), respectively.	62

Figure 3-15. Actuation strain of nanocomposites as a function of applied electric field. 62

Figure 3-16. Estimated work densities of Al/acrylate nanocomposites. 63

Figure 4-1. A schematic illustration of how the crosslinking sites are formed and broken. Furan-maleimide adducts, one of the Diels-Alder pairs, were selected as the dynamic bonds forming the crosslinking sites. 68

Figure 4-2. The synthesis route of FM-A: (i) ethyl acetate, room temperature, 24 hrs; (ii) ethanolamine, ethanol, reflux, 4 hrs; (iii) acryloyl chloride, triethyl amine, DCM, 0 °C to room temperature, 24 hrs..... 69

Figure 4-3. (a) ¹H NMR and (b) ¹³C NMR (400 MHz, DMSO) spectra of as-synthesized FM-A. 74

Figure 4-4. The synthesis route of a PADA elastomer. Note that Xlinker was co-dissolved with other monomers before UV curing but it remain inert during UV curing and thermal treatment at 130 °C. It reacted with Polymer 2 during treatment at 70 °C at the last step resulted in a crosslinked polymer network. 76

Figure 4-5. TGA curves of PADA-10_70 and PADA-10-r from 50 °C to 180 °C in air atmosphere with a heating rate of 5 °C/min and the derivative curve of PADA-10_70's TGA curve..... 77

Figure 4-6. (a) A schematic illustration of thermal treatments. The as-synthesized films were at their rigid states (Stage 1, PADA-X-r). Soft states (Stage 2, PADA-X-s) were achieved though heating the films at 130 °C for 30 min and then fast cooling down to room temperature. Rigid states (Stage 3, PADA-X-r) could be regained though heating the films at 70 °C for another 24 hrs and cooling down to room temperature. (b) The moduli of elastomer formulations with different weight parts of FM-A at both rigid and soft states, and (c) the moduli change ratio (**R**) between the

two states. **(d)** Cycling test of one of the formulations, PADA-5. These elastomers samples were thermally adjusted between PADA-5-r and PADA-5-s as shown in **(a)** for 5 cycles..... 81

Figure 4-7. Various moduli of PADA-4 elastomers could be achieved through thermal treatments.

(i) PADA-4-r samples were heated at **(a)** 90 °C, **(b)** 110 °C, **(c)** 130 °C and **(d)** 160 °C followed by a fast cooling down to room temperature to achieve PADA-4-s90, PADA-4-s110, PADA-4-s and PADA-4-s160. (ii) Samples were aged at room temperature for 2 hrs and their moduli did not show a significant change. (iii) Samples were heated at 70 °C for 24 hrs in **(a)**, **(b)** and **(c)** and for 48 hrs in **(d)**. Moduli were normalized as the modulus of PADA-4-r was set as 1..... 82

Figure 4-8. (a) Stress-strain curves of PADA-4 elastomers. A dumbbell-shaped sample was stretched to rupture at a rate of 3.33 mm/s. **(b)** UV spectra of PADA-4 elastomers. **(c)** Swelling ratios of PADA-4 elastomers in chloroform. 83

Figure 4-9. The comparison of measured moduli and estimated moduli from both UV spectra and swelling test at different de-bonding temperatures. 85

Figure 4-10. (a) The structure of a capacitive sensor. **(b)** The stress-strain curves of the sensors made of PADA-4-r and PADA-4-s at a stretch rate of 1 mm/s. **(c)** The capacitive sensing results at a stretch rate of 1 mm/s. **(d)** The capacitance-stress curves of the sensors. Note that in **(c)** and **(d)**, the thickness of the capacitor is normalized to 100 μm (d_0). 87

Figure 4-11. Actuation curves of PADA-4-r and PADA-4-s. Average actuation strains at each nominal 10 MV/m electric field were plotted. Both films were prestretched 5% by 5%..... 88

List of Tables

Table 1-1. Comparisons of various actuation technologies. ^{3,6}	2
Table 1-2. DE materials.	5
Table 1-3. DE actuator configurations.	19
Table 2-1. Formulas (weight part) with various amount of acrylic acid.....	24
Table 2-2. Calculated blocking force and dielectric constant.	29
Table 2-3. The summarized actuation performances of the synthesized elastomers.	31
Table 3-1. Dielectric elastomers with high dielectric constants.....	39
Table 3-2. Properties of the synthesized nanocomposite DEs.	57
Table 4-1. Formulations (parts of weight) of synthesized elastomers.	70
Table 4-2. Moduli of the formulated elastomers at three stages in one cycle.....	78
Table 4-3. Comparison of the actuation performances of PADA-4-r and PADA-4-s.	88

Acknowledgements

I would like to give my sincerest thanks to my dissertation advisor, Professor Qibing Pei, for his guidance and financial support during my PhD study. Professor Pei has offered me not only inspiring ideas and encouragement in research but also has taught me how to think, how to define and solve problems and be creative.

Also, I would like to thank Professor Yu Huang, Professor Yong Chen and Professor Yunfeng Lu for serving as my committee members and their help. I also took their courses which gave me insights in different aspects of materials science.

Especially, I would like to thank Dr. Xiaofan Niu, Dr. Paul Brochu and Dr. Hristiyan Stoyanov for training me on experimental design and equipment operation and sharing their experience and suggestions. Without their help, the first days in my research could be far more difficult. I would also like give my thanks to Mr. Zhi Ren, Dr. David McCoul, Dr. Jiajie Liang, Dr. Junpeng Li, Mr. Chao Liu, Dr. Chaokun Gong, Dr. Qi Chen, Mr. Jacob Hajagos, Mr. David Kishpaugh and other lab colleagues for their help and valuable discussion. I would also thank Dr. Sergey Prikhodko and Dr. Ignacio Martini for offering me training on multiple characterization skills in materials science. Meanwhile I appreciate the help from several undergraduate students who worked with me: Ms. Suki Naifang Zhang, Mr. Zhixin Jason Xie, Ms. Erin Askounis, Mr. Shenshen Li and Ms. Lisa Chieh.

Outside the academic field, I also want to thank Dr. Charlie Zhai and Dr. Mengzhi Pang in Apple Inc. for offering me an internship opportunity. This 6-month internship provided me with the insight of semiconductor industry and ideas in career planning.

A big thanks to my friends who have made my life in UCLA bright and fun, especially Ms. Huier Gao, Ms. Shuyu Charlotte Chou, Dr. Huanping Zhou, Ms. Chia-Jung Cara Hsu, Dr. Si Chen, Ms. Xiaodan Zhu, Dr. Pu Wang, Mr. Yongjia Li, Dr. Tse-bin Song and Mr. Wei Zhang.

My special thanks come to my parents, Ms. Ling Wei and Mr. Falin Hu, for their selfless support during not only during my PhD study but also my entire life. Also my boyfriend, Dr. Jiechen Wu, for his encouragement.

Vita

2010

B. E.

Polymer Materials and Engineering

Tsinghua University, Beijing, China

2010 - 2015

Ph.D. Candidate

Materials Science and Engineering

University of California, Los Angeles, CA

Publications

W. Hu, Z. Ren, J. Li, E. Askounis, Z. Xie and Q. Pei, “New dielectric elastomers with tunable moduli”, Under review.

W. Hu and Q. Pei, “Materials design and optimization of dielectric elastomers”, Book chapter, Under review.

W. Hu, D. McCoul, S. J. Biggs and Q. Pei, “Dielectric elastomers as EAPs: Applications”, Book chapter, In preparation.

W. Hu, S. N. Zhang, X. Niu, C. Liu and Q. Pei, “An aluminum nanoparticle-acrylate copolymer nanocomposite as a dielectric elastomer with a high dielectric constant”, *Journal of Materials Chemistry C*, 2014, 2, 1658-1666.

W. Hu, X. Niu, S. N. Zhang, X. Yang and Q. Pei, “Synthesis and electromechanical characterization of a new acrylic dielectric elastomer”, *Proceedings of SPIE*, 2013, 8687, 86872U.

Z. Ren, W. Hu, S. Li, X. Niu and Q. Pei, “A shape memory electroactive polymer with a sharp plastic-rubber transition toward a facile rigid to rigid deformation”, In preparation.

J. Li, J. Liang, L. Li, F. Ren, W. Hu, J. Li, S. Qi and Q. Pei, "Healable capacitive touch screen sensors based on transparent composite electrodes comprising silver nanowires and a furan/maleimide Diels-Alder cycloaddition polymer", *ACS Nano*, 2014, 8, 12784-12882.

P. Brochu, H. Stoyanov, R. Chang, X. Niu, W. Hu and Q. Pei, "Capacitive energy harvesting using highly stretchable silicone-carbon nanotube composite electrodes", *Advanced Energy Materials*, 2014, 4, 1300659.

J. Li, J. Liang, X. Jian, W. Hu, J. Li and Q. Pei, "A flexible and transparent thin film heater based on a silver nanowire/heat-resistant polymer composite", *Macromolecular Materials and Engineering*, 2014, 299, 1403-1409.

Z. Ren, X. Niu, D. Chen, W. Hu and Q. Pei, "A new bistable electroactive polymer for prolonged cycle lifetime of refreshable Braille displays", *Proceedings of SPIE*, 2014, 9506, 950621.

J. Liang, L. Li, K. Tong, Z. Ren, W. Hu, X. Niu, Y. Chen and Q. Pei, "Silver nanowire percolation network soldered with graphene oxide at room temperature and its application for fully stretchable polymer light-emitting diodes", *ACS Nano*, 2014, 8, 1590-1600.

C. Gong, J. Liang, W. Hu, X. Niu, S. Ma, H. T. Han and Q. Pei, "A healable, semi-transparent silver nanowire-polymer composite conductor", *Advanced Materials*, 2013, 25, 4186-4191.

X. Niu, H. Stoyanov, W. Hu, R. Leo, P. Brochu and Q. Pei, "Synthesis of a new dielectric elastomer exhibiting large actuation strain and suppressed electromechanical instability without prestretching", *Journal of Polymer Science B: Polymer Physics*, 2012, 51, 197-206.

X. Niu, R. Leo, D. Chen, W. Hu and Q. Pei, "Multilayer stack actuator made from new prestrain-free dielectric elastomers", *Proceedings of SPIE*, 2013, 8687, 86871M

1. Introduction

1.1. Background

1.1.1. Mechanisms of dielectric elastomer

Dielectric elastomers (DEs) represent a new category of electroactive materials and are being investigated for a wide variety of electromechanical transducers such as actuators with various form factors and sizes, strain sensors and energy harvesters.^[1-3]

The DE device structure comprises an elastomer film sandwiched between two compliant electrodes, which is essentially a soft capacitor. As schematically illustrated in **Figure 1-1**, in actuation mode, when the voltage is on, opposite charges are introduced onto the compliant electrodes. The soft capacitor will shrink in thickness while expand in area in response to the electrostatic stress.^[4] Thus the electrical energy is transferred into mechanical energy. The generation mode basically is the reverse of the actuation mode in which mechanical energy is transferred into electrical energy.

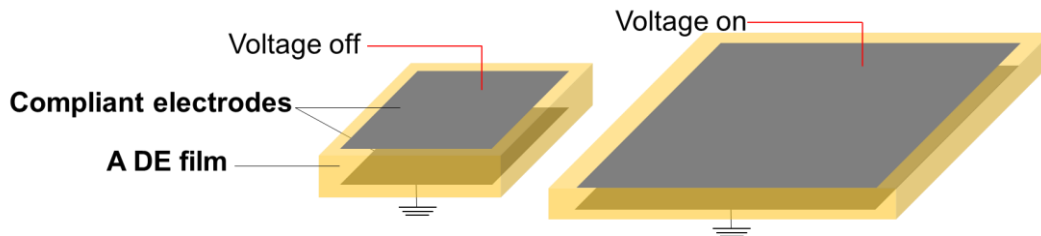


Figure 1-1. A schematic illustration of a dielectric elastomer actuator.

The actuation thickness strain (s_z) can be calculated using Equation (1):

$$s_z = \varepsilon_0 \varepsilon_r E^2 / Y \quad (1)$$

where ε_0 , ε_r , E and Y are the vacuum permittivity (8.85×10^{-12} F/m), dielectric constant or permittivity of the dielectric elastomer, applied electric field and apparent modulus of the dielectric elastomer.^[5]

Electroactive systems have been drawing great attention for their great potential application in robotics. Widely investigated systems include shape memory polymers, piezoelectric ceramics, conducting polymers and ferroelectric polymers in addition to dielectric elastomers. These technologies, together with the properties of mammalian skeletal muscles, are compared and listed in **Table 1-1**.

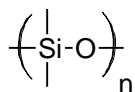
Table 1-1. Comparisons of various actuation technologies.^[3,6]

Property	Density [g/cm ³]	Modulus [MPa]	Strain [%]	Energy density [kJ/m ³]
Mammalian skeletal muscle	1	10 - 60	20 - 40	8 - 40
Shape memory alloy	6	20 k - 80 k	1 - 8	> 1 k
Piezoelectric ceramic	8	70 k	0.2	100
Conducting polymer	1.2	500	2 - 12	70 - 100
Ferroelectric polymer	2	400 -1200	3 - 10	1 k
Dielectric elastomer	1	0.1 - 3	~ 100	1 k

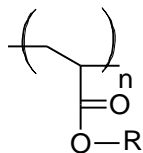
When compared with other electroactive systems and materials, DEs offer several advantages, including: (1) large strain and force output, (2) light weight, (3) large actuation strain and high energy density, (4) quiet operation, and (5) low cost.

1.1.2. Study of dielectric elastomer

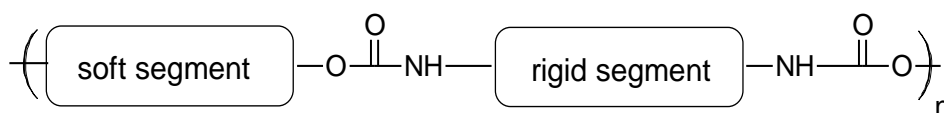
The dielectric and mechanical properties of the DE films are the key to the performance of the DE devices. Major DEs currently under investigation include crosslinked silicones^[7] and polyacrylates^[8], thermoset or thermoplastic polyurethanes^[9], and triblock copolymers comprising two rigid end blocks and a soft middle block^[10,11]. Schemes of some representative DEs are shown in **Figure 1-2**.



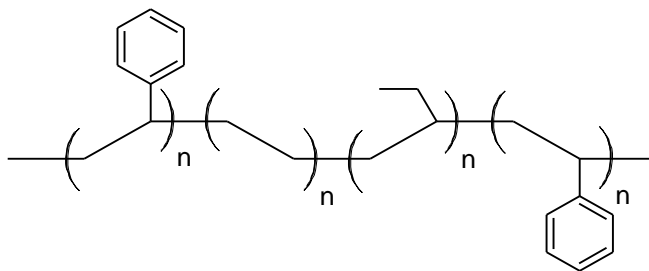
Polydimethylsiloxane (PDMS), a silicone



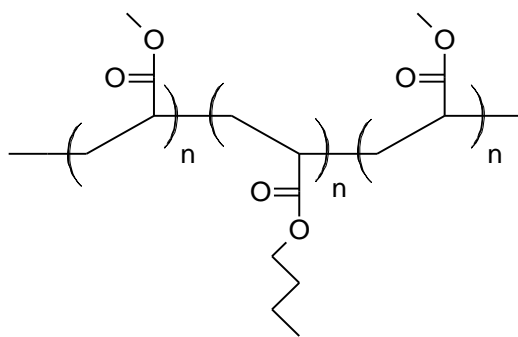
Polyacrylate, R refers to alkyl group or other functional groups



Polyurethane



Polystyrene-block-(ethylene-co-butylene)-block-polystyrene (SEBS), a triblock copolymer



Polymethylmethacrylate-block-polybutylacrylate-block-polymethylmethacrylate (PMMA-PnBA-PMMA), a triblock copolymer

Figure 1-2. Chemical structures of representative DE materials.

Silicones are attractive as these elastomers have low glass transition temperatures, low viscoelasticity, and fast response to both mechanical and electrical stimuli thanks to the high freedom of rotation of the of silicone backbone and low inter polymer chain interaction. Other advantageous features of silicones include resistance to moisture and chemicals, and stability over a broad temperature range. On the other hand, silicones have low dielectric constant, typically less than 3, resulting from the lack of polar moieties. Since most commercial silicones come as viscous pre-crosslinked viscous fluids, efforts have been made to increase the dielectric constants of silicones by adding various high dielectric fillers or highly polarizable groups before curing.

Polyurethane elastomers are either thermoplastic or thermoset depending on the functionalities of employed hydroxyl ended oligomers and isocyanate compounds. In both thermoset and thermoplastic polyurethanes, the rigid urethane blocks function as physical crosslinking sites providing the elasticity while the soft blocks allow large deformation. However, without chemically crosslinking, the thermoplastic polyurethanes suffer from creep or stress relaxation. The thermoplastic polyurethanes are also more sensitive to temperature than thermoset polyurethanes due to the melting of the urethane blocks when heated. The high polarity urethane group promotes polyurethanes' dielectric constants up to 10, higher than silicones. Like silicones, most commercial polyurethanes are supplied as un-cured oligomers, so it is feasible to alter the commercial formulation with additives and fabricate thin films with designed thickness.

Polyacrylates have been an important DE material ever since the high performance of 3M™ VHB™ adhesive film was first discovered.^[5] This commercial material comes as cured films, but it can still be modified by swelling with known acrylate monomers^[12] or plasticizers^[13]. Several new formulations based on commercial monomers or oligomers have also been developed targeting at specific requirements.^[14] Comparing with the precursors of silicones and

polyurethanes, the acrylate monomer solutions have relatively low viscosity so that no additional solvent is required during processing. The solutions can be molded into films through bulk polymerization. Polyacrylates have dielectric constants around 5 and usually demonstrate superior dielectric strengths and actuation strains.

As in the triblock copolymers with two rigid polymer end blocks and a soft block in between, the end blocks form rigid domains that function as physical crosslinkers. Meanwhile, the soft block allows for large deformation similar as in thermoplastic polyurethanes. Polystyrene-block-(ethylene-co-butylene)-block-polystyrene (SEBS) and polymethymathacrylate-block-polybutylacrylate-block-polymethymathacrylate (PnBA-PMMA-PnBA) are two major triblock copolymers utilized as DEs. Their mechanical and electrical properties can be tuned by changing the molecular weight of each block or by applying dielectric solvents to swell the polymer.^[10,11]

Fluoroelastomers^[15], polyesters^[16], polybutadiene^[17], and other elastomers have also been investigated as DEs although the overall performance appear to be lower than the polymers above.

Table 1-2 lists representative DEs reported in recent literatures, including commercial products without or with alteration and new polymers developed in research laboratories. Composite DEs will be discussed in **Section 3**.

Table 1-2. DE materials.

Material	Category	ϵ_r at 1 kHz	Modulus [MPa]	Elongation [%]	Dielectric strength [MV/m]	Maximum actuation [%]

Nusil CF19-2186 ^[5,18]	Silicone	2.8	1.0	600	350	64 (area)
Dow Corning HS3 ^[5,19]	Silicone	2.8	0.1	550	128	117 (linear)
Dow Corning Sylgard 186 ^[4]	Silicone	2.8	0.7	-	144	-32 (thickness)
Silicone-IPN ^[7]	Silicone	-	0.5	400	58	45 (area)
Dow Corning DC 3481 ^[20]	Silicone	3.3~3.7	0.35~0.56	-	32	10 (area)
Dow Corning 730 ^[17,21]	Fluoro-silicone	6.9	0.5	240	80	28 (thickness)
Deerfield PT6100S ^[4]	Polyurethane	7	17	-	160	11 (thickness)
Estane TPU588 ^[9]	Polyurethane	6	-	-	8	8 (thickness)
TPU LPT 4210 UT50 ^[15]	Polyurethane	6.0 ^a	3.36	421	218	-
Bayfol EA102 ^[15]	Polyurethane	7.1 ^a	1.44	300	130	-
3M™ VHB™ ^[5]	Polyacrylate	4.8	3.0	> 1050	412	158 (area)
VHB-IPN ^[12]	Polyacrylate	3.6	2.5	150	300	233 (area)

Formulated polyacrylate^[14]	Polyacrylate	4.8	1	170	237	90 (area)
SEBS 161-oil^[10]	Swollen triblock copolymer	-	1.3 ^b	-	203	> 100 (linear)
SEBS 217-oil^[10]	Swollen triblock copolymer	-	1.1 ^b	-	195	> 100 (linear)
MBM-146-45^[22]	Swollen triblock copolymer	4.1	0.08	380	28	110 (area)
PnBA-PMMA-TL^[11]	Swollen triblock copolymer	3.0	7.6	419	4.4	20 (area)
PnBA-PMMA-THF^[11]	Swollen triblock copolymer	2.9	12.31	294	5	8 (area)
Polyester-1^[16]	Polyester	5.6	0.08	1100	16	12 (area)
Polyester-2^[16]	Polyester	7.7	1.9	60	34	5.5 (area)
Aldrich PBD^[17]	Polybutadiene	4.0	1.7	-	76	12 (area)

Solvane 250 ^[15]	Fluoro-elastomer	14 ^a	800	525	250	-
Lauren L1431-C ^[4]	Fluoro-elastomer	12.7	2.5	-	32	8 (thickness)
ACN rubber ^[23]		14	4		50	20 (thickness)

^a This value is measured at 1/8 Hz.

^b This value is compressive modulus in z direction.

1.1.3. Optimization of dielectric elastomers – Design guidelines for dielectric elastomers

1.1.3.1. Dielectric properties

Dielectric properties, including dielectric constant, dielectric loss, leakage current, and dielectric strength are all decisive factors for DEs' actuation properties and application performance.

A. Dielectric constant and loss

A dielectric material is polarized when exposed to an external electric field. Polarization (P) is defined as the macroscopic density of the permanent and induced electric dipole moments in the material. P is calculated as:

$$P = \epsilon_0(\epsilon_r - 1)E \quad (2)$$

As for a capacitor, the capacitance (C) can be calculated as:

$$C = \epsilon_0\epsilon_r A/d \quad (3)$$

where A and d are the area and the thickness of the capacitor, respectively. This equation is also often used to characterize the dielectric constant.

In a dynamic operation, the dielectric permittivity can be expressed in a complex form:

$$\varepsilon^*(\omega) = \varepsilon'(\omega) - j\varepsilon''(\omega) \quad (4)$$

where ω is the operation frequency, and $\varepsilon'(\omega)$ and $\varepsilon''(\omega)$ are the real and imaginary parts of the dielectric constant, respectively. The real part $\varepsilon'(\omega)$ responds to the polarization for the energy storage and $\varepsilon''(\omega)$, often referred as loss factor, represents that of the dissipative part. The dissipative behavior is sometimes characterized by loss tangent ($\tan(\delta_e)$) defined as:

$$\tan \delta_e = \varepsilon'' / \varepsilon' \quad (5)$$

There are several mechanisms in microscopic scale contributing to the macroscopic polarization:

(1) electronic polarization: a distortion of the electron cloud around the nuclei upon the external electric field; (2) distortion polarization: also referred as atomic polarization, the bending and stretching motions of the molecules; and (3) orientation polarization: rotation of permanent dipoles or displacement of ions.

All the three polarization mechanisms contribute to the macroscopic polarization at low frequencies. However, dielectric constant is a function of frequency and every polarization mechanism has a characteristic time. A typical dielectric constant – frequency behavior is presented in **Figure 1-3**.^[24]

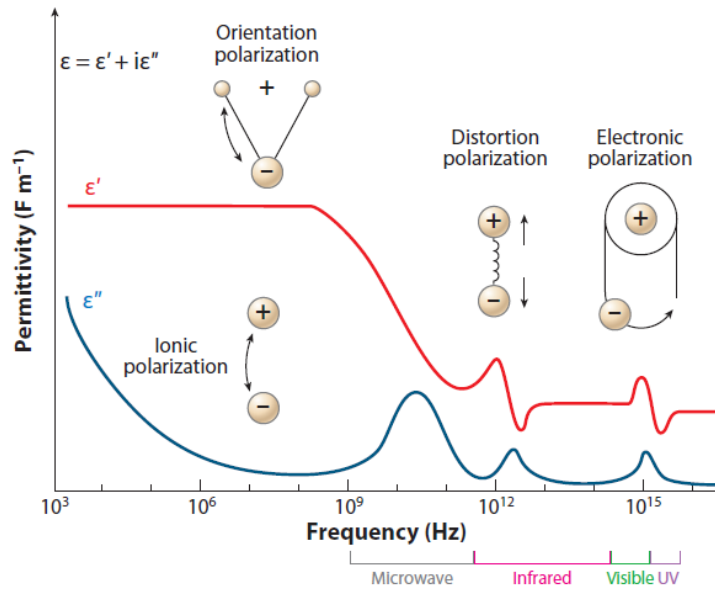


Figure 1-3. Dielectric behavior over frequency. (adopted from [24])

Electronic polarization has the fastest, almost instant response to the applied electric field up to beyond 10^{15} Hz, distortion polarization occurs at frequencies no greater than 10^{14} Hz, while orientation polarization only responds to low frequencies ($< 10^9$ Hz). When considering composite elastomers with high dielectric constant fillers, interfacial polarization between filler and matrix plays a role as well but it has an even lower response speed than that of orientation polarization. When polarization cannot catch up with the alternating applied electric field, there will be an increase in dielectric loss. However, when the applied electric field has a much higher frequency such that the polarization ceases to respond, the corresponding dielectric loss would turn to decrease. Therefore, every polarization mechanism exhibits a peak loss with frequency.

The dielectric constants of polymers depend mainly on their chemical structures. Polar groups contribute to both distortion and orientation polarizations, and thus increase the dielectric constant. For example, silicones usually have dielectric constants below 3 due to absence of polar groups, as listed in **Table 1-2**. However, ϵ_r of Dow Corning 730, a fluoro-silicone, is 6.9 thanks to the

high density of C-F groups in this polymer. The introduction of strong dipoles has been a popular approach to enhancing dielectric constant. This topic will be discussed in **Section 3**.

Permittivity plays a key role in the actuation performances of DE devices. Elastomers with high permittivity are ideal DE materials. Unfortunately, most of the known elastomers with high permittivity also exhibit low dielectric strength and high dielectric loss, which are detrimental to actuation performance. This topic will be further discussed in **Section 3**.

B. Dielectric strength and leakage current

The dielectric strength of a DE refers to the maximum electric field the material can survive without failure. As Equation (1) shows, the dielectric strength defines the limiting performance of a DE. However, the measured dielectric breakdown is often dependent on experimental conditions such as film thickness, apparent modulus, moisture, and electrode material. Several mechanisms could initiate dielectric breakdowns:^[25,26]

(1) Thermal breakdown: Thermal breakdown happens when the Joule heat generated by the leakage current across the DE film cannot be effectively dissipated. The resulted heat in film would raise the conductivity of the film, thus the leakage current, and further increase the leakage current, resulting in a positive feedback. Once above a threshold, the elastomer film would be melt locally, creating low-breakdown path.

(2) Electronic process: The breakdown starts from ionization in a local region. At this region, electron avalanches. The discharging causes erosion of the dielectric, and thus rapid propagation of a conducting channel.

(3) Electromechanical instability: As schematically shown in **Figure 1-4**, an elastomer film undergoes a characteristic rapid increase in stress, then a plateau region, followed by a very steep rise in the stress until the rupture of the film via the breaking of covalent bonds. The actuation stress/strain curve will follow the quadratic curve in the figure. For sufficiently high driving voltage, the reduction in film thickness and increase in electric field form a positive feedback loop and the film will continue to be driven thinner and thinner until the local electric field exceeds the dielectric strength of the film, as indicated by the intersection of the quadratic curve and elastic stress curve. This induces eventual dielectric breakdown. However, if the film is pre-stretched, the origin of the actuation stress/strain curve will shift to O'. The resulting actuation stress/strain curve will be less likely to intersect the elastic stress/strain curve; therefore the actuation will be more stable.^[3]

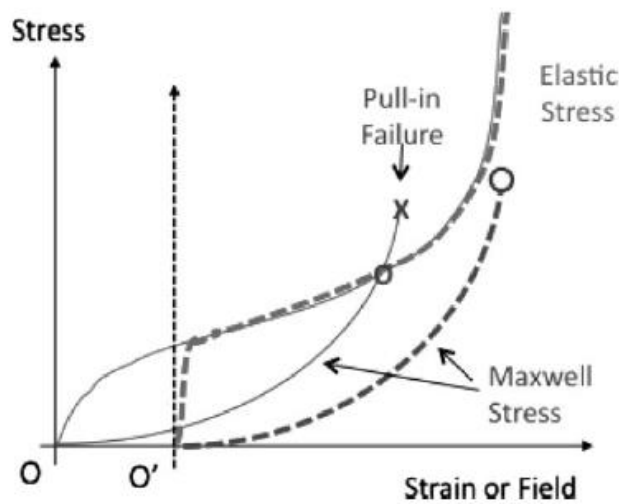


Figure 1-4. Characteristic stress of a DE film as a function of mechanical strain or electric field (constant voltage condition). The chart with origin at O are for a non-prestrained film at O' for the prestrained film. The cross (×) indicates dielectric breakdown and the bar (-) indicates stable actuation strain. Small o and large O represent the apparent breakdown field and actual breakdown strength respectively. (adopted from [3])

(4) Environmental effect: The breakdown is started by ionization of surrounding medium such as air molecules. It usually occurs at the edge of the electrodes.

Overall, the dielectric breakdown of a DEA often starts from a local breakdown. The apparent, practically useful dielectric strength can often be improved by suppressing the presence of local defects or “weak spots” such as non-uniformity of film thickness, residual catalyst, and dust particles. Yuan et al. utilized carbon nanotubes as self-clearing electrode with which a local breakdown is open-circuited as the ultrathin carbon nanotube electrode is burned away around the breakdown spot. A DE actuator can thus be made to survive after numerous breakdown events without significant loss of actuation performance. Immersion in dielectric oil could reduce the chance of air discharging.^[27]

C. Leakage current

Leakage current through a DE film is inevitable since DE is not perfectly insulating. It decreases the actual voltage on the DE component and consumes electrical energy without exerting mechanical work.

The works by Gisby et al. and Di Lillo show that the 3M™ VHB™ does not show an Ohmic behavior.^[26,28] The leakage current increases exponentially with the applied electric field due to the excitation of more electrons in valence band into the conduction band at higher electric field, and thus increase of electrical conductance.

1.1.3.2. Mechanical properties

The moduli of the DE polymer at various strains place a key role in the actuation as Equation (1) shows. Other mechanical properties are also important factors such elongation and stress at rupture and viscoelasticity. In this section, viscoelasticity will be discussed in length since it is influential on the reliability of DEs.

Viscoelasticity

Viscoelasticity is a result of molecule movement delay and inter chain friction. Mechanical loss factor is often used to characterize the viscoelasticity of a polymer:

$$\tan \delta_m = E'' / E' \quad (6)$$

where E'' and E' are the loss modulus and storage modulus. Viscoelasticity will harm the device performances in (1) reducing response speed, (2) lowering reliability due to creep and stress relaxation and (3) dissipating electro-mechanical energy into heat.^[29] 3MTM VHBTM is an example of DEs with high viscoelasticity resulted from strong inter chain interactions. **Figure 1-5** shows an actuator with 3MTM VHBTM as the active material. The delay in response is seen both when a driving voltage is applied on and removed.^[15]

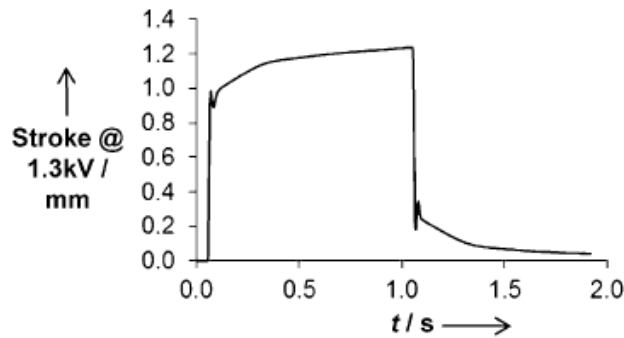


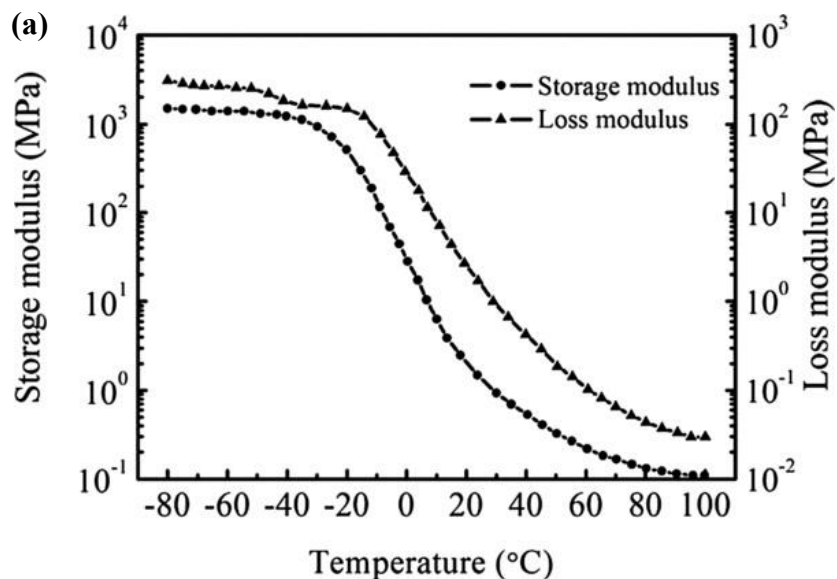
Figure 1-5. A 3MTM VHBTM actuator's performance as a function of time. The actuation voltage is applied at 0.05 s and removed at 1.05 s. (adopted from [15])

Overall, viscoelasticity is not a desirable property for DE. However, it might not be eliminated completely.

1.1.3.3. Environmental effects

A. Temperature

Temperature may affect a DE's performance in three aspects: material's chemical structure, dynamic mechanical property and dielectric constant. Sheng et al. conducted quantitatively study on 3M™ VHB™ as a representative polyacrylate DE. In a thermal gravity analysis in nitrogen atmosphere, 3M™ VHB™ started to lose weight at 260 °C followed by a rapid loss at 385 °C. The storage modulus of 3M™ VHB™ was found very sensitive with temperature change around room temperature. It is 1.2 GPa below - 30 °C, decreases rapidly above - 20 °C due to glass transition, and reaches 0.1 MPa at 100 °C. (See **Figure 1-6.**) Such a large variation of modulus in the ordinary operation temperature range is undesirable. It could be overcome via the addition of plasticizers to lower the glass transition temperature.^[13] The permittivity of VHB increases with temperature from - 40 °C to 0 °C, which coincides with the glass transition and it attributed to the change in orientational freedom of dipoles in the polymer as a function of temperature. The authors also observed a dielectric constant decrease above 0 °C, and explained it as a result of dipole density decrease due to thermal expansion.^[30]



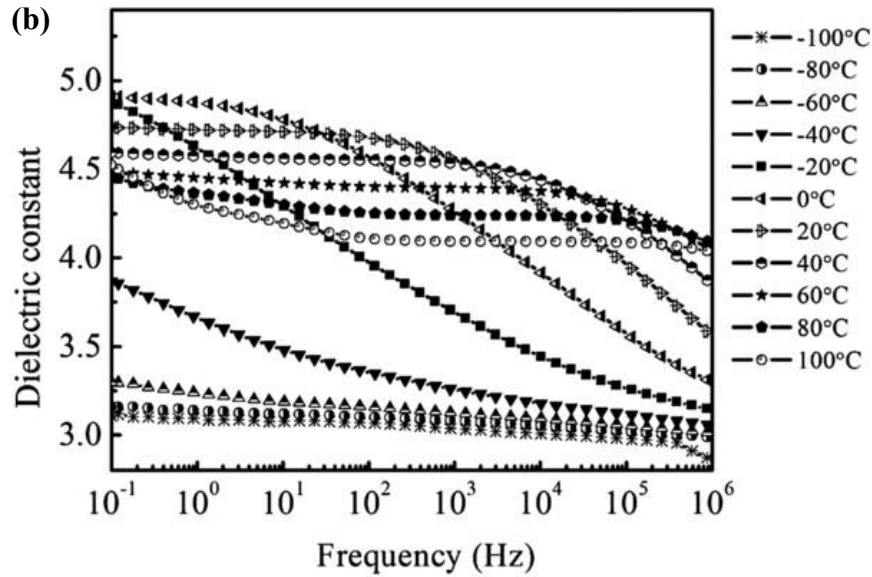


Figure 1-6. 3M™ VHB™’s (a) Storage and loss moduli as a function of temperature at a frequency of 0.1 Hz; and (b) dielectric constants of different temperatures as a function of frequency. (adopted from [30])

Biggs et al. also studied the effect of temperature on the actuation performances of 3M VHB as well as a silicone elastomer. As shown in **Figure 1-7**, the 3M™ VHB™ actuator shows a stroke increase from $-40\text{ }^{\circ}\text{C}$ to room temperature due to decrease in modulus. However, the stroke decreased as temperature is further raised. In comparison, silicone shows a very stable actuation from $-40\text{ }^{\circ}\text{C}$ up to $80\text{ }^{\circ}\text{C}$ because of stable mechanical and dielectric properties.^[15]

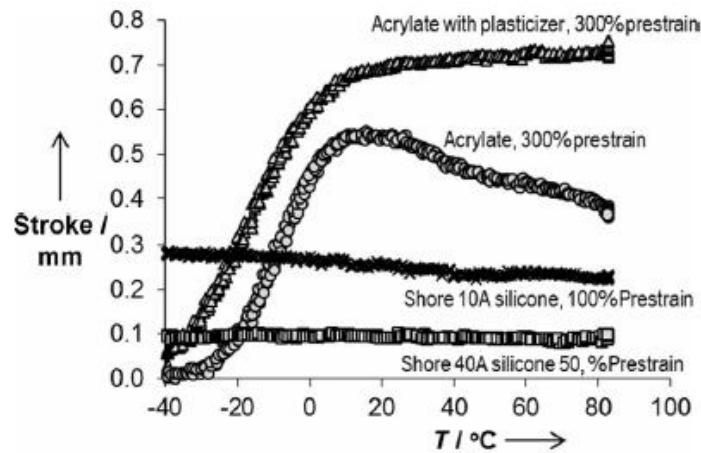


Figure 1-7. Performance of actuators of 3M™ VHB™ and a silicone as a function of temperature. (*adopted from [15]*)

B. Humidity

Moisture absorbed in a polymer network would increase the material's conductivity so that the soft capacitor would suffer a higher leakage current and an early electric breakdown during high electric field operation. The absorption of moisture in a DE polymer is determined by free volumes in the polymer and interaction between water molecules and constituent bonds on the polymer chains. Strong dipole and hydrogen bond-forming bonds tend to absorb more moisture. For the same polymer structure, an elastomer with lower crosslink density can be swollen more than a more densely crosslinked elastomer.

Biggs et al. studied how humidity affects the reliability of a 3M™ VHB™ actuator, and found that the mean cycles to failure dropped two orders when humidity increased from 20 %RH to 60 %RH.^[15] This high moisture sensitivity is likely caused by the presence of polar and hydrogen bonding forming moieties, such as the carbonyl group and carboxylic acid group, in this polyacrylate copolymer.

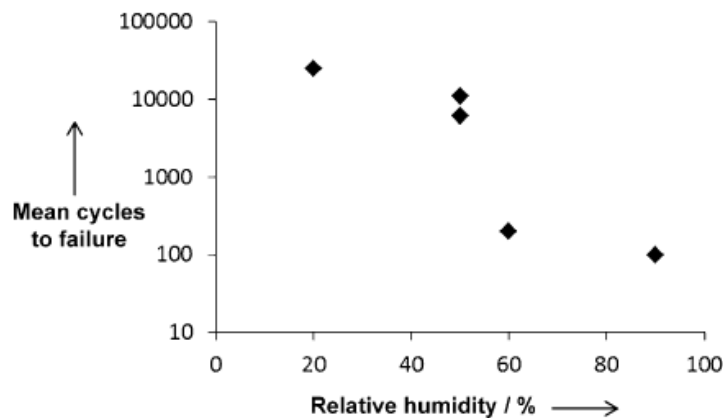


Figure 1-8. Effect of relative humidity on actuation cycles to failure of 3M™ VHB™ acrylate actuators at room temperature. (*adopted from [15]*)

Silicones are much less susceptible to moisture due to absence of highly polar or hydrogen bonding forming groups. A silicone based device could be operated at 25 °C/70% RH for 7.6 million cycles, with a mean time to failure of 20 million cycles at 65 °C/85% RH.^[15]

1.1.3.4. Fabrication of DE films

DE actuators generally require electric fields of 10 to 100 MV/m to produce useful force or strain. Thinner films are preferred to reduce the driving voltage. However, to fabricate elastomer thin films is even more challenging than other plastic polymers due to their low stiffness.

High molecular weight polymers or pre-polymers, such as most silicones and polyurethanes, were usually mixed with solvents and drop casted into films. Crosslinking reactions occur during and after solvent evaporation. The resulted film thickness usually exceeds ~ 50 μm to ensure a uniform film thickness. A clean room environment is preferred to achieve better quality. Bulk polymerization though UV and heat is suitable for formula with low viscosity prepolymer without solvents or by-product during crosslinking. Lotz et al. developed a process to fabricate multilayer actuators. Uncured silicone parts were mixed and spin coated. After the silicone film thermally cured, graphite powder was sprayed on. Then the process is repeated to fabricate more layers. The film thickness can be adjusted by spin speed. A minimum thickness of 4 μm was achieved.^[31]

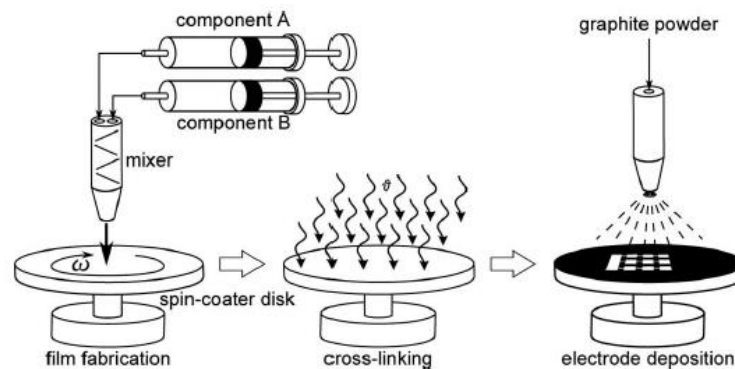


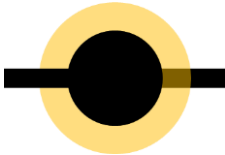

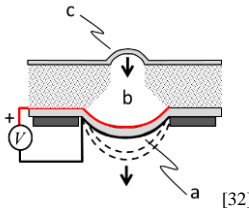

Figure 1-9. Lotz’s process for fabricating multilayer DEAs. (*adopted from [31]*)

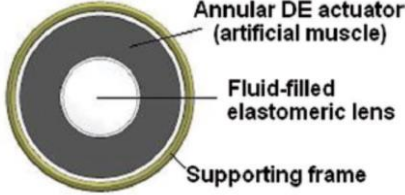
1.1.4. Applications of dielectric elastomers

1.1.4.1. Actuators with various configuration

DE actuators have been integrated into multiple complex systems such as braille display, tunable lenses and robotics. Basic configurations of DE actuators include: planar, stacking, diaphragm, spring roll and annular actuators. The configurations and applications are listed in **Table 1-3**.

Table 1-3. DE actuator configurations.

Configuration	Structure	Comments and applications
<p>Planar actuator</p>		<p>Basic DE actuator. Material characterization and patterning.</p>
<p>Stacking actuator</p>		<p>Increase displacement in thickness direction. Increase actuation blocking force. Linear actuator.</p>
<p>Diaphragm actuator</p>		<p>Tactile display, Braille display and microfluidic channel.</p>
<p>Spring roll actuator</p>		<p>Electrode can be patterned to achieve multiple degree of freedom.</p>

		Walking robot and flying vehicle.
Annular actuator	 <p>Annular DE actuator (artificial muscle) Fluid-filled elastomeric lens Supporting frame</p> <p>[34]</p>	Tunable lens.

A planar actuator is the basic actuator structure which is usually used to characterize the actuation performance of a DE or an electrode material. Stacking actuator contains multiple layers of planar actuators which can enlarge the deformation in thickness direction and increase the actuation blocking force. Diaphragm actuator comprises a confining ring so that the film would buckle up. A spring roll actuator contained a compressed spring wrapped with a DE film with pasted electrodes. Depending on the electrode pattern and the actuated portion of the DE film, the spring roll actuator was able to show multiple actuation modes. An annular actuator is usually used in tunable lens.

1.1.4.2. Products and prototypes

There are a few commercial products utilizing the special advantages of DE technologies including the capacitive sensors for human motion measurement by StretchSense^[35], tunable lenses by Optotune^[36], and headphone with vibration motion by Vivitouch Technology^[37]. Meanwhile efforts have been made on various prototypes such as bio-inspired robots which can walk or fly, braille displays and microfluidic channels.

1.2. Motivation of this thesis

It has been 15 years since the superior actuation performances of dielectric elastomers were discovered. Great achievements have been established in several subjects in this field, including mechanics study and modeling, prototypes fabrication and material improvements. However, most of the currently employed DE materials, including acrylic adhesive, silicone and polyurethane elastomers, are commercial polymers manufactured for other applications such as pressure sensitive adhesives, encapsulation and coating. Furthermore, the exact chemical structure or formulation of these polymers are kept as industrial secrets, making it difficult to modify the formulation for enhanced DE performance or specific application requirements. Therefore, it is of great interest to design and develop new polymeric materials from molecular level specifically for DE applications.

1.3. Scope and layout of the dissertation

This dissertation is divided into five chapters.

Chapter 1, the current chapter, gives an introduction of the thesis, including the basic mechanisms the dielectric elastomer, the state of art in DE material development in materials' properties and processing and configurations and applications of DE actuators.

Chapter 2 describes the formulation of a group of polyacrylate DEs targeting at high actuation performances. The effects of an acid component, acrylic acid, on both mechanical and electromechanical properties of these DEs, were discussed.

Chapter 3 introduces the synthesis of a group of DEs targeting at high permittivity. The permittivity was increased through addition of Al nanoparticles. The as-prepared nanocomposite elastomer demonstrated a high permittivity of 8.4 while maintain high breakdown strength.

Chapter 4 discusses a new type DEs with controllable stiffness. The mechanical properties of these elastomers can be administered by dynamic bonding formation via simple thermal treatment. Capacitive sensors and actuators are fabricated with this new DE and can be operated at different modes.

Chapter 5 gives an outlook of future researches in this field and concludes the dissertation.

2. Dielectric Elastomers with High Actuation Strain

2.1. Background of this study

3M™ VHB™ adhesives have been used as dielectric elastomers for a lot of applications. The second network was introduced into this elastomer to suppress the electromechanical instability during actuation.^[12] Plasticizers were used as well to broaden the operation temperature range.^[13] However, these adhesive films come as film rolls with confidential formulation, making it difficult to understand the structure-property relationship and further improve this material. Moreover, these film rolls have pre-set thicknesses, not suitable for certain applications.

A group of acrylate copolymers were synthesized as new dielectric elastomers targeting at high actuation strains. Acrylate monomers were selected for two reasons:

- (1) Acrylates have various structures and can be used to form polymers with versatile properties.
- (2) Acrylates are reactive and easily cured when exposed to ultra-violet (UV) light. UV curing process is fast, low cost, and scalable and has low environmental impact.

In the set of formulations, n-butyl acrylate was selected as the core building block to synthesize these new acrylate copolymers because poly (n-butyl acrylate) is soft at ambient temperature with a glass transition temperature of ~ -50 °C.^[38] This would contribute to a large actuation strain. A difunctional urethane acrylic ester resin (CN 9021) was added as a long chain crosslinker as it has a flexible chain and its mono polymer has a tensile strain up to 1000 %. A silicone diacrylate (CN 9800) was used as the second crosslinker to avoid crystallization. Acrylic acid is another important component in the formula since its carboxyl acid group is quite polarizable and may contribute to a high permittivity. In this study, various amounts of acrylic acid were investigated.

2.2. Experimental design

2.2.1. Materials

The monomers, n-butyl acrylate ($\geq 99\%$) and acrylic acid (99%, anhydrous), and the photoinitiator, 2,2-dimethoxy-2-phenyl acetophenone (99%) (DMPA) were purchased from Sigma-Aldrich. CN 9021 and CN 9800, were supplied by Sartomer Company. All the chemicals were used without further purification.

The adhesive tape, 3M™ VHB™ 4905, was used as a reference material. This tape has a thickness of 500 μm .

2.2.2. Film preparation

Four formulas, listed in **Table 2-1**, with various amounts of acrylic acid were investigated.

Table 2-1. Formulas (weight part) with various amount of acrylic acid.

Formulation	n-butyl acrylate	Acrylic acid	CN 9021	CN 9800	DMPA
AA-0	100	0	13	1.3	0.5
AA-6	100	6	13	1.3	0.5
AA-13	100	13	13	1.3	0.5
AA-20	100	20	13	1.3	0.5

In a typical procedure, a pre-polymer solution was injected into a glass mold coated with commercial Rain-X hydrophobic coating. The thickness of the liquid layer is defined by spacer tapes on the edges of glass pieces. The UV light, supplied from a UVP B-100 lamp, was shone on the liquid layer for 15 minutes as the monomers were cured to form a solid film. Then film was taken out of the glass mold and baked on a hot plate at 80 °C for one hour to let un-polymerized

monomers evaporate and release the inner stress developed in the curing process. The as-cured films are soft, stretchable and transparent.

2.2.3. Tensile test

Tests followed ISO 37:1994 by a dynamic mechanical analyzer (DMA, TA instruments RSAIII). Films were cut into a standard dumbbell shape with an effective area of 2 mm width by 12 mm length with a laser cutter. All tested samples have a thickness between 500 μm and 600 μm . Samples were stretched to the limitation of the DMA stage with a rate of 3.33 mm/s.

2.2.4. Actuation characterization

AA-0, AA-6, AA-13 and AA-20 films were stretched by 300 % biaxially and confined with plastic frames. Circular actuators were made by pasting carbon grease on both sides of the stretched films using shadow masks. AA-13 films were further investigated with 200 %, 250 %, 350 % and 400 % biaxial prestrains.

Actuation voltages were applied starting at 800 Volts and increased at 200 Volts increments till 2400 Volts. The voltage was then increased at 100 Volts increments till the failure of each actuator. Each actuation voltage was hold for 10 seconds. Areas during actuation were recorded with a web camera and measured with a LabView program.

2.2.5. Actuation blocking force measurement

The synthesized films were first stretched 300 % biaxially. Single walled carbon nanotube was dispersed into chloroform solvent with a concentration of 4 mg/ml through ultra-sonication for 3 hrs. The dispersion was sprayed onto both surfaces of the stretched films with an overlapping electrode area of 40 mm by 6 mm which defines the active area of the actuator. Rigid frames were then applied as shown in **Figure 2-1** for clamping onto DMA. The clam position was adjusted to

ensure 300 % prestrain of the DE films in the vertical direction. The films would shrink in x direction due to Poisson's effect. Voltages increasing from 500 Volts to 2500 Volts at 100 Volts increments were applied. The force at vertical direction (y axis in **Figure 2-1**) required to maintain the 300 % prestrain was measured by the DMA. The force changes between voltage-on and voltage-off states were taken as the blocking force corresponding to the bias voltage.

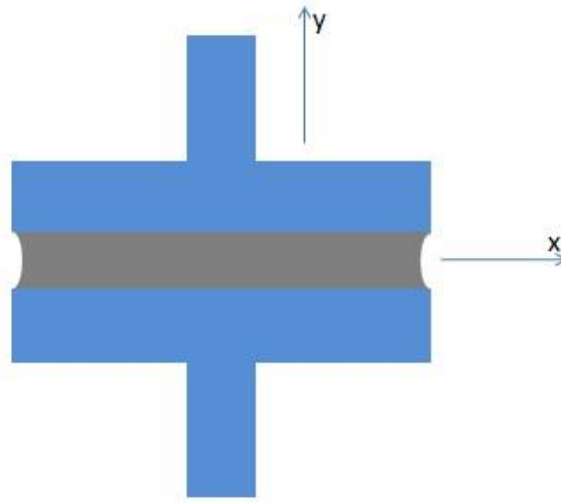


Figure 2-1. An actuator for blocking force test.

2.2.6. Actuation lifetime measurement

2.2.6.1. Actuation lifetime at a static voltage

AA-13 films were stretched by 300 % biaxially. Circular actuators were made as described in Section 2.2.4. To improve the lifetime performance, self-clearing electrodes with single walled carbon nanotubes were deposited as described in Section 2.2.5. These carbon nanotube electrodes were blanket covered with dielectric oil for stable self-clearing. Constant voltages were applied to obtain 150 % actuation area strain. The transient current during the constant voltage actuation was measured with a Keithley multimeter and recorded by a LabView program. The actuation area was

recorded with a web camera and the calculated area strain was recorded with the same LabView program. The actuation voltage was maintained until terminal failure of each sample.

2.2.6.2. Actuation cycle lifetime

AA-13 films were stretched to 300 % biaxial prestrain. Circular actuators were made using carbon grease electrodes. Square wave voltages with 0.05 Hz and 0.5 Hz frequency between 0 volts and a predetermined high voltage that drove an actuator sample to 150 % area strain were applied. The transient area of the active area was recorded with a web camera and recorded with a LabView program. The cyclic actuation was continued until terminal failure of each sample.

2.3. Results and discussion

2.3.1. Mechanical properties

Stress-strain curves were plot in **Figure 2-2**. Note that the final points at 1100 % tensile strain of all the four stress-strain curves are not elongation rupture but the limitation of the DMA.

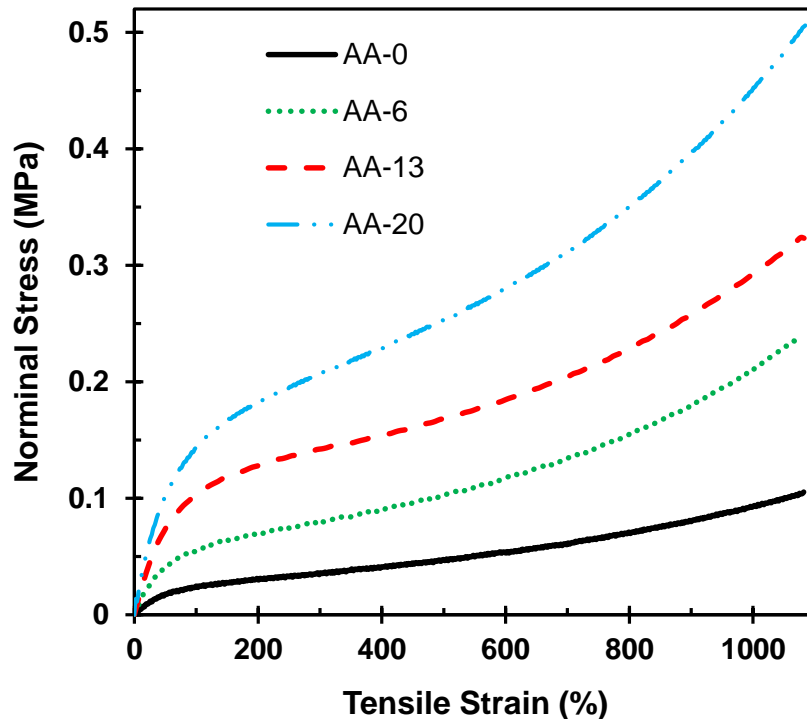


Figure 2-2. Stress-stain curves of AA-0, AA-6, AA-13 and AA-20.

All the four curves follow a typical hyperelastic stress-strain characteristic: the stress increases rapidly at first, then undergoes a plateau region and a rapid increase at the end. **Figure 2-2** indicates that the increase of acrylic acid amount results in an increase of stiffness.

2.3.2. Measurement of dielectric constant

Dielectric constants of different formulations were determined by blocking force tests. According to the derivation in **Ref [39]**^[39], the permittivity can be calculated from blocking force by Equation (7):

$$F_y/z_o = x_o \varepsilon_r \varepsilon_o E^2 / \alpha_y = k E^2 \quad (7)$$

where F_y is the blocking force in y direction measured by DMA, x_o and z_o are length and thickness before prestrain, and α_y is prestrain ratio of the width (y) direction, respectively. V is the applied voltage. F_y/z_o is proportional to E^2 and ε_r can be calculated by Equation (8).

$$\varepsilon_r = k \alpha_y / x_o \varepsilon_o \quad (8)$$

Figure 2-3 shows the plots of F_y/z_o and E^2 of different formulations and the linear fit of each curve. 3MTM VHBTM 4905 adhesive was tested as well as a reference. **Table 2-2** shows the calculation results of block force tests.

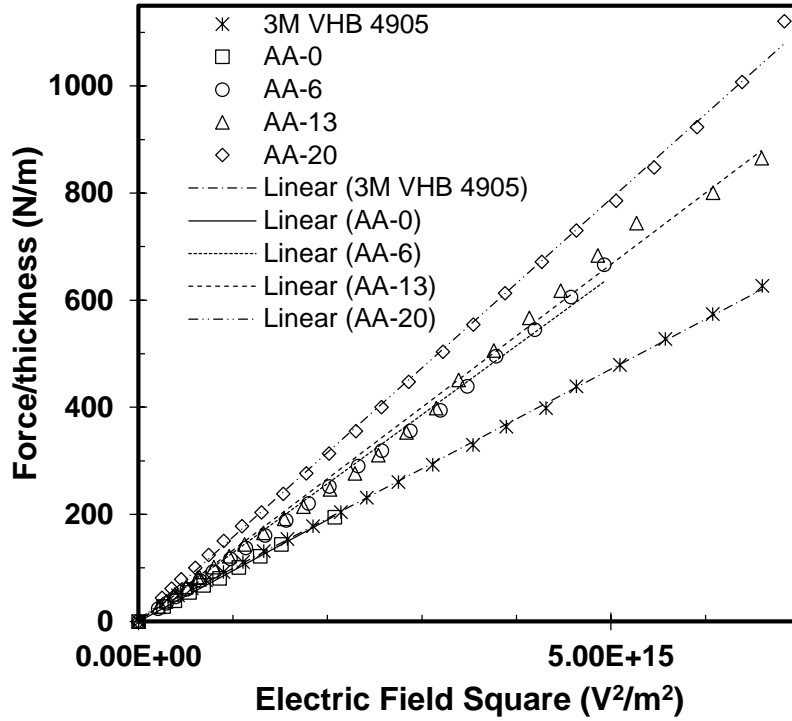


Figure 2-3. Blocking force test of AA-0, AA-6, AA-13 and AA-20. 3M™ VHB™ 4905 was tested as a reference.

The calculated blocking force using the linear fit was listed in **Table 2-2**.

Table 2-2. Calculated blocking force and dielectric constant.

Sample	Linear fit slope k [10 ⁻¹⁴ J/V ²]	Coefficient of determination R ²	ε _r
AA-0	9.45	0.999	4.3
AA-6	9.48	0.999	5.8
AA-13	12.87	0.996	6.0
AA-20	13.34	0.995	7.1
3M™ VHB™ 4905	15.79	0.999	4.3

2.3.3. Actuation performance

2.3.3.1. Actuation of all elastomers with 300% by 300% prestrain

Actuation curves of AA-0, AA-6, AA-13 and AA-20 at 300 % by 300% biaxial prestrain were plotted in **Figure 2-4**.

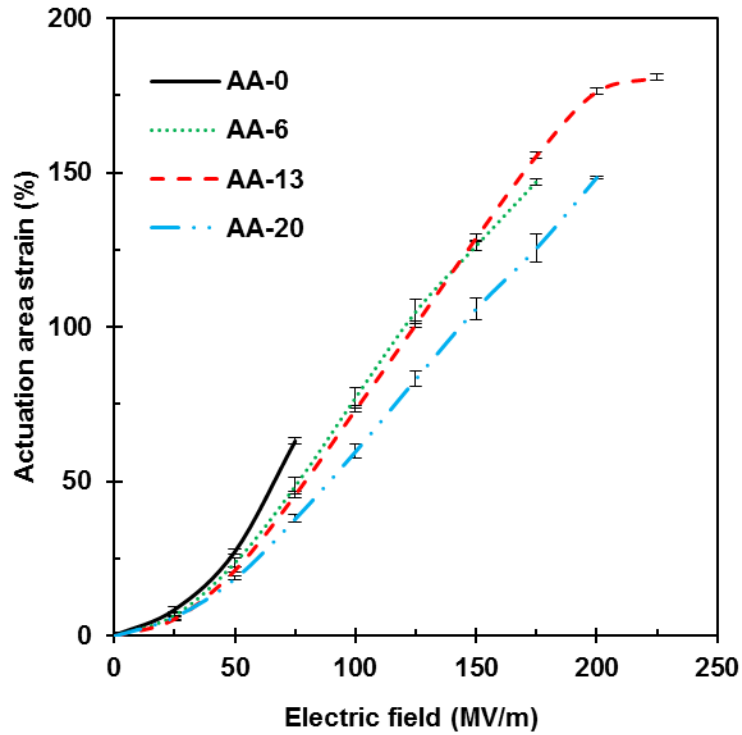


Figure 2-4. Actuation performances of AA-0, AA-6, AA-13 and AA-20 elastomers. All elastomers were pre-stretched 300% by 300% biaxially.

2.3.3.2. Actuation of AA-13 elastomer at various prestrain ratios

As AA-13 had shown superior performance than other formulations. It was studied with other pre-stretched ratio. The actuation curves were plotted in **Figure 2-5**.

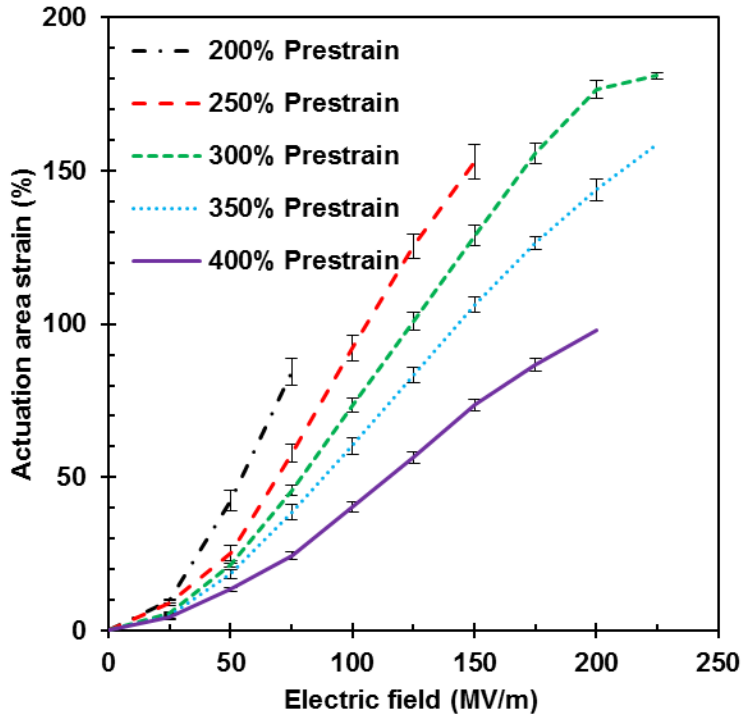


Figure 2-5. Actuation performances of AA-13 with various prestrain ratios.

The key actuation performance data of these elastomer actuators were summarized and listed in **Table 2-3**.

Table 2-3. The summarized actuation performances of the synthesized elastomers.

Sample	$E_{b, \max}$ [MV/m]	$S_{a, \max}$ [%]	p_{\max} [MPa]	$u_{e, \max}$ [MJ/cm ³] ^[5]
AA-0 300% by 300%	65	43	0.2	0.03
AA-6 300% by 300%	170	148	1.5	0.67
AA-13 300% by 300%	222	186	2.6	1.4
AA-20 300% by 300%	191	137	2.3	0.99

AA-13 200% by 200%	93±3	113±9	0.5	0.17
AA-13 250% by 250%	157±3	165±4	1.3	0.64
AA-13 350% by 350%	221±2	162±1	2.6	1.3
AA-13 400% by 400%	206±3	104±2	2.3	0.80

2.3.3.3. Actuation lifetime at a static voltage

Four samples with carbon grease electrodes actuated at a constant voltage and a measured strain of approximately 150 % showed lifetimes of 295 s, 435 s, 309 s and 191 s, respectively. To further improve the performance, 4 samples with self-clearing electrode were tested at the same conditions. The lifetimes were increased to 3000 s, 1130 s, 1000 s and 3400 s, respectively. **Figures 2-6** and **2-7** show the actuation strains and leakage currents of one self-clearing sample and one sample with carbon grease electrodes, respectively. In **Figure 2-6**, the sharp peaks indicate self-clearing occurrences.^[27] And the final leakage current peaks in both figures indicate terminal failure of the actuators. It is concluded from **Figure 2-6** that this material is self-clearable and can survive a long life time.

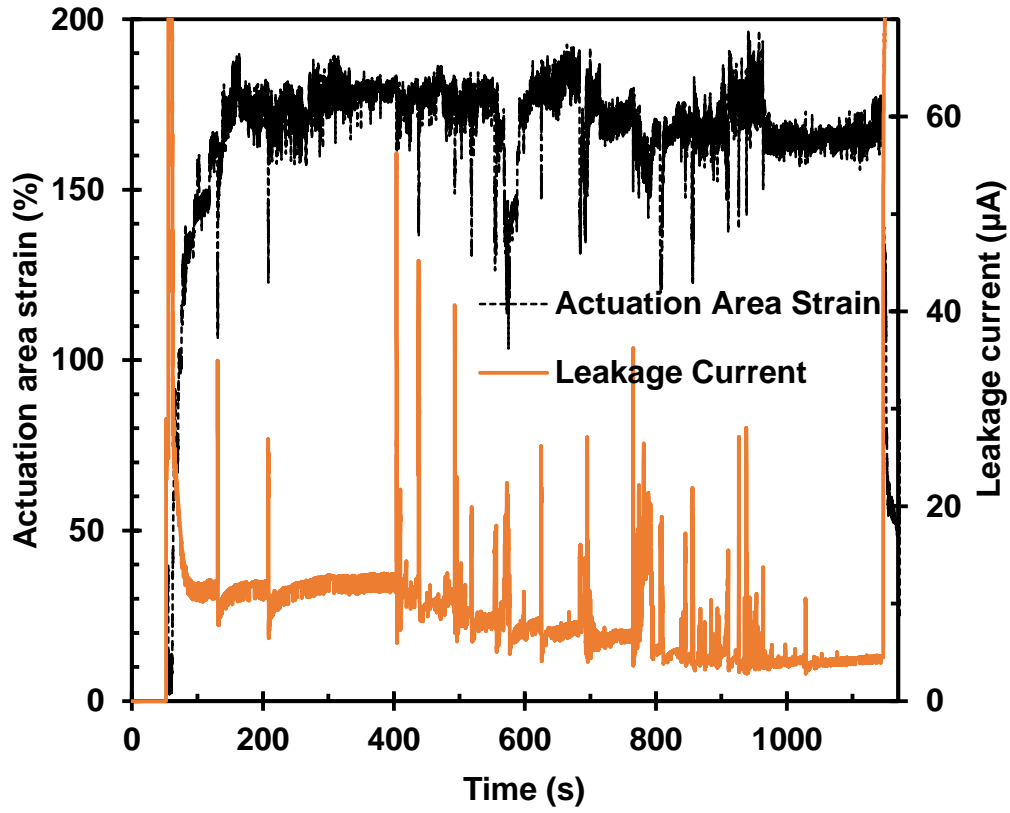


Figure 2-6. Lifetime measurement of an actuator with self-clearing electrodes. The leakage current of the actuator was monitored while constant actuation voltage was maintained to keep the actuation strain at ~ 150 % area strain.

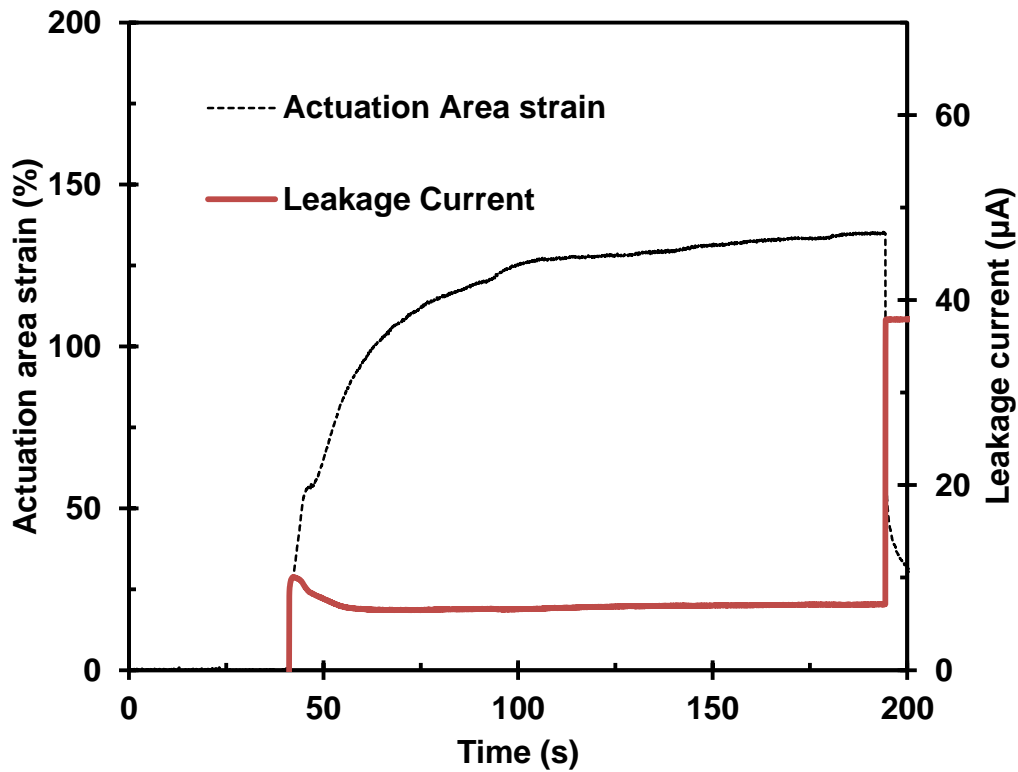


Figure 2-7. Lifetime measurement of an actuator with carbon-grease electrodes. The leakage current of the actuator was monitored while constant actuation voltage was maintained to keep the actuation strain at ~ 150 % area strain.

2.3.3.4. Actuation cycle lifetime

Four samples with carbon grease electrodes were tested under AC actuation (square wave and 0.5 Hz) to determine the cycle reliability. The samples were actuated to show an area strain of ~ 110 %. The lifetimes were 6600 cycles, 1285 cycles, 1536 cycles and 2380 cycles, respectively. **Figure 2-8** shows the actuation of one of the samples. During the cycle lifetime measurement, the actuation strain increased gradually and then approached to a stable number (~ 100 %), indicative of a viscoelastic behavior of this material.

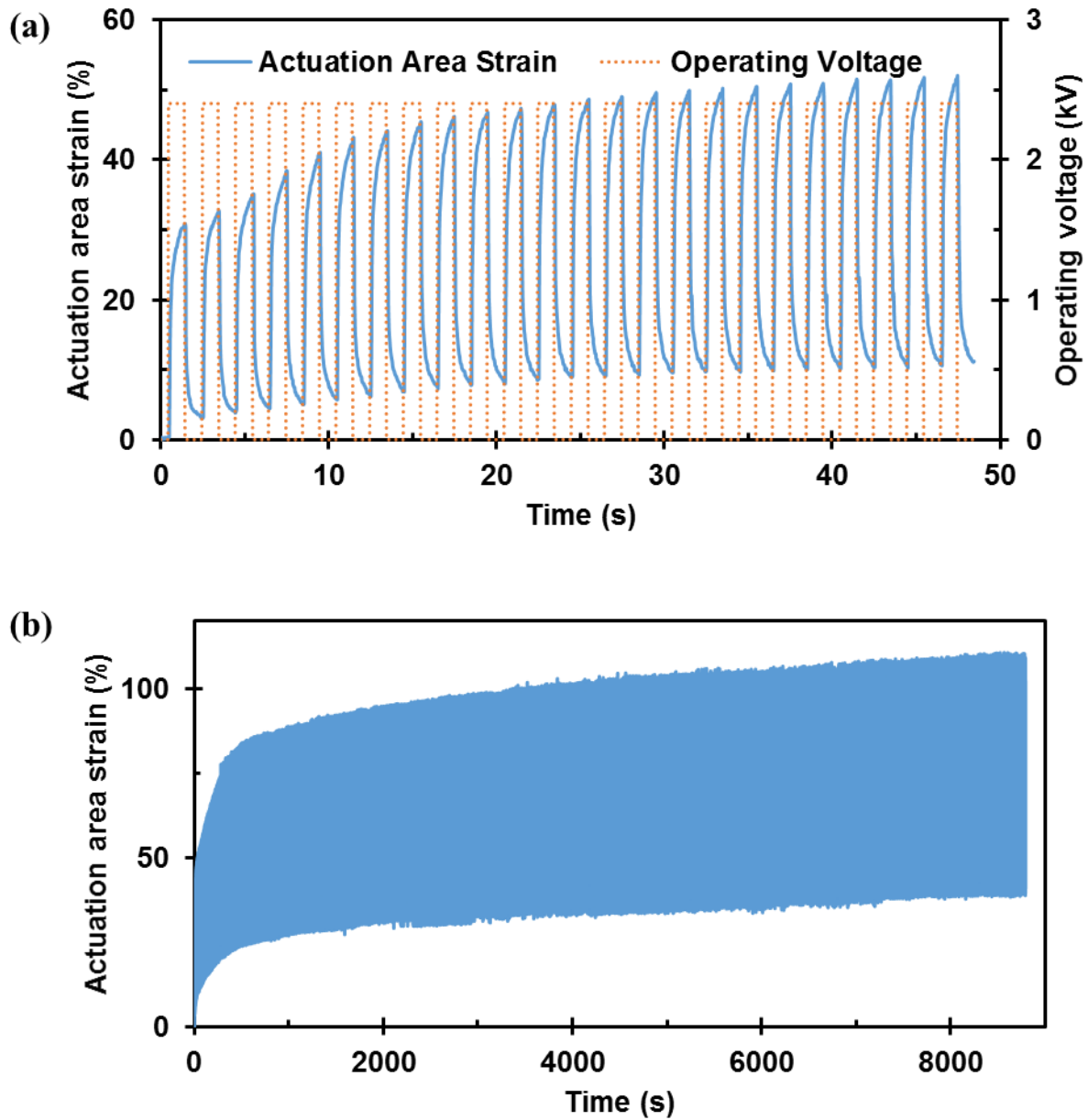


Figure 2-8. Cycle lifetime measurement at 0.5 Hz. AC voltage was applied to achieve a peak actuation area strain of ~ 110 %. Actuation strain at (a) initial 50 sec (25 cycles) and (b) until failure of the actuator.

2.3.4. Effect of acrylic acid

As plotted in **Figure 2-9**, the addition of acrylic acid affects the dielectric elastomers in several aspects: (1) an increase in stiffness; (2) an increase in dielectric constant; and (3) an improvement in the actuation performance with an optimized amount of acrylic acid.

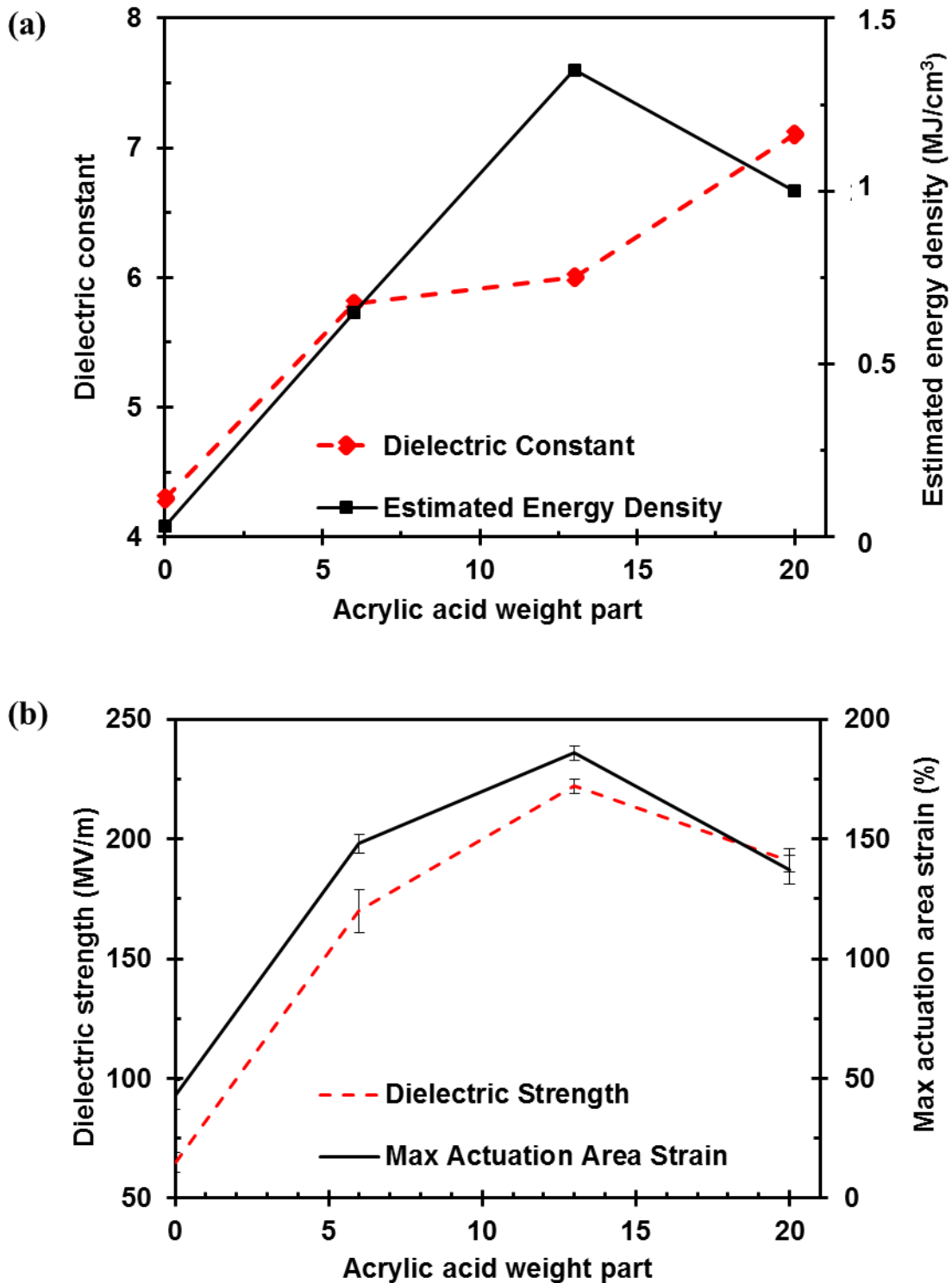


Figure 2-9. (a) Dielectric constant and energy density and (b) actuation performances change with different weight parts of acrylic acid.

These changes result from the molecular structure of the formulated polymers.

(1) The hydrogen bond between the hydrogen atom in the acid side group and the oxygen atom in the ester group in the polymer chain give rise to a stiffness increase. The stiffer films have a smaller chance of undergoing electro-mechanical instability. Therefore there is an increase of dielectric strength. However, when the acid amount is further increased, there may be a higher current leakage at high electric field, so the dielectric strength decreases after the optimal concentration (AA-13).

(2) A higher amount of acrylic acid also contributes to a higher dielectric constant since the carboxyl acid side groups are quite polarizable. The higher dielectric constant also gives rise to a higher energy density together with the increased dielectric strength.

2.3.5. Effect of pre-strain

It has been reported that prestrain can improve the actuation performance of dielectric elastomers. The improvement comes from suppressing electro-mechanical instability so that the breakdown field is increased. **Figure 2-10** shows how prestrain influences the actuation performance of the developed DE materials.

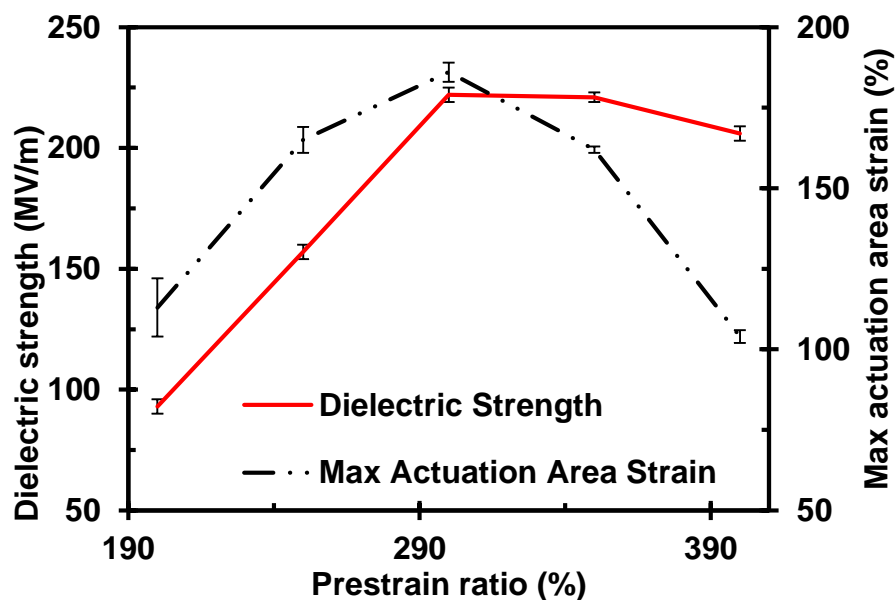


Figure 2-10. Actuation performances of AA-13 with different prestrain ratios.

After 300 %, the breakdown field almost remains unchanged. This phenomenon indicates that the electro-mechanical instability can be overcome once the biaxial prestrain ratio reaches 300 %.^[40] If the dielectric constant is considered unchanged at different prestrains, samples with 300 % prestrain is an optimal condition to obtain large actuation strain and high energy density.

2.4. Conclusions

A group of acrylic dielectric elastomers based on n-butyl acrylate and acrylic acid were synthesized and characterized. Polarizable carboxylic acid group increases the stiffness. The dielectric constant is also increased from 4.3 without acid to 7.1 when the acid content is 20 weight parts. The formula with 13 weight parts of acrylic acid and 300% biaxial prestrain shows a maximum actuation area strain of 186 %, a breakdown field of 222 MV/m, and energy density of 1.4 MJ/m³. These values are comparable with the VHBTM elastomers. The new DE polymer also show fairly long static and cyclic actuation lifetimes at greater than 100 % area strains.

3. Enhancing Dielectric Constant Using Nanocomposite

3.1. Background of this study

3.1.1. The need of high dielectric constant

A high dielectric constant is desirable for improving DEs' performances such as actuation outputs, capacitive sensing sensitivity and energy generating. Meanwhile, the other purpose of using high dielectric constant DE is to reduce to driving voltage of DE devices to maintain a required output. The driving voltages of DE actuators or generators are usually in the scale of kilo volts which brings in both safety concern and complexity in electric circuitry. Using thin elastomer film could be one approach to reduce the driving voltage while produce same actuation strain. However, in this case, the actuation pressure would be limited and the process of thin film fabrication is difficult since DEs are soft. Therefore, developing new DE materials with higher dielectric constant can be another approach to achieve useful output.

3.1.2. Approaches to enhance dielectric constant

There are three general methods of increasing the dielectric constants of DEs, including: (1) incorporation of ceramic fillers with high permittivity; (2) addition of conductive fillers; and (3) covalently linkage of highly polarizable organic groups. Some DEs with high dielectric constants are listed in **Table 3-1**.

Table 3-1. Dielectric elastomers with high dielectric constants.

Material	Composite		Neat polymer		S _{max} [%]
	ϵ_r	E_b [MV/m]	ϵ_r	E_b [MV/m]	
SEBS_TiO ₂ _15 _v ^{a[41]}	5.0	27	2.3	37	13 in area

Silicone_TiO₂_15_w ^[42]	-	78	-	83	17 linear
Silicone_PANI_27.5_w ^[43]	6.5	68	2.2	66	3 in area
PU_CNT_1_w ^[44]	8.4 ^b	5.5	7.6 ^b	7.6	1.1 linear
Silicone_PHT_6_w ^[45]	9.4	8.5	2.8	14	2.4 linear
Silicone_dipole_13.4_w ^[46]	5.98	39	3	130	1.3 in area
Silicone_dipole_0.25_w ^[47]	3.1	-	2.1	-	-

^a M_F_L_{v or w} means Matrix_Filler_Loading percentage volume or weight.

^b These values were measured at 50 Hz.

3.1.1.1. Incorporation of ceramic fillers with high dielectric constants

This method is widely used in producing high-k dielectrics for high energy density capacitor applications. Several models were adopted to predict the effective dielectric constant of these composites.^[48–50]

The classic model predicts that the effective permittivity of a composite in between the equivalent series connection, the lower bound, and the parallel connection, the upper bound:

$$\varepsilon_{r,\min} = \frac{\varepsilon_1 \varepsilon_2}{(\varepsilon_1 v_1 + \varepsilon_2 v_2)} \quad (9)$$

$$\varepsilon_{r,\min} = \varepsilon_1 v_1 + \varepsilon_2 v_2 \quad (10)$$

where ε_r , ε_1 and ε_2 are the dielectric constants of the composite and the two mixing components, respectively, and v_1 and v_2 are their volume fractions. However, in real cases, there is generally a large contrast between fillers' and matrixes' dielectric constants. Therefore, the range predicted by the classic model is too broad and not practical.

The Clausius-Mossotti, Lorenz-Lorentz, Rayleigh and Maxwell-Garnett models are all essentially based on polarizability of small size and spherical particle inclusion assumption. Starting with a bottom-up approach, assuming spherical fillers are embedded in a continuous matrix, the polarizability of a single particle can be written as:

$$\alpha = V(\varepsilon_f - \varepsilon_m) \left[\frac{3\varepsilon_m}{(\varepsilon_f + 2\varepsilon_m)} \right] \quad (11)$$

where ε_f and ε_m are the dielectric constants of the filler (dispersed phase) and the matrix (continuous phase), respectively, α is the polarizability of the particle, V is the volume of the particle. With this, the effective dielectric constant of the mixture can be calculated from the polarizability and density of the fillers as in Equation (12):

$$\varepsilon_r = \varepsilon_m + \frac{n\alpha}{(1 - n\alpha/3\varepsilon_m)} \quad (12)$$

where n is the filler density in the composite. Equation (12) is named Clausius-Mossotti formula or Lorenz-Lorentz formula. If we substitute α by Equation (11), we can get Maxwell-Garnett formula, also referred as Maxwell-Wagner formula:

$$\varepsilon_r = \varepsilon_m + \frac{3v_f\varepsilon_m(\varepsilon_f - \varepsilon_m)}{[\varepsilon_f + 2\varepsilon_m - v_f(\varepsilon_f - \varepsilon_m)]} \quad (14)$$

Rayleigh formula is essentially the same as Equation (14) with a different form.

When v_f is very small (usually less than 0.1), Equation (14) can be written as Sillars formula or Landau-Lifshitz formula which is Equation (15):

$$\varepsilon_r = \varepsilon_m + \frac{3v_f\varepsilon_m(\varepsilon_f - \varepsilon_m)}{(\varepsilon_f + 2\varepsilon_m)} \quad (15)$$

Yamada formula is another version of Equation (15) but considering other shapes of inclusion:

$$\varepsilon_r = \varepsilon_m + \frac{mv_f\varepsilon_m(\varepsilon_f - \varepsilon_m)}{[m\varepsilon_m + (1 - v_f)(\varepsilon_f - \varepsilon_m)]} \quad (16)$$

where m is a constant related to the shape of the filler. When m equals 3, Equation (16) is the same as Equation (15).

Other predicting rules include: coherent potential formula, Bruggeman formula (polder-Vansanten formula or Bottcher formula) and Logarithmic formular (Lichtenecker formular).

Coherent potential formula is based on wave propagation in random media, in the case of spherical fillers, the formula is:

$$\varepsilon_r = \varepsilon_m + \frac{3v_f\varepsilon_r(\varepsilon_f - \varepsilon_m)}{[\varepsilon_f + 2\varepsilon_m - v_f(\varepsilon_f - \varepsilon_m)]} \quad (17)$$

The Bruggeman formula is based on Wagner approach and fits well in the case of concentrated filler loading:

$$\frac{\varepsilon_f - \varepsilon_r}{\varepsilon_r^{1/3}} = (1 - v_f) \frac{(\varepsilon_f - \varepsilon_m)}{\varepsilon_m^{1/3}} \quad (18)$$

Logarithmic formular is describing random mixing:

$$\ln\varepsilon_r = v_m \ln\varepsilon_m + v_f \ln\varepsilon_f \quad (19)$$

These models can provide an initial guide of material selection. In real cases, the mixing of two dielectrics may be even more complicated due to non-uniform filler sizes and shapes, different interfacial properties and interactions between fillers and polymer matrixes.

During composite synthesizing, the first problem is the non-compatibility of two materials. A surface treatment of the inorganic fillers is helpful. In the work of Stoyanov et al., TiO₂ nanoparticles with a dielectric constant of 128 were incorporated in an SEBS polymer. The surface

of these nanoparticles were coated with short PDMS oligomer chains with low polarity similar to the matrix SEBS polymer. (See **Figure 3-1**.) The resulted composite appeared uniform in micro scale. In comparison, composites with uncoated TiO₂ nanoparticles at same loading content showed large aggregates in 100- μ m scale.^[41]

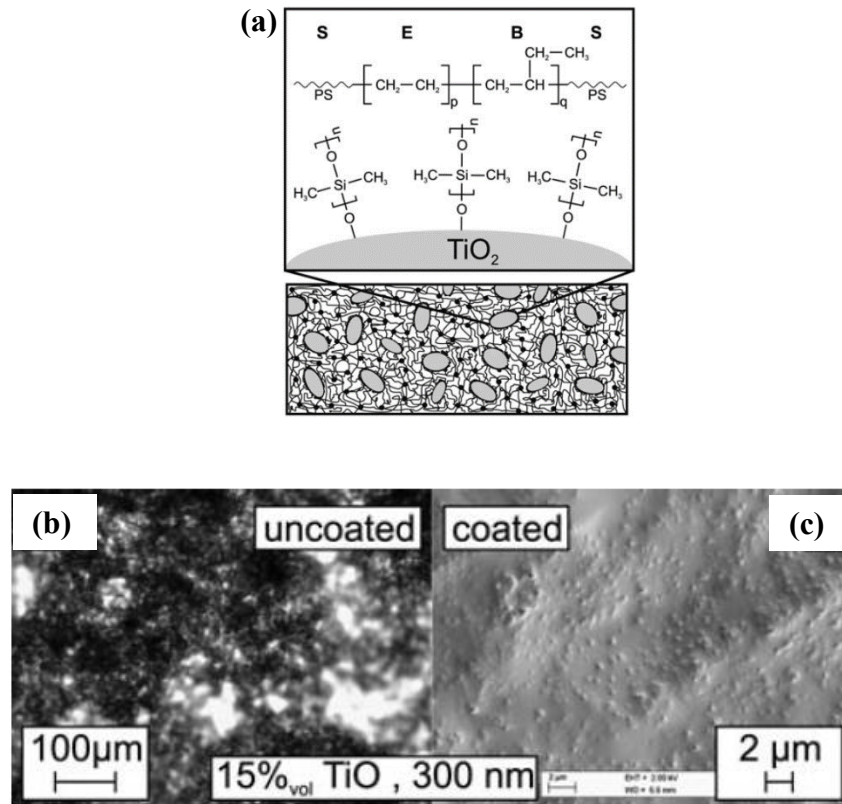


Figure 3-1. (a) Schematic representation of the composite structure and chemical properties of the particle surface. (b) Optical micrograph of composite with 15 vol% uncoated TiO₂; and (c) SEM of cryo-fracture surface of composite with silicone coated TiO₂. (adopted from [41])

In another work of Stoyanov and Brochu, the same silicone coated TiO₂ nanoparticles were dispersed in PDMS. With the loading amount of 30 wt%, there is a fairly small decrease in dielectric strength. Although information of morphology was not provided, the robust dielectric strength provides an indication of absence of large aggregates. Overall the dielectric constant has a 2.7 times increase.^[42]

While improvements have been achieved, a great amount of fillers is needed to get a high dielectric constant both in theory prediction and in experiment. The high amount of fillers tends to bring in aggregations. Even with surface modified nano sized fillers, aggregation is non-avoidable at a certain loading amount. These aggregates may result in (1) air traps, which create local low dielectric strength areas and facilitates discharging; (2) pathways from connected ceramic fillers showing low resistivity and (3) limit the fabrication of thin films. Except the aggregations, high filler loading is mechanically stiffening DEs, which limits the actuation strain.^[41,51]

3.1.1.2. Incorporation of metallic fillers

Compared with high permittivity ceramic fillers, metallic ones can be viewed to have infinite permittivities charges can move more freely inside conductors. Therefore they are more effective to increase the overall dielectric constant. Percolation theory is another method to explain these composite systems. At high filler loading, the metallic particles are approaching each other so the whole bulk material can be viewed as a super capacitor with very thin layer of dielectrics, so the whole material has a large high dielectric constant. According to percolation theory, the effective dielectric constant is determined by:

$$\epsilon_r = \epsilon_m / (f_c - f)^q \quad (20)$$

where ϵ_{mr} and ϵ_r are the dielectric constants of the matrix and the composites respectively; f is the fraction of filler loading; f_c is the critical loading fraction or percolation threshold fraction; and q is a scaling constant. An infinite high dielectric constant is expected when f is approaching f_c .^[52] Even before percolation threshold is reached, a descent dielectric constant can be achieved in some conductive filler/polymer composites.

3.1.1.3. Introduction of covalently bonded polarizable organic groups

To avoid the naturally poor compatibility of inorganic fillers and polymers, efforts have been made to modify pure polymers by grafting strong dipole moieties onto polymer chains. Kussmaul et al. synthesized a dipole molecule, N-allyl-N-methyl-p-nitroaniline (See **Figure 3-2.**), with a vinyl group which can be linked to un-cured silicone chain. With the addition of 13.4 wt% of dipole molecules, the dielectric constant increased from 3.00 to 5.98.^[46]

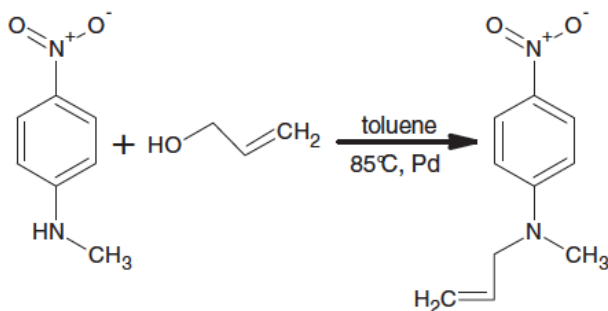


Figure 3-2. Synthesized dipole, enabling the subsequent grafting reaction to silicone. (adopted from [46])

Due to the noticeable polarities difference between typical dipole molecules and silicones, potentially there would be phase separation with increasing amount of dipoles. Madsen et al. synthesized and studies several dipole molecules with three vinyl groups so that these molecules can be silicones' crosslinkers. (See **Figure 3-3 (a).**) When contributing to dielectric polarization, these molecules also ensure a uniform crosslinking network. (See **Figure 3-3 (b).**) With one particular dipole crosslinker, 0.25 wt% loading amount raised the dielectric constant from 2.3 to 3.1.^[47]

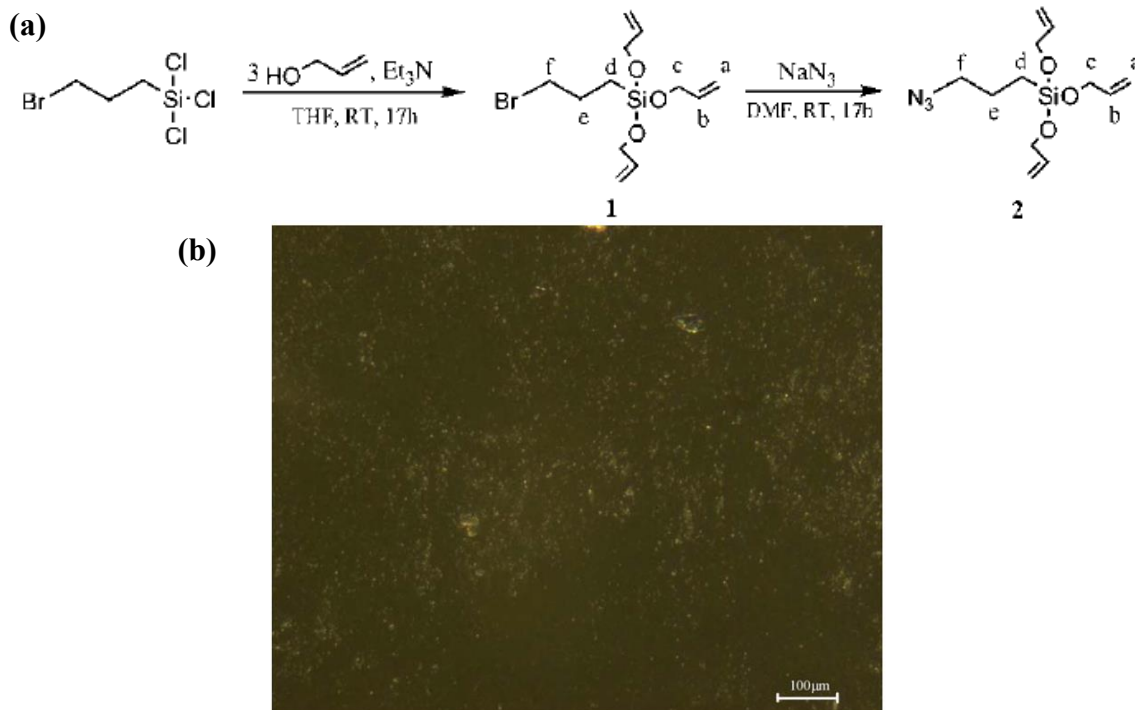


Figure 3-3. (a) An example of preparation of a dipole crosslinker; (b) a fluorescent microscopy image of a film with dipole crosslinker. (adopted from [47])

3.2. Experimental design

3.2.1. Materials

Phosphoric acid 2-hydroxyethylmethacrylate ester, hydroquinone, acetonitrile, n-butyl acrylate (nBA), and azobisisobutyronitrile (AIBN) were purchased from Sigma-Aldrich and used as received. CN 9021 was obtained from Sartomer Company and used as received. Spherical Al nanoparticles with an average diameter of 18 nm and an specific surface area $> 60 \text{ m}^2/\text{g}$ were purchased from US Reserch Nanomaterials, Inc. and stored in glove box filled with N_2 gas before use.

3.2.2. Surface modification of Al nanoparticles

The surface modification of aluminum nanoparticles follows a published work.^[53] In a typical procedure, 1 g Al nanoparticle was carefully transferred to a flask in a glove box filled with N_2 . 90

ml acetonitrile was flushed by Ar and transferred to the flask with Al nanoparticles through a cannula. The mixture was ultrasonicated for 10 min to achieve a black dispersion. To this dispersion, 2.5 g of phosphoric acid 2-hydroxyethylmethacrylate ester and 0.05 g of hydroquinone co-dissolved in 10 ml acetonitrile were flushed with Ar and cannula transferred to the reaction vessel at once. The resulting dispersion was stirred for 16 hrs while being heated in an oil bath at 60 °C and protected with Ar gas. Then the nanoparticles were washed with acetone and collected by centrifugation for 3 cycles, and then dried in vacuum.

The as-modified Al nanoparticles were characterized using a Perkin Elmer Pyris Diamond Thermogravimetric Analysis (TGA). In one test, the particles were heated to 500 °C in N₂ atmosphere. In the other test, both as-received and as-modified Al nanoparticles were heated at 80 °C in air atmosphere for one hour. The FT-IR spectrum of the as-modified Al nanoparticles was obtained with a Jasco FT-IR 420. Solubility tests were carried out using n-butyl acrylate and DI-water.

3.2.3. Nanocomposite film preparation

A typical procedure to prepare a nanocomposite DE film was as follows: a pre-polymer solution was prepared by mixing 45 weight parts of nBA and 55 parts of CN 9021. Different weight parts of as-modified Al nanoparticles, 0, 5, 10 and 15 parts, were added into the pre-polymer solution. The resulting dispersion was ultrasonicated until it reached homogeneity. 1 weight part of AIBN was then added, and the mixture was shaken for dissolution. The dispersion was injected into a mold made of two pieces of glass in parallel separated by 200 μm with a spacer. The liquid dispersion was cured at 80 °C on a hot plate for 1 hour. The cured film was peeled off and annealed at 80 °C for another hour. The as-prepared nanocomposite films were labeled as A-00, A-05, A-10 and A-15 and the numbers represented the weight parts of the surface-modified Al nanoparticles.

The cross-sections of these nanocomposite films were observed using a Nova Nano 230 SEM. The surface was pre-coated with sputtered gold before imaging.

3.2.4. Tensile test

Type IV dumbbell-shaped samples for tensile tests were made with a cutting die, defined in ISO 37. Stress-strain tests at a tensile rate of 3.33 mm/s were carried out on an RSAIII Dynamic Mechanical Analyzer of TA Instruments.

3.2.5. Dielectric constant measurement

The dielectric properties were characterized at both low voltage (1 V) using a GwInstek LCR-819 LCR meter and high voltage (200 V) using a Self Sensing Unit (SSU) developed in the Biomimetic Laboratory in the University of Auckland, New Zealand.

The nanocomposite samples for the low voltage dielectric measurement were prepared by the same method described above except that the glass pieces were pre-coated with a 200 nm thick Al coating deposited by physical vapor deposition in vacuum. The nanocomposite films were kept between the glass pieces during the dielectric measurement. The capacitances defined by the overlapping area of the Al electrodes were measured with 1 V excitation in the frequency range of 100 Hz to 100 kHz and the dielectric constant was calculated accordingly.

Nanocomposite samples for high voltage capacitance measurement were made by biaxially stretching the films by 100 % by 100 % and spray-coating carbon nanotubes onto both surfaces as contact electrodes. An electric field around 4 MV/m is applied for the dielectric constant measurements. Commercial 3M™ VHB™ adhesive 4905 film and cured Nusil CF-19-2186 silicone films were tested by the same methods for reference.

3.2.6. Resistivity measurement

Resistances of the nanocomposite films were determined by measuring the leakage currents under applied voltages. The sample films were pre-stretched by 100 % biaxially, and mounted onto a plastic frame to maintain the prestrain. Carbon nanotubes were sprayed as the contact electrodes. High voltages were supplied from an HV box fabricated in-house, and the leakage current were measured using a Keithley 200 multimeter.

3.2.7. Actuation performance characterization

DE elastomer films were pre-stretched 100 % biaxially and coated with carbon grease electrodes. High voltages were supplied from the HV box fabricated in house. The area changes of the actuator, defined as the overlapping area of the tow opposite electrodes, were recorded by a web camera controlled by a LabView program. Voltages were applied with 200 V increments until the breakdown of a specific actuator. At each voltage, the voltage was held for 10 seconds to obtain a stable actuation strain. For each DA formulation, 5 samples were tested and a characteristic set of data are presented.

3.3. Results and discussion

3.3.1. Bonding nanoparticle to polymer matrix

The as-received Al nanoparticles had a self-passivated oxide shell as shown in **Figure 3-4**.

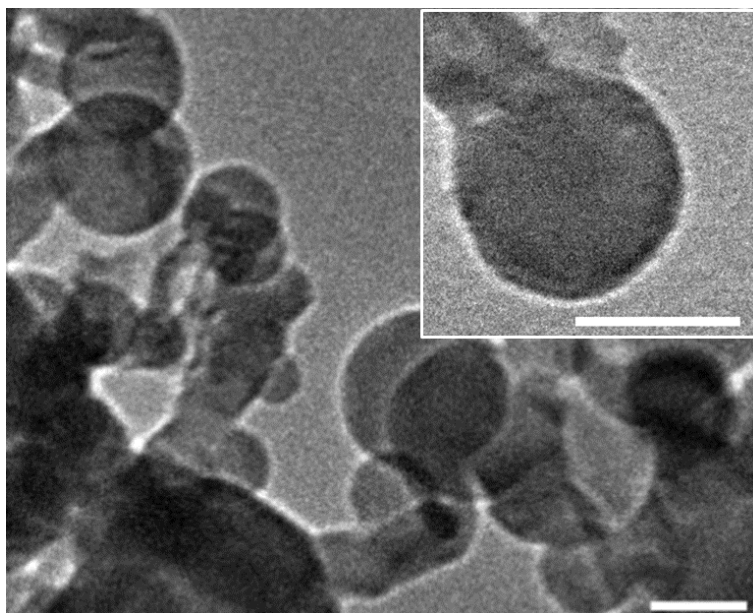


Figure 3-4. TEM images of as-received nanoparticles. (Scale bar: 40 nm)

These nanoparticles were modified with phosphoric acid 2-hydroxyethylmethacrylate ester following a reported procedure as illustrated in **Figure 3-5**.^[53] The phosphoric acid forms strong bonding onto the oxide shell. The methacrylate was thus tethered to the particle surface.

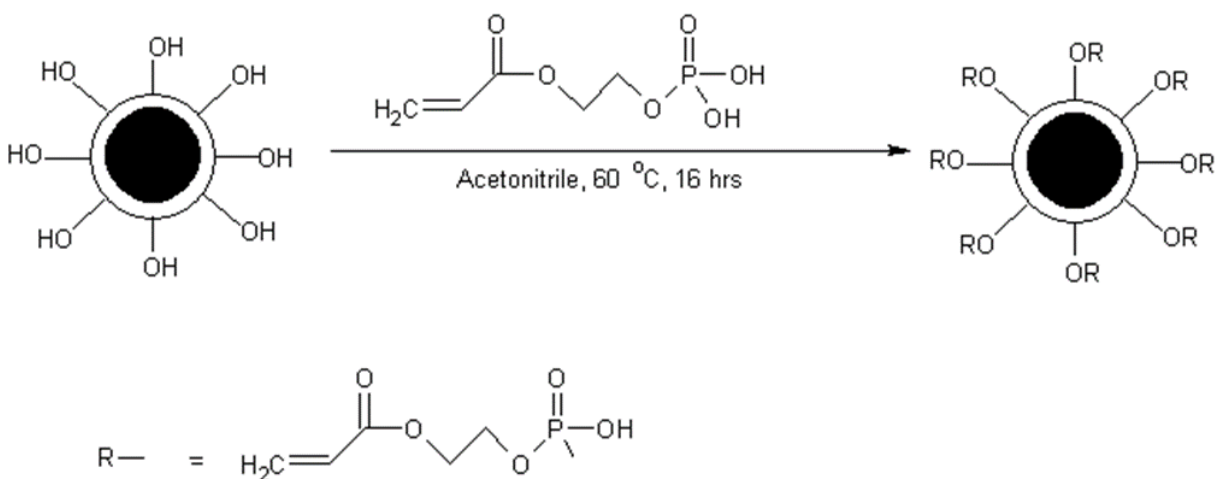


Figure 3-5. Surface modification of Aluminum nanoparticles.

The surface modification was confirmed by Fourier transform infrared (FT-IR) (**Figure 3-6**): vibrational peaks at 1720 cm^{-1} attributed to C=O stretching, 1635 cm^{-1} to C=C stretching, and 1457

cm^{-1} to H-C-H scissor bending from the ligand were observed for the functionalized nanoparticles. These peaks are not present in the FT-IR of the Al nanoparticles before functionalization.

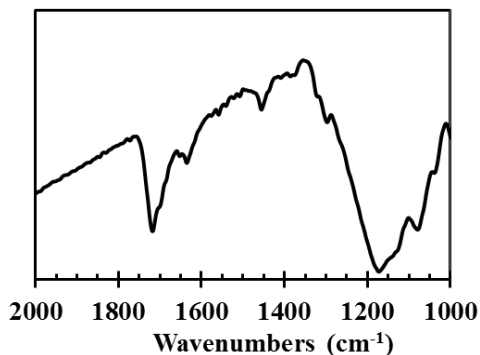


Figure 3-6. FT-IR spectrum of surface-modified Al nanoparticles.

Thermogravimetric analysis (TGA) of the functionalized nanoparticles in N_2 showed a gradual weight loss in the temperature range of 150-280 °C and a rapid loss between 280-330 °C (**Figure 3-7**), which is consistent with the work of Al nanoparticle surface modification in [Ref \[58\]](#).

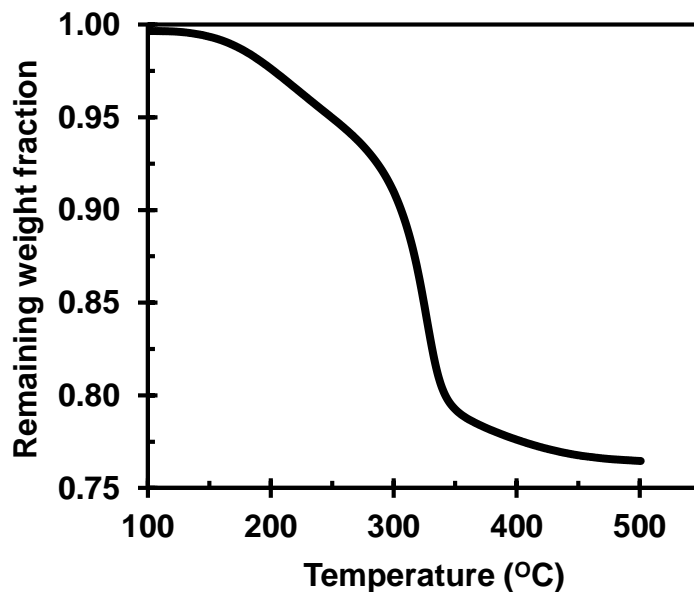


Figure 3-7. The TGA curve of surface-modified Al nanoparticles.

The total weight loss up to 500 °C is 24 wt%. The grafting density of the organics introduced during the functionalization reaction can be estimated by Equation (21):

$$\text{Grafting Density} = \frac{\text{weight loss fraction}}{1 - \text{weight loss fraction}} \times \frac{N_A}{MW \times SSA} \quad (21)$$

where N_A and MW are Avogadro's constant and molecular weight of the ligand, respectively. The grafting density is calculated to be 16 molecules/nm². The density of hydroxylated groups on Al oxide surface was reported to be in the range from 3 to 15 groups/nm².^[54] Therefore, we expected the chemical bonding of ligand and nanoparticle surface was saturated and some ligands may be physically bonded.

The stability of as-received and as-modified Al nanoparticles was studied using TGA as well. These particles were heated in air at 80 °C for one hour, which is the match the curing condition of the nanocomposite films. As shown in **Figure 3-8**, no mass increase was observed during heating, indicating oxidation hardly happened.

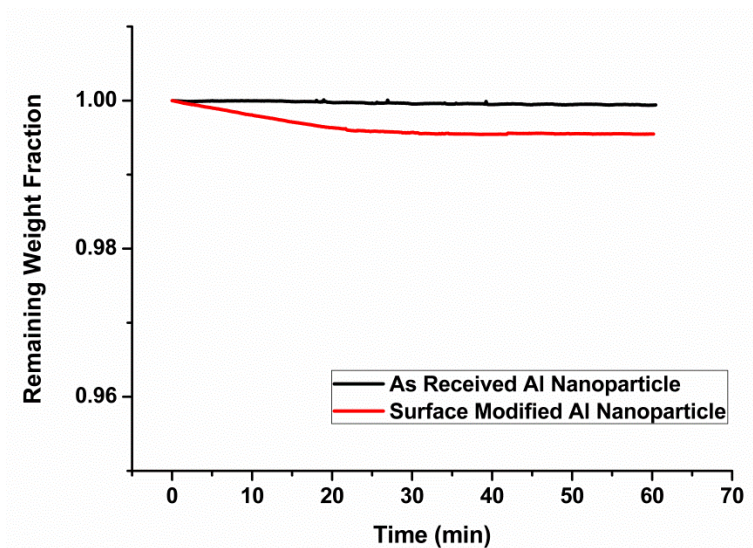


Figure 3-8. TGA curves of as-received and as-modified Al nanoparticles at 80 °C in air atmosphere for one hour.

Both the as-received Al and as-modified Al nanoparticles were dispersed in n-butyl acrylate to test the dispersibility. The dispersions of as-received Al and as-modified Al were dropped on the top of DI-water (**Figures 3-9 (a) (c)**). The as-modified Al nanoparticles did not settle down over half

an hour (**Figures 3-9 (d)**), but the as-receive Al nanoparticles settled down fairly fast (**Figure 3-9 (b)**). The surface modification has greatly improved the dispersibility of the nanoparticles in the low-polarity acrylate monomer.

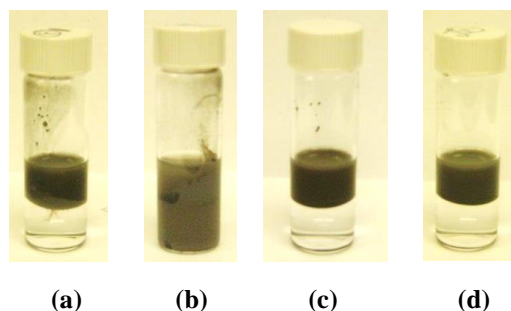


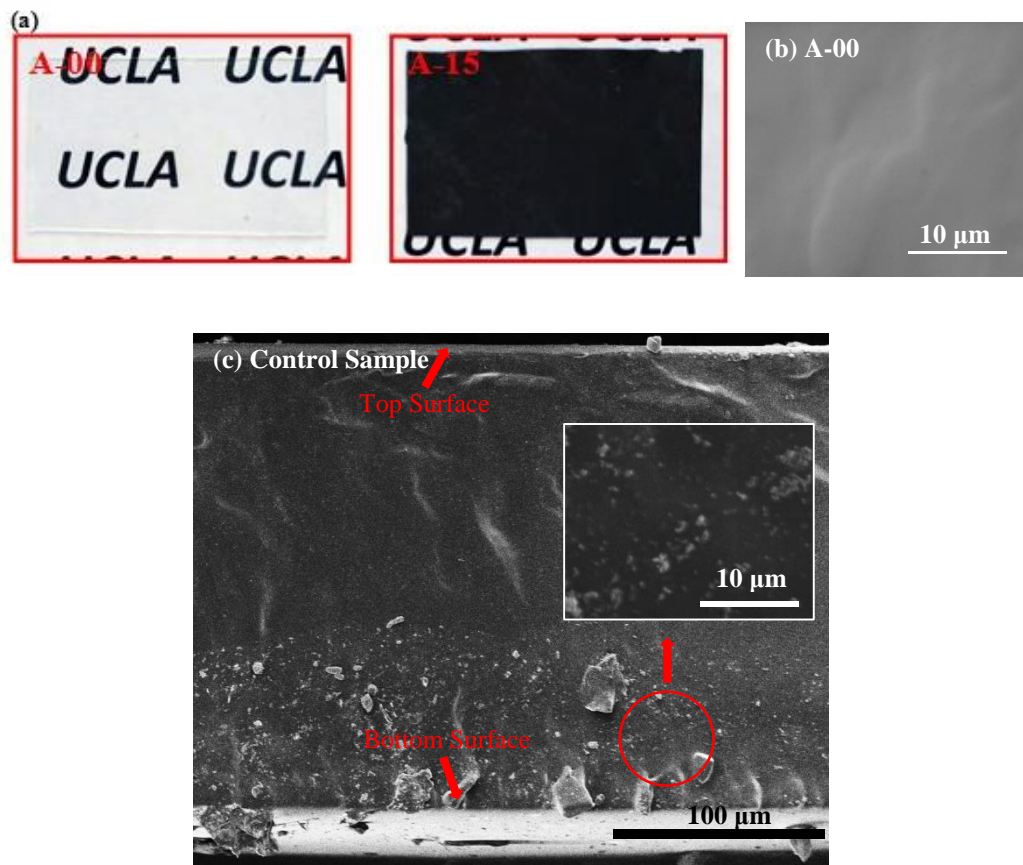
Figure 3-9. Solubility of surface-modified Al nanoparticles. The dispersions of as-received Al (**a**) and as-modified Al nanoparticles (**c**) were dropped on the top of DI-water. The dispersions of (**b**) as-received Al and (**d**) as-modified Al nanoparticles on water after 30 mins.

3.3.2. Film preparation

For the nanocomposite synthesis, an acrylate co-monomer solution consisting of n-butyl acrylate and CN 9021 was employed. In our previous study of DE materials, such a copolymer would produce fairly high actuation performance. CN 9021 is a urethane diacrylate; its homopolymer has an elongation at break being 1100%, which is a good attribute to obtaining large actuation strain from the corresponding nanocomposites. The functionalized nanoparticles were dispersed into the acrylate co-monomer solution (100 weight parts) at weight parts of 5, 10, and 15 to prepare the nanocomposites, referred to as A-05, A-10, A-15, respectively. The neat copolymer without nanoparticles is named A-00. The dispersions were injected into glass molds and thermally cured to form solid films. Particle loading higher than 15 weight parts resulted in very viscous dispersions which could not be injected into the glass mold. Based on the densities of poly(n-butyl acrylate), CN 9021 resin, phosphoric acid 2-hydroxyethylmethacrylate ester and Al, the volume concentration of the Al nanoparticles in the nanocomposites were calculated to be 0%, 1.4%, 2.7%,

and 4.0% for A-00, A-05, A-10, and A-15, respectively (**Table 3-2**). The nanocomposite containing 1.4 vol% of as-received Al nanoparticles, the same Al volume concentration as A-05, was also prepared as a control sample. A-00 films are transparent and all the nanocomposite films show a dark color (See **Figure 3-10 (a)**).

Scanning electron microscopic (SEM) images of the samples' cross sections confirm a uniform dispersion of nanoparticles in the acrylate copolymer. As expected, A-00 is fairly homogenous except for the surface roughness formed when the sample was freeze-broken to create the cross section (**Figure 3-10 (b)**). The control sample shows large agglomerates of nanoparticle clusters settled on the bottom of the film (**Figure 3-10 (c)**), while sample A-05 with the same volume concentration results in a uniform film (**Figure 3-10 (d)**). A-10 (**Figure 3-10 (e)**) and A-15 (**Figure 3-10 (f)**) films show a uniform dispersion as well.



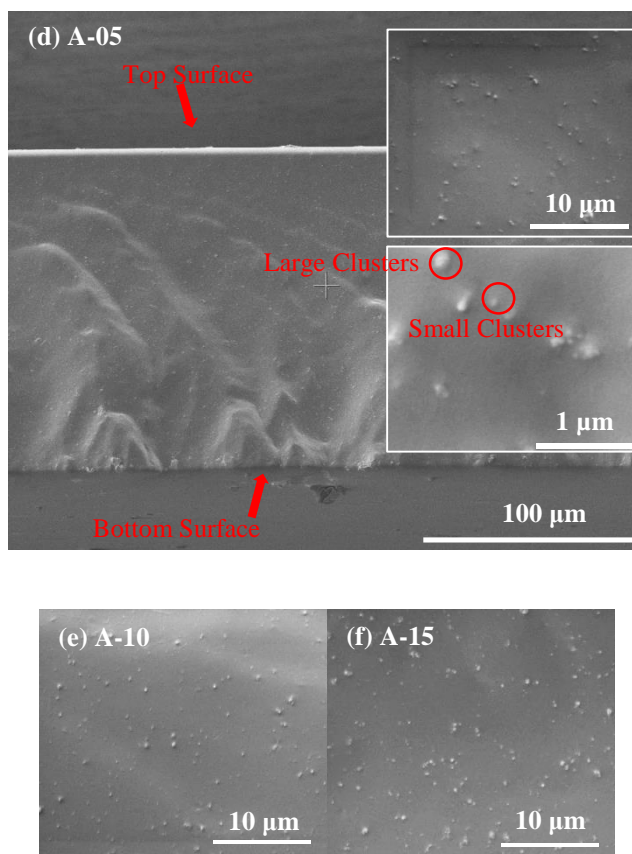


Figure 3-10. (a) Optical photographs of samples A-00 and A-15; SEM images of cross sections of (b) A-00, (c) control sample using unmodified nanoparticles, (d) A-05, (e) A-10 and (f) A-15.

Sizes of the nanoparticle clusters are as large as several micrometers in control samples but range from 80 nm to 200 nm in films with the surface-modified nanoparticles (**Figure 3-10 (c) (d)**). The cluster sizes are larger than the diameters of as-received nanoparticles. The slight agglomeration was generated during the surface modification when several particles could be wrapped together by the organic compound due to the high SSA of the nanoparticles. This has been observed in other Al nanocomposite systems as well.^[53] One drawback of commercial dry nanopowders is the difficulty to obtain individually dispersed nanoparticles in solution. However, the surface modification still contributes to a good uniformity due to the Van der Waal interaction between organic shell and monomer solution, and the copolymerization between methacrylate on nanoparticle surface and acrylate matrix.^[55,56]

3.3.1. Mechanical properties

The tensile stress-strain response of the nanocomposites was tested. Young's moduli and apparent moduli at 300% and 500% strains were determined from the curves and listed in **Table 3-2**. Note that the area change of cross sections was considered when moduli were calculated. The results show that while the nanocomposite stiffness increases with increasing loading of nanoparticles, the elongation of rupture does not change much, which could indicate that the nanoparticles were uniformly dispersed in the polymer matrix, and there were few micro-scale cracks which would significantly reduce the elongation of rupture.

Table 3-2. Properties of the synthesized nanocomposite DEs.

Sample	Al Vol [%]	Dielectric Properties		Mechanical Properties ^c			Electromechanical Properties				
		ϵ_r ^a	Conductivity [10 ⁻¹⁰ S/m] ^b	Y ^d	M_{300} ^e	M_{500} ^f	Elongation [%]	$E_{b,max}$ [MV/m]	$s_{a,max}$ [%]	s_a @ 140 MV/m [%]	p @ 140 MV/m [MPa] ^g
				[MPa]							
A-00	0	5.0±0.1	0.91	0.16	0.72	0.72	671	179	134	101	0.87
A-05	1.4	6.1±0.1	2.5	0.28	0.76	2.46	666	220	172	101	1.1
A-10	2.7	7.2±0.1	3.0	0.38	1.20	3.12	612	157	90	73	1.2
A-15	4.0	8.4±0.2	6.9	0.53	1.40	3.88	691	140	56	56	1.5
Control Sample	1.4	-	7.5	-	-	-	-	12	0	-	-

^a Measured at 200 V, 400 Hz; ^b Estimated from the linear fit of leakage current density – electric field curve; ^c The change of cross section areas of samples were considered when moduli were calculated; ^d Modulus at 0% strain calculated from stress-strain response; ^e Apparent modulus at 300% linear strain calculated from stress-strain response; ^f Apparent modulus at 500% linear strain calculated from stress-strain response; ^g Calculated.

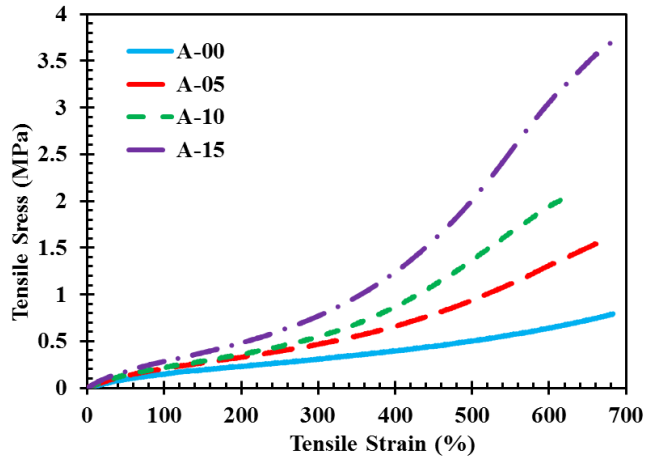


Figure 3-11. Tensile test of aluminum nanocomposites.

3.3.2. Measurement of dielectric constant

The dielectric permittivity, measured using a GwInstek LCR-819 LCR meter in the frequency range from 100 Hz to 100 kHz with 1 V amplitude and an average of 0 V, showed a considerable increase with the addition of Al nanoparticles (**Figure 3-12**). The permittivity at 100 Hz increases from 5.3 in the neat acrylate copolymer films to 8.5 for A-15, while the dielectric loss remains low. There is a minimum in the dielectric loss spectrum at around 2 kHz, which was observed in the TiO₂/ SEBS nanocomposite system as well^[41]. The minimum point is a combination of two types of “universal” dielectric responses.^[57] At low frequency, the dielectric loss decreases with the increase of frequency giving a carrier-dominated response. With the increase of frequency, peaks will appear in a dipole-dominated response. A minimum would appear between the two responses.

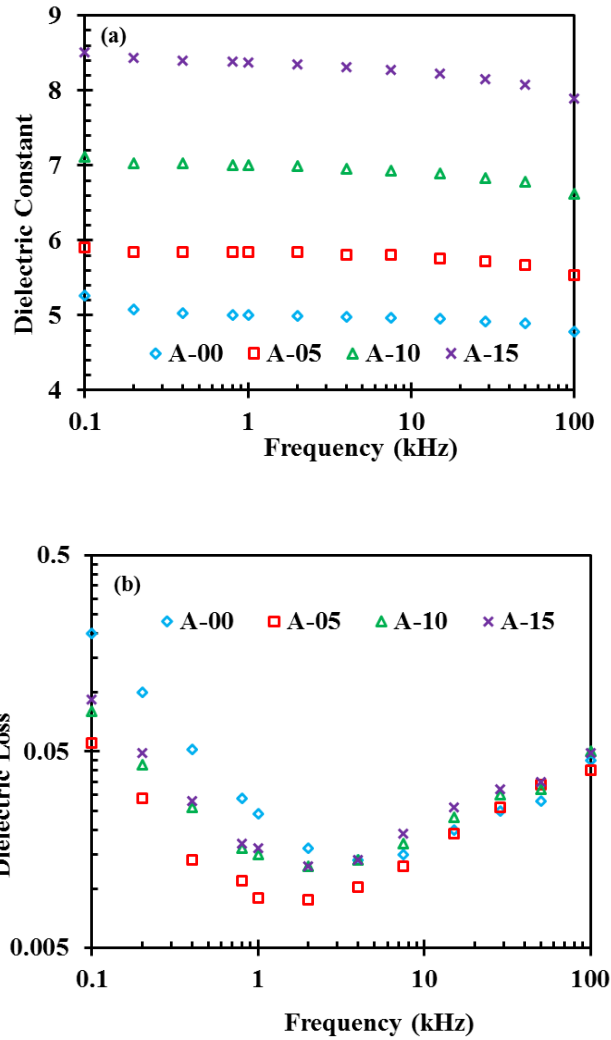


Figure 3-12. (a) Dielectric constants and (b) dielectric losses of A-00, A-05, A-10 and A-15 from 100 Hz to 100 kHz.

Capacitances were also measured at high voltages that are closer to the operating voltages of the actuators. A sinusoidal AC signal with an amplitude of 50 V and an average of 200 V at 400 Hz was applied. The measured capacitances were consistent with the results obtained under low voltage. As references, the dielectric constants of 3M VHB 4905 adhesive and CF-19-2186 silicone films were measured to be 4.4 ± 0.2 and 2.3 ± 0.1 , respectively by the same method.

Figure 3-13 shows the dielectric constants of the nanocomposites.

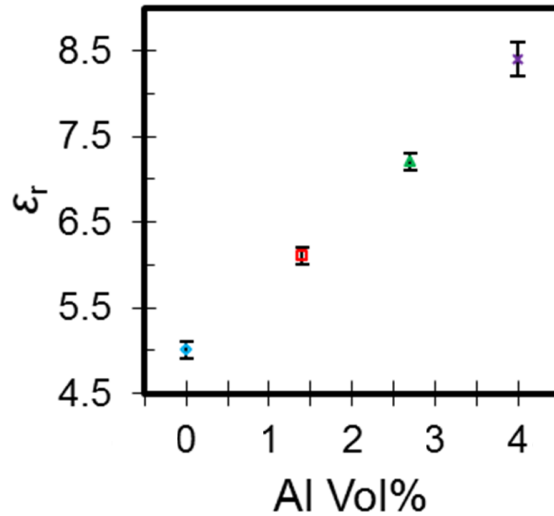


Figure 3-13. Dielectric constants at various loadings measured at 200 V AC and 400 Hz.

Compared with a typical percolation behavior which shows a sharp increase approaching the critical filler fraction, these nanocomposites show a linear increase at relatively low volume fraction. Except for the scenario in which percolative network forms a super capacitor, the conductor-insulator composite can be explained by the polarization of each dispersed metal nanoparticles. In the presence of an applied electrical field, electrons in a metal nanoparticle will move such that each nanoparticle forms a dipole, which cumulatively results in a polarization that is similar to a dielectric compound. Therefore, the addition of Al nanoparticles is equivalent to the addition of strong dipoles which contributes to the increase of dielectric constant.^[58,59]

3.3.3. Measurement of leakage current

The leakage currents from 0 MV/m to 60 MV/m electric fields were measured on pre-stretched samples. The active area was mounted on a plastic frame. In this field range, there was no observable actuation or wrinkling of the nanocomposite films; the Maxwell stress is smaller than the tension caused by the pre-stretching. Therefore, the changes in electrode conductance and sample shape should be negligible, and the measured leakage current reflects the intrinsic property

of the nanocomposites. These leakage current vs. field curves could be fit linearly to estimate the conductivities of the nanocomposites (**Figure 3-14** and **Table 3-2**). Note that only the neat polymer matrix shows an Ohmic behavior, indicative of no obvious change in film conductivity with electric field. With increased amount of Al nanoparticles, the leakage current increases superlinearly with the electric field, which indicates that the conductivity increases with the increase of the electric field. Similar observation was made in polyacrylate and titanate/SEBS nanocomposite systems, where the conductivity increase has been considered to result from the voids or impurities.^[28,41] The loading of Al nanoparticles can be considered as impurities which create localized states for the electrons in the electronic band structures of the DEs. With the electric field increasing, more electrons would be able to jump to the conduction band, contributing to an increased conductivity. The transition from Ohmic to non-Ohmic behavior as the loading of Al nanoparticles is increased does not induce a dramatic increase of the leakage current, which bodes well for dielectric actuation. The control sample was tested at the same condition. Its leakage current was higher than A-15 at the same low electric field up to 15 MV/m. The dielectric breakdown occurs at higher field, so the leakage current at high field could not be determined for the control samples.

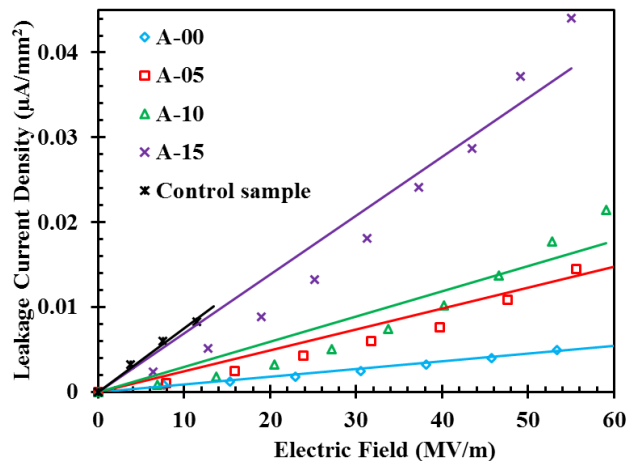


Figure 3-14. Measured leakage current density of nanocomposite samples with electric field. The electrode area and thickness of the samples were 11.4 cm² and ~50 μm (after pre-stretching), respectively.

3.3.4. Actuation performance

Circular actuators were made by pre-stretching nanocomposite elastomer films by a 100% × 100% ratio and coating a thin layer of carbon grease on both surfaces. The circular overlapping area of the compliant electrodes defines the active area of the actuators. The actuation area strains were determined from the area change of the active area imaged with a web camera. The driving voltage was increased at small increment until dielectric breakdown occurred. **Figure 3-15** shows the measured strains at each 20 MV/m increment from 0 to 140 MV/m. The control sample dielectrically broke down at below 20 MV/m and no observable actuation was obtained before breakdown. All nanocomposite films using surface-modified Al nanoparticles show high field strength and large actuation strain. From A-00 to A-05, the field strength is significantly improved. (See **Table 3-2.**) One plausible explanation is that A-05 is stiffer than A-00, and the probability of undergoing electromechanical instability is lowered.^[14,40]

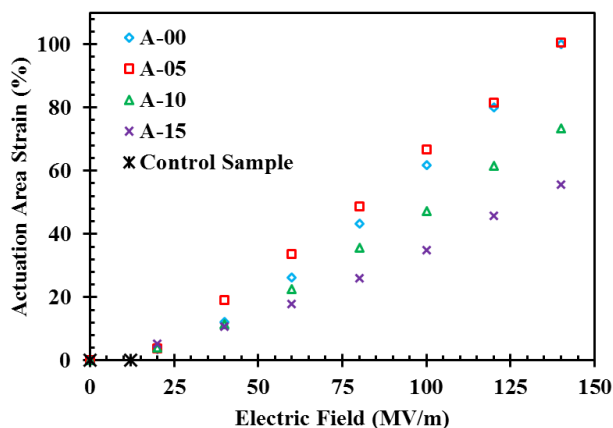


Figure 3-15. Actuation strain of nanocomposites as a function of applied electric field.

With higher nanoparticle loading, the field strength is diminished, but remains fairly high in A-15. Thanks to the increasing permittivity with nanoparticle loading, the actuation pressure at a given

field increases with nanoparticle loading. For A-15, the calculated actuation pressure at 140 MV/m is 1.5 MPa, which is comparable to the maximum actuation pressure of high performance DE materials at much higher electric field. The strains at 140 MV/m show a generally declining trend with nanoparticle loading. Apparently, the stiffness increases with nanoparticle loading faster than the dielectric permittivity does. The actuation performances of the nanocomposites are summarized in **Table 3-2**. Work density w , which is the specific mechanical energy density of an actuator at a driving voltage, can be estimated as:

$$w = -p \frac{2s_a + s_a^2}{2(1+s_a)^2} \quad (22).^{[42]}$$

Figure 3-16 plots the calculated work density based on the measured strain and stress. The work density increased with the nanoparticle loadings, albeit at a rather small pace due to increasing stiffness of the nanocomposites.

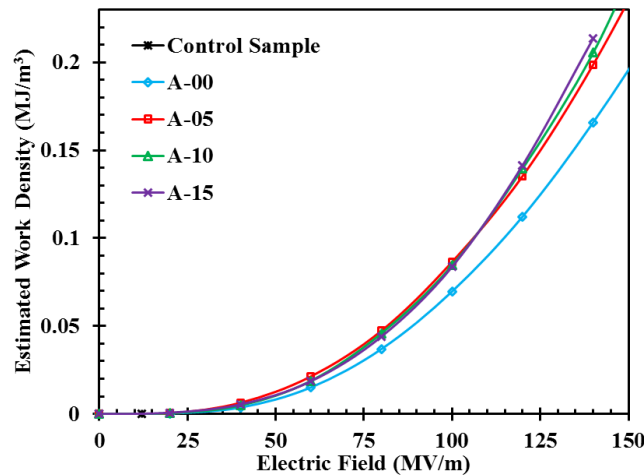


Figure 3-16. Estimated work densities of Al/acrylate nanocomposites.

As listed in **Table 3-1**, high dielectric constants have been achieved in these nanocomposites, however, the reported field strength and actuation strain are substantially lower than the A-15 in this work. A major advantage we are taking here is the use of an acrylate copolymer as the matrix

for the nanocomposite. Acrylate copolymers, as shown in the 3M™ VHB™ 4910 and 4905 adhesives, have a relative high dielectric constant for neat polymers, high elongation at rupture, and high field strength. Its overall actuation performance is much higher than silicone and polyurethane elastomers that the other reported nanocomposites are based upon. The ability to synthesize acrylate copolymers from readily available monomers allows us to develop nanocomposites with further enhanced actuation properties.

Metallic nanoparticles show a great advantage over high dielectric constant ceramic nanofillers. Metals can be considered to have an infinitely high dielectric constant since electrons are free to move within it, although dielectric constant is usually referred to an insulating material. To obtain a dielectric constant greater than 8, only 4 vol% Al nanoparticles were incorporated into acrylate copolymer matrix in this work. In comparison, in the reported lead magnesium niobate-lead titanate/silicone nanocomposites, 10 vol% of nanoparticles were introduced^[60] and in titanate/SEBS nanocomposites, 30 vol% of nanoparticles were added^[41]; these two nanocomposites were too stiff to be actuated to large strains.

The formation of conductive paths in conductor/insulator nanocomposites is a major hurdle to clear before a high field strength can be obtained. Surface modification of conductive nanofillers with an insulating material has been shown to be effective to suppress inter-nanofiller aggregation. In the nanocomposites of CNT/polyurethane (CNT-PU)^[44] and poly(hexylthiophene)/silicone (PHT-PDMS)^[45] where the conductive fillers were not covered or wrapped by an insulating layer, the dielectric strength is rather low. On the other hand, polyaniline/silicone nanocomposites^[43] where polyaniline particles have an insulating shell, maintain a high dielectric strength comparable with the matrix polymer. In our approach, the Al nanoparticles are wrapped with methacrylate

functional groups that not only help shield the conductive core, but also form covalent bonds to the matrix polymer chains.

3.4. Conclusions

Al/acrylate copolymer nanocomposites have been synthesized comprising uniformly dispersed nanoparticles that are covalently bonded in the polymer matrix. The addition of nanoparticles increases the stiffness of the matrix and its dielectric constant. The nanocomposite containing 4 vol% Al nanoparticles has a high dielectric constant at 8.4, with large elongation at rupture, high field strength, and low leakage current at high field, all being essential to make for a high performance DE material. The maximum actuation strain of 56 % is dramatically higher than reported values for DE polymers and nanocomposites with comparable dielectric constants.

4. Dielectric Elastomers with Tunable Moduli

4.1. Background of this study

The electro-mechanical responses of dielectric elastomers are greatly influenced by the materials' mechanical properties such as modulus, elongation of rupture and viscoelasticity. Although the actuation strain could be tuned through changing the applied electric field according to Equation (1), in some electroactive systems, variable strain is needed while constant actuation pressure is maintained. Therefore, elastomers with tunable moduli would be desirable in these cases such as adaptive grippers^[61,62] and micro-fluid channels^[63]. These elastomers can further mimic natural muscles which are able to adapt to changing work requirements.

Previous strategies tuning the stiffness of polymers fall in two categories: (1) phase transition or microstructure change through external stimuli and (2) addition/reduction of external soft media such as gas and solvent. Examples for Category (1) include photoresponsive liquid crystal polymer controlled through ultraviolet light^[64], shape memory polymer controlled by temperature^[65] and magneto-rheological elastomers controlled by magnetic field^[66]. All of these material systems require maintaining the external sources during operation which brings in extra cost, device complexity, and energy consumption. A good example for Category (2) systems is a structure built from cellulose nanofibers and a rubber matrix modulated by water and IPA solvents.^[67,68] The common drawback of Category (2) is that the use of non-solid material would limit their application due to package and reliability issue.

In this chapter, a new elastomeric material whose stiffness can be altered via simple thermal treatment is demonstrated.

A synthetic elastomer generally has a specific modulus pre-determined by the polymer's molecular structure. In theory of rubber elasticity, the tensile modulus (Y) of an ideal elastomer at small strain is determined by:

$$Y = \frac{3\rho RT}{\overline{M}_c} \quad (23)$$

where ρ , R , T and \overline{M}_c are the density of the elastomer, the gas constant (8.31 J/K-mol), the absolute temperature, and the average molecular weight of chain segments between crosslinking sites, respectively.^[69] \overline{M}_c is a term to describe the crosslinking density of an elastomer network, where a larger \overline{M}_c means a lower crosslinking density. As indicated in Equation (23), polymer chain segment length is a key factor of an elastomer's stiffness. Therefore, our strategy tuning the stiffness is to change the chain segment length using dynamic covalent bonding, which could reversibly form and break the crosslinking sites as illustrated in **Figure 4-1**.

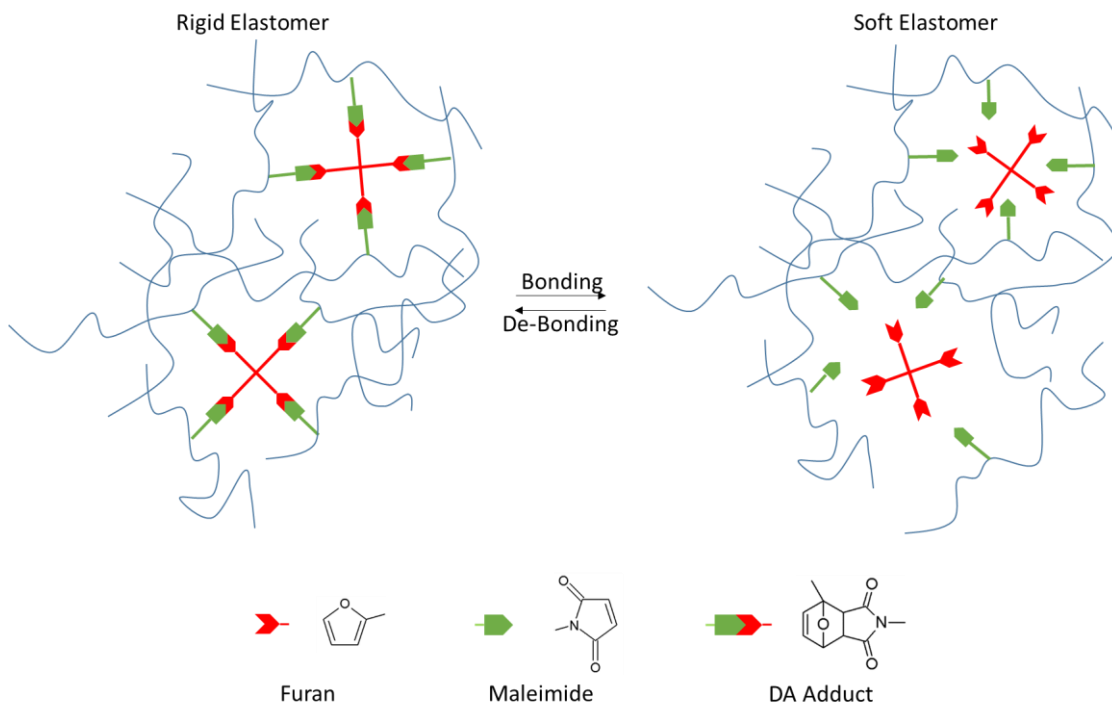


Figure 4-1. A schematic illustration of how the crosslinking sites are formed and broken. Furan-maleimide adducts, one of the Diels-Alder pairs, were selected as the dynamic bonds forming the crosslinking sites.

Diels-Alder (DA) reaction offers an effective method to form dynamic covalent bonds, and has been widely utilized in self-healing materials thanks to the good reversibility of the DA reaction.^[70]

Among DA pairs, furan derivatives as the diene and maleimide derivatives as the dienophile have drawn great attention since they usually have moderate reaction (forming DA bonds) and retro-reaction (breaking DA bonds) temperatures.^[71–73] In this chapter, a series of polyacrylate dielectric elastomers containing furan-maleimide adduct moieties were synthesized to exploit this reversible reaction. The resulting copolymers are elastomers exhibiting multiple states of moduli inter-switchable via thermal treatments. The rigid states have a modulus three times as high as that of the soft states. The elastomers were employed to fabricate capacitive sensors and actuators that could be operated in different modes.

4.2. Experimental design

4.2.1. Synthesis of FM-A

4.2.1.1. *Materials*

Maleic anhydride, ethanolamine, acryloyl chloride, triethyl amine (TEA), ethyl acetate, ethanol and anhydrous dichloromethane (DCM), N-butyl acrylate and 2,2-dimethoxy-2-phenylacetophenone were purchased from Sigma-Aldrich and used as received. 2-(2-ethoxyethoxy) ethyl acrylate was obtained from Sartomer Company and used as received. Furan was purchased from Alfa-Aesar. All chemicals were used as received without further purification.

4.2.1.2. *Synthesis of FM-A*

FM-A was synthesized following the procedure in [Ref \[74\]](#)^[74] with modifications. The route contained three steps, as illustrated in **Figure 4-2**.

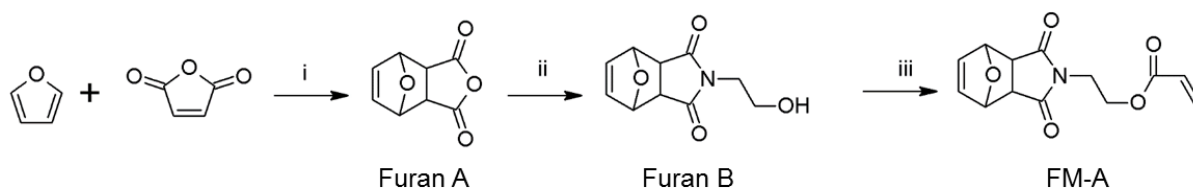


Figure 4-2. The synthesis route of FM-A: (i) ethyl acetate, room temperature, 24 hrs; (ii) ethanolamine, ethanol, reflux, 4 hrs; (iii) acryloyl chloride, triethyl amine, DCM, 0 °C to room temperature, 24 hrs.

The synthesis procedure is described as below:

(i) 20 g (0.204 mol) maleic anhydride was dispersed in 25 ml ethyl acetate and then 19.8 ml (18.5 g, 0.272 mol) furan were added into a round bottom flask. Maleic anhydride was not fully dissolved at first but the solution gradually turned into transparent followed by precipitation of white solid. After 24 hrs' stirring at room temperature, the white solid (Furan A) was collected via vacuum filtration and dried in a vacuum line.

(ii) 10 g (60.2 mmol) Furan A and 20 ml ethanol were added into a round bottom flask. A solution of 3.74 ml (3.78g, 61.8mmol) ethanolamine in 3 ml ethanol was added into the flask drop wisely. After refluxing for 4 hrs in Ar atmosphere, the solution was cooled down and transferred into a fridge. One hour later, a white solid, Furan B, was collected via vacuum filtration and dried in a vacuum line.

(iii) 3 g (14.4 mmol) Furan B and 2.6 ml (1.89g, 18.6 mmol) TEA were dissolved in 60 ml anhydrous DCM and the reaction was protected with Ar gas and kept in ice bath. 1.37 ml (1.53 g, 17.0 mmol) acryloyl chloride was drop wisely added into the solution. Then the reaction was kept from 0 °C to room temperature for 22 hrs. The resulted solution was washed with NH₄Cl aqueous solution and water followed by chromatography column purification.

4.2.2. Preparation of PADA elastomer films

A typical procedure for the preparation of a DA elastomer film is as follows: A pre-polymer solution was prepared by co-dissolving all the components as listed in **Table 4-1**.

Table 4-1. Formulations (parts of weight) of synthesized elastomers.

Formulation	nBA	EOEA	FM-A	Xlinker	DMPA
PADA-2.5	87	11	2.5	1.9	1
PADA-3	86	11	3	2.3	1
PADA-4	85	11	4	3	1
PADA-5	84	11	5	3.8	1
PADA-10	80	10	10	7.5	1
PADA-10'	80	10	10	0	1

Xlinker was synthesized following the method in [Ref \[71\]](#) published by the same group.^[71] This compound was used in the formulation of a thermally healable polymer/Ag nanowire composite. The solution was injected into two glass slides with a spacer to define the thickness of the liquid layer. The pre-polymer solution was first cured through a conveyor equipped with a 2.5 W/cm² Fusion 300S type “H” UV curing bulb, at a speed of 4.0 feet/min for two passes. Then the resulted film was gently removed off the glass slides and then heated at 130 °C for 2 hrs on a hot plate followed by another 24-hour heating at 70 °C. The as synthesized films were named as PADA-X-r.

4.2.3. TGA of PADA elastomers

A PADA-10-r film was characterized using a Perkin Elmer Pyris Diamond TGA with a heating rate of 5 °C/min in air atmosphere from 50 °C to 180 °C. In comparison, a PADA-10_70 film was

synthesized through the same method except the heating step at 130 °C was skipped. PADA-10_70 was characterized through TGA with the same conditions.

4.2.4. Stiffness change via reversible DA reaction

The dynamic mechanical moduli and loss tangents of the DA elastomer films were measured with a TA RSA3 DMA. Films with a measured thickness of ~ 100 µm were cut into ~ 5 mm wide strips by a razor blade and loaded onto the DMA with an active length of ~ 10 mm. 5 samples were tested for each formulation at 1 Hz frequency and < 3% strain.

All films except DA-10' were tested at least at for one cycle at three stages:

Stage 1: The sample was as prepared and marked as PADA-X-r.

Stage 2: The sample was heated at 130 °C for 30 min and fast cooled down to room temperature with compressed air blowing. As the thermal treatment would break DA bonds, the sample became softer and was marked as PADA-X-s.

Stage 3: The sample was heated at 70 °C for 24 hrs. As DA bonds would reform, the sample returned to its as-prepared rigid state which is PADA-X-r.

The control sample, PADA-10' film, was tested only at Stages 1 and 2. The PADA-5 films were tested for 5 cycles to determine the reversibility.

The PADA-4 films were tested at other de-bonding temperature: 90 °C, 110 °C and 160 °C and the corresponding resulted softer samples were marked as PADA-4-s90, PADA-4-s110 and PADA-4-s160. Their moduli were measured with DMA as well. To observe the stability, PADA-4-s90, PADA-4-s110, PADA-4-s and PADA-4-s160 were relaxed at room temperature for 2 hrs

and their moduli were measured again. These samples were further heated at 70 °C for 24 hrs or longer to return to the rigid state (PADA-4-r).

4.2.5. Other characterizations

Stress-strain curves of PADA-4 films were obtained on the same DMA. An elastomer film was cut into a standard dumbbell shape with an active length of 12 mm and a width of 2 mm using a laser cutter. The sample was stretched at 3.33 mm/s till rupture.

The UV absorption spectra of the PADA-4 films were obtained using a Shimadzu PharmaSpec UV-1700 UV-Visible spectrophotometer. A sample for UV spectrum was prepared using quartz slides as the mold instead of regular glass slides. One of the quartz slides was carefully peeled off after UV curing. The film was kept attaching on the other quartz slide during further thermal treatments and measurements.

In swelling test, a DAPA-4 film was cut into round-shaped plates and swelled in chloroform for 16 hrs. Diameters of these plates before and after swelling were measured.

4.2.6. Application as capacitive Sensors

PADA-4-r and PADA-4-s were fabricated into capacitive sensors whose structure is schemed in **Figure 4-10**. The area of one sensor was 6 cm × 2 cm within which an area of 2 cm × 5 cm had overlapped electrodes (the area of the capacitor). The stress-strain curves of the capacitive sensors were tested on a TA RSA3 DMA at a stretch rate of 1 mm/s. The capacitors were further stretched using a Zaber A-LSQ300A-E-1 motorized linear stage at the same rate. Meanwhile the capacitances were measured on a Self Sensing Unit (SSU) developed in the Biomimetics Laboratory in the University of Auckland, New Zealand. During measurement, a sinusoidal AC signal with an amplitude of 50 V and an average of 400 V at 400 Hz was applied.

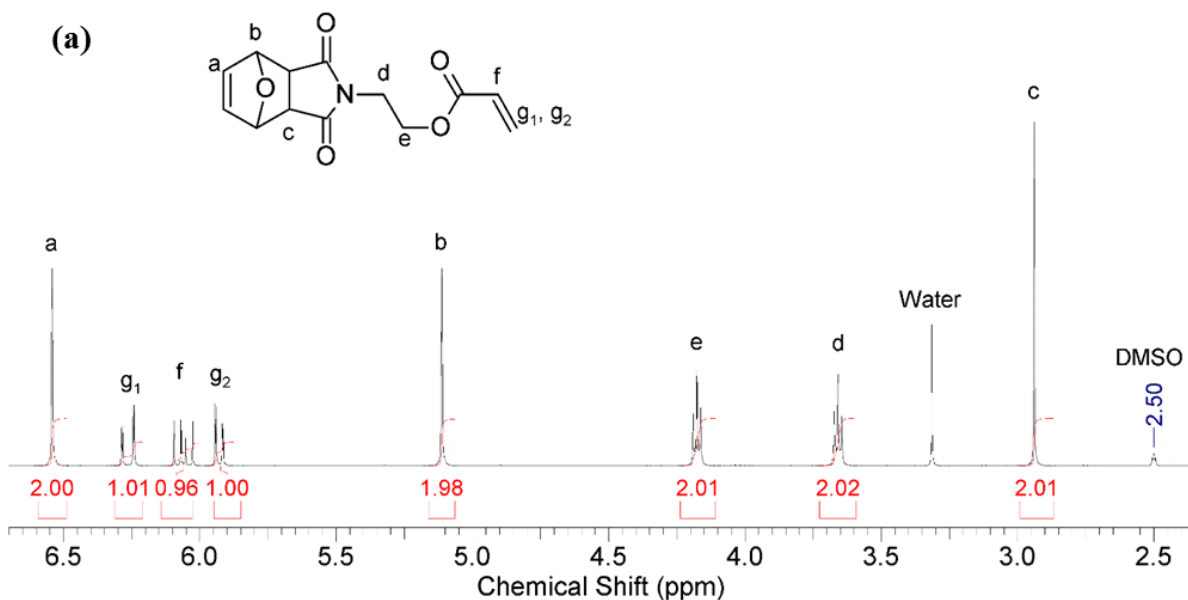
4.2.7. Application as actuators

PADA-4-r and PADA-4-s were fabricated into actuators with 5% by 5% biaxial prestrain. Carbon grease was coated onto both sides of the films as electrodes. High voltages were supplied from the HV box fabricated in-house. The area change of the active area, defined as the overlapping area of the two electrodes, were recorded by a web camera controlled by a LabView program. Voltages were applied to obtain 10 MV/m increments in the nominal electric field regarding to the unactuated thickness of each film. 4 samples were tested for both rigid and soft films, respectively.

4.3. Results and discussion

4.3.1. Synthesis of FM-A

The chemical structures of FM-A and the intermediate products were confirmed by NMR spectra. The peaks appeared in ^1H NMR spectra of Furan A are: (400 MHz, DMSO- d_6) δ 6.58 (t, 1H), 5.35 (t, 1H), 3.31(s, 1H). And those of Furan B are: (400 MHz, DMSO- d_6) δ 6.54 (s, 1H), 5.12 (s, 2H), 3.42 (m, 2H), 2.92 (m, 2H). The product, FM-A appeared white powder. Its ^1H NMR and ^{13}C NMR spectra were displayed in **Figure 4-3**.



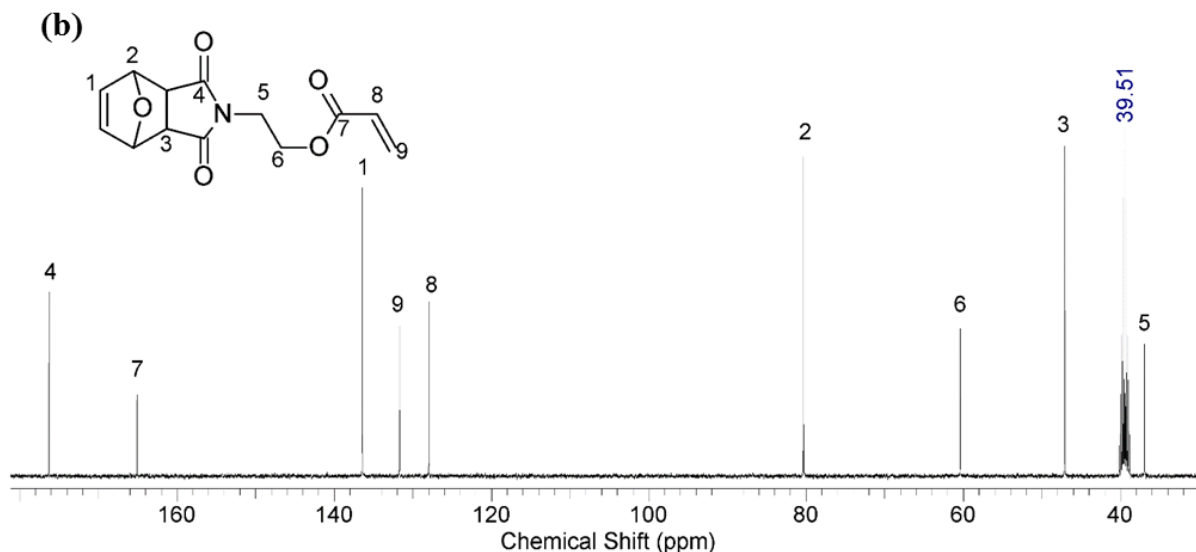


Figure 4-3. (a) ^1H NMR and (b) ^{13}C NMR (400 MHz, DMSO) spectra of as-synthesized FM-A.

Note that this furan-maleimide group on this monomer was not to provide a crosslinking site in the as-synthesized polymer but to protect the maleimide group from copolymerizing with other acrylate co-monomers.^[75]

4.3.2. Preparation of DA elastomer films

Five formulations with different concentrations of co-monomers and crosslinker (Xlinker) were investigated as shown in **Table 4-1**. Copolymers consisting of n-butyl acrylate (nBA) have demonstrated high actuation strains and high energy densities as dielectric elastomers. Therefore, n-butyl acrylate was selected as the base monomer. 2(2-ethoxyethoxy) ethyl acrylate (EOEA) was added to improve the solubility of FM-A in nBA. The Xlinker with four furan end groups in each molecule was previously synthesized in the same group and used in a self-healing polymer composite. The copolymers are called PADA-X where X stands for the weight part of FM-A. A control formulation, PADA-10', without Xlinker, was also synthesized. Each co-monomer, Xlinker, and a photo-initiator, 2, 2-dimethoxy-2 phenylacetophenone (DMPA), were admixed at

the weight ratios shown in **Table 4-1** to afford clear solutions. Note that in all the formulations, the furan moieties maleimide moieties are equimolar.

The synthetic route for the elastomers is schematically illustrated in **Figure 4-4**. The three acrylate monomers (nBA, EOEA and FM-A) copolymerized into a linear chain (Polymer 1 in **Figure 4-4**) with pendant DA adducts provided by FM-A. The Xlinker remains intact and dissolved in Polymer 1 during the UV curing. The film was then heated at 130 °C for 2 hrs and then at 70 °C for 24 hrs to effect a metathetic reaction between the pendant DA moieties and the Xlinker compound: The DA moieties underwent retro-DA reaction and released furan molecules, and the resulting pendant maleimide moieties (in Polymer 2) underwent DA reaction with the furan groups on the dissolved Xlinker at 70 °C to afford a crosslinked elastomer network. This metathetic route was taken because the maleimide moieties could participate in the free-radical co-polymerization of the acrylate groups. The DA adduct with furan molecules protected maleimide moieties through the UV curing process and could be easily de-protected by retro-DA reaction. The resulted elastomer films were transparent with slightly tint. The films were relatively rigid as the DA bonds were formed, and called PADA-X-r, where r indicated rigid.

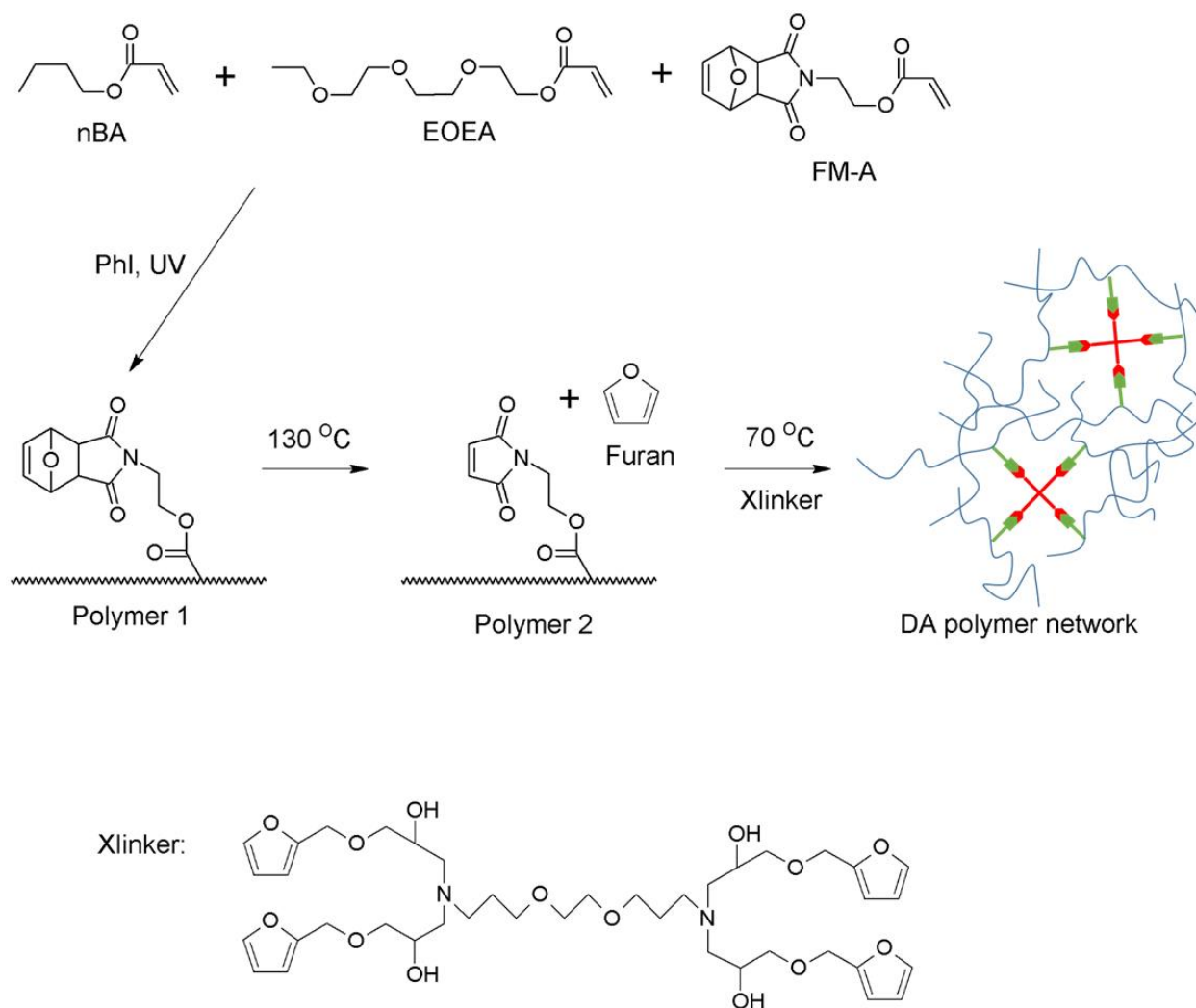


Figure 4-4. The synthesis route of a PADA elastomer. Note that Xlinker was co-dissolved with other monomers before UV curing but it remain inert during UV curing and thermal treatment at 130 °C. It reacted with Polymer 2 during treatment at 70 °C at the last step resulted in a crosslinked polymer network.

The scenario was confirmed with thermogravimetric analysis (TGA). As calculated from the formulation of PADA-10, the weight percentage of evaporated furan molecules is 2.4 theoretically.

As shown in **Figure 4-5**, the as-synthesized PADA-10 sample (PADA-10-r) remained stable up to 180 °C while heating in air atmosphere at the rate of 5 °C/min. In comparison, another sample, PADA-10_70, was synthesized from the same pre-polymer solution but the heating step at 130 °C for 2 hrs had been skipped. Different from PADA-10-r, PADA-10_70 showed a weight loss of 2.7 wt% from 50 °C to 180 °C. As indicated in its derivative curve in **Figure 4-5**, the major weight

loss of PADA-10_70 happened from 110 °C to 155 °C which had a peak value at 138 °C. The temperature range matched well with where the retro-DA reaction happened in furan-maleimide adducts and the value of weight loss was in good agreement with the theoretical number.⁷³

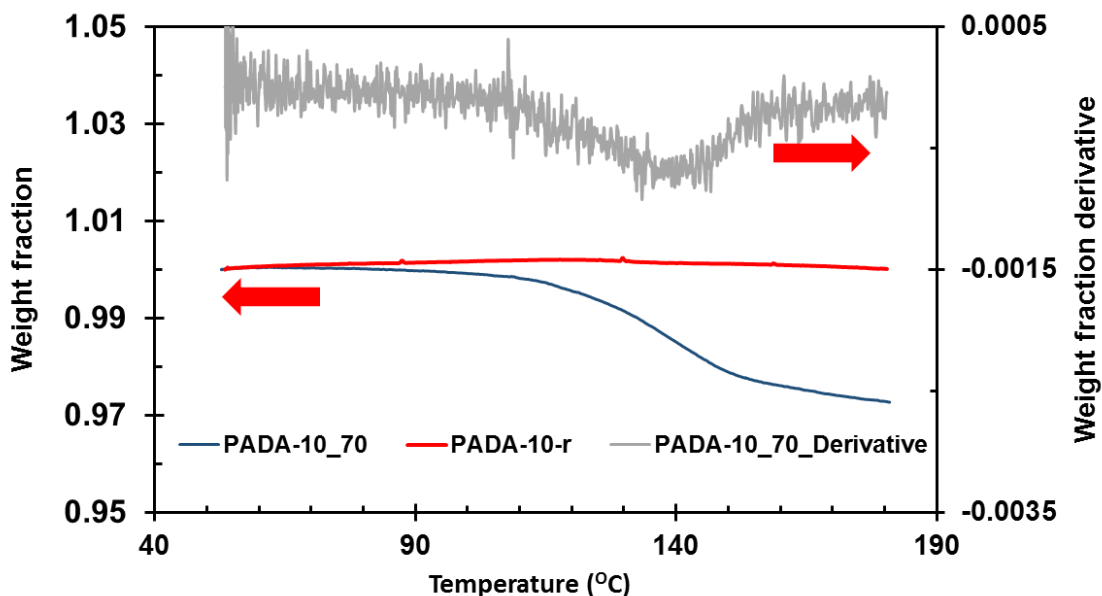


Figure 4-5. TGA curves of PADA-10_70 and PADA-10-r from 50 °C to 180 °C in air atmosphere with a heating rate of 5 °C/min and the derivative curve of PADA-10_70's TGA curve.

4.3.3. Stiffness change via reversible DA reaction

Since the mechanical properties of elastomers heavily depend on their crosslinking densities, forming and breaking the DA crosslinking sites would create two or even more stiffness states in one elastomer. The rigid state corresponds to the highly crosslinked state as synthesized with short chain segments while the soft state is achieved by partially breaking DA bonds, resulting in long chain segments between crosslinking sites. The soft elastomer could return to its rigid state by reforming DA bonds. As shown in **Figure 4-6 (a)**, Stage 1 samples refer to those as-synthesized (PADA-X-r). The Stage 2 (PADA-X-s) samples were obtained by heating PADA-X-r samples at 130 °C for 30 min followed by fast cooling down to room temperature. The Stage 3 samples (also PADA-X-r) were obtained by heating the PADA-X-s samples at 70 °C for 24 hrs. The elastic

moduli (E') and loss tangents ($\tan \delta$) were measured using a dynamic mechanical analyzer (DMA) and listed in **Table 4-2**. All the formulations showed an obvious difference in modulus between Stage 1/3 and Stage 2 except PADA-10'. This proved that it was the dynamic DA bonding that contributed to the change of moduli.

Table 4-2. Moduli of the formulated elastomers at three stages in one cycle.

Elastomer	Stage 1 (PADA-X-r)		Stage 2 (PADA-X-s)		Stage 3 (PADA-X-r)	
	E' [MPa]	$\tan \delta$	E' [MPa]	$\tan \delta$	E' [MPa]	$\tan \delta$
PADA-2.5	0.20±0.02	0.118±0.008	0.099±0.003	0.271±0.006	0.214±0.003	0.114±0.003
PADA-3	0.30±0.02	0.08±0.01	0.12±0.01	0.22±0.03	0.27±0.02	0.09±0.01
PADA-4	0.52±0.03	0.045±0.008	0.26±0.02	0.10±0.02	0.54±0.03	0.039±0.003
PADA-5	1.23±0.09	0.026±0.004	0.41±0.03	0.084±0.009	0.94±0.06	0.033±0.003
PADA-10	2.24±0.09	0.026±0.001	1.32±0.06	0.031±0.001	2.31±0.07	0.026±0.001
PADA-10'	1.01	0.028	1.06	0.026		

As demonstrated in **Table 4-2** and **Figure 4-6 (b)**, at both rigid and soft state, the moduli of the formulated elastomers increased with the addition of FM-A and Xlinker. The increase of moduli can be attributed to the increase of crosslinking density. Another reason is the addition of rigid monomer. Compared with nBA and EOEA, FM-A has a relatively bulky and rigid side group which hardens of the elastomers. The moduli change ratio, between rigid and soft states, of an elastomer is

$$R = \frac{E'(Stage1)+E'(Stage3)}{2 \times E'(Stage2)} \quad (24).$$

All the elastomers displayed very similar moduli change ratio, around 2, which indicated that the chain segment length became to about twice in the soft state and half of the crosslinking site was broken.

The elastomers could be adjusted from PADA-X-r and PADA-X-s repeatedly thanks to the good reversibility of the DA reactions. One of the elastomers, PADA-5, was tested for 5 cycles as shown in **Figure 4-6 (d)**. Both moduli and loss tangents were consistently changed between rigid and soft states.

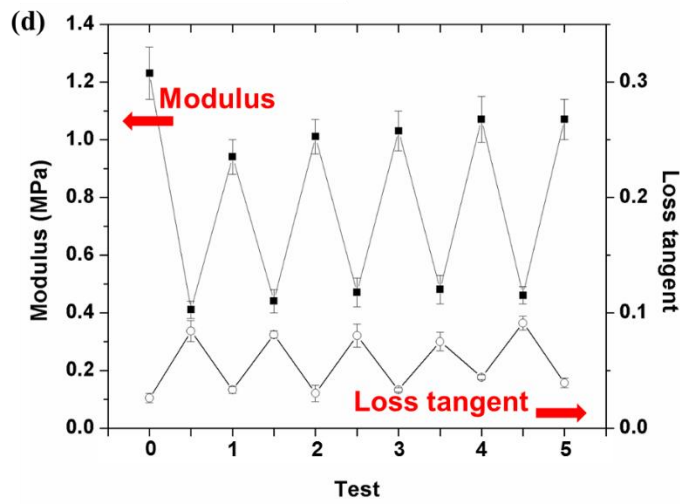
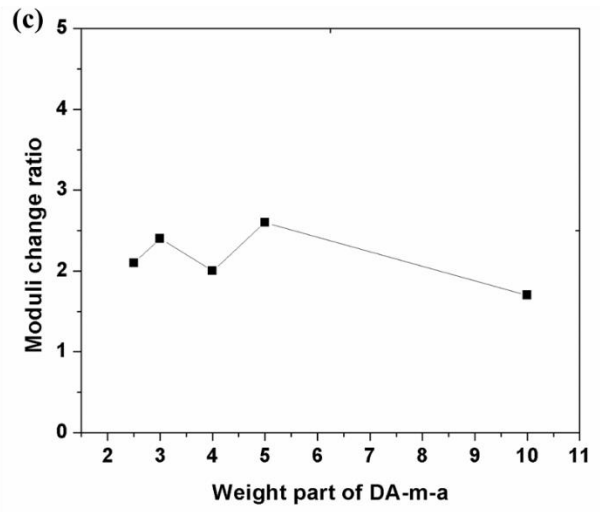
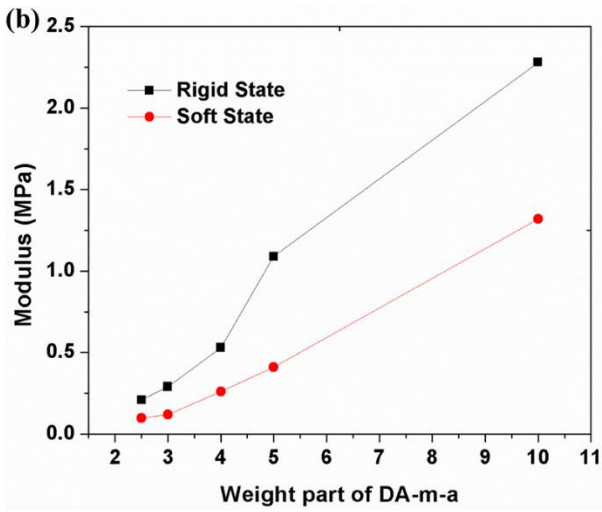
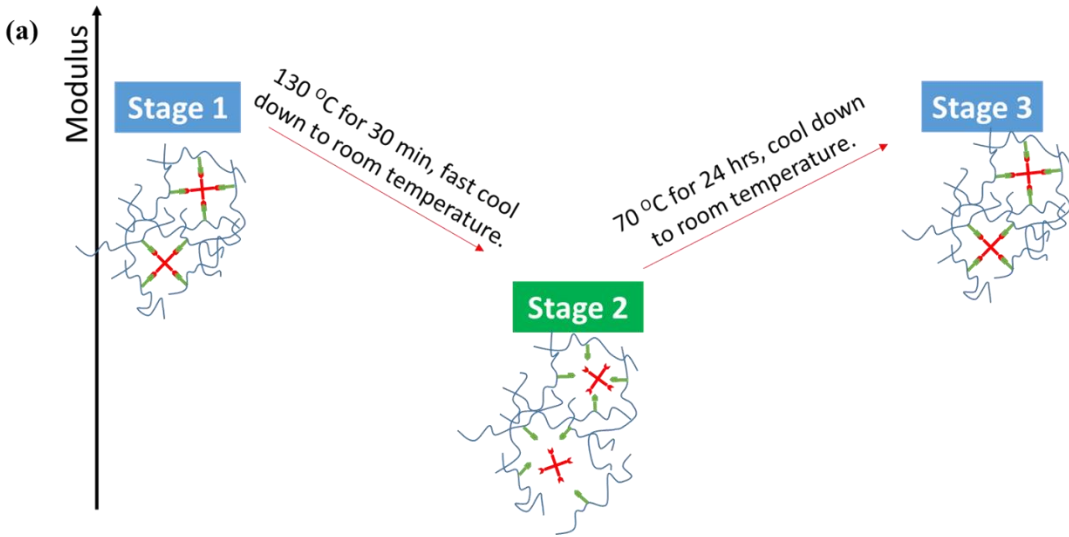


Figure 4-6. (a) A schematic illustration of thermal treatments. The as-synthesized films were at their rigid states (Stage 1, PADA-X-r). Soft states (Stage 2, PADA-X-s) were achieved through heating the films at 130 °C for 30 min and then fast cooling down to room temperature. Rigid states (Stage 3, PADA-x-r) could be regained through heating the films at 70 °C for another 24 hrs and cooling down to room temperature. **(b)** The moduli of elastomer formulations with different weight parts of FM-A at both rigid and soft states, and **(c)** the moduli change ratio (R) between the two states. **(d)** Cycling test of one of the formulations, PADA-5. These elastomers samples were thermally adjusted between PADA-5-r and PADA-5-s as shown in **(a)** for 5 cycles.

4.3.4. Achieving multiple states by controlling crosslinking density

While stiffness difference between PADA-X-r and PADA-X-s was demonstrated, more states could be achieved through treatments at different de-bonding (retro-DA) temperatures. Lower de-bonding temperatures would relatively retard the retro-DA reaction and result in moderately crosslinked states while high de-bonding temperatures tend to break DA bonds more completely.^[76] PADA-4-r elastomers were heated at different de-bonding temperatures, 90 °C, 110 °C and 160 °C other than 130 °C and fast cooled down to room temperature (step i in **Figure 4-7**) resulting in PADA-4-s90, PADA-4-s110 and PADA-4-s160, respectively. While PADA-4-s had a modulus equal to half of that of PADA-4-r, the ratios of the moduli of PADA-4-s90, PADA-4-s110 and PADA-4-s160 to that of PADA-4-r were 0.85, 0.67 and 0.34 measured with DMA, respectively. After aging at room temperature for 2 hrs (step ii in **Figure 4-7**), the moduli of PADA-4-s90, PADA-4-s110, PADA-4-s and PADA-4-s160 did not show a significant increase. Generally, DA reaction is favorable at room temperature thermodynamically. Therefore, PADA-4-r should be the stable form of all the PADA-4 elastomers at room temperature. However, the soft states could be maintained for a relatively long time due to the slow DA reaction, which is good for most applications. After heating at 70 °C for another 24 hrs (step iii in **Figure 4-7 (a), (b) and (c)**), PADA-4-s90, PADA-4-s110 and PADA-4-s regained their original stiffness. However, PADA-4-s160 needed 48 hrs' heating at 70 °C (step iii in **Figure 4-7 (d)**) to return to the original modulus.

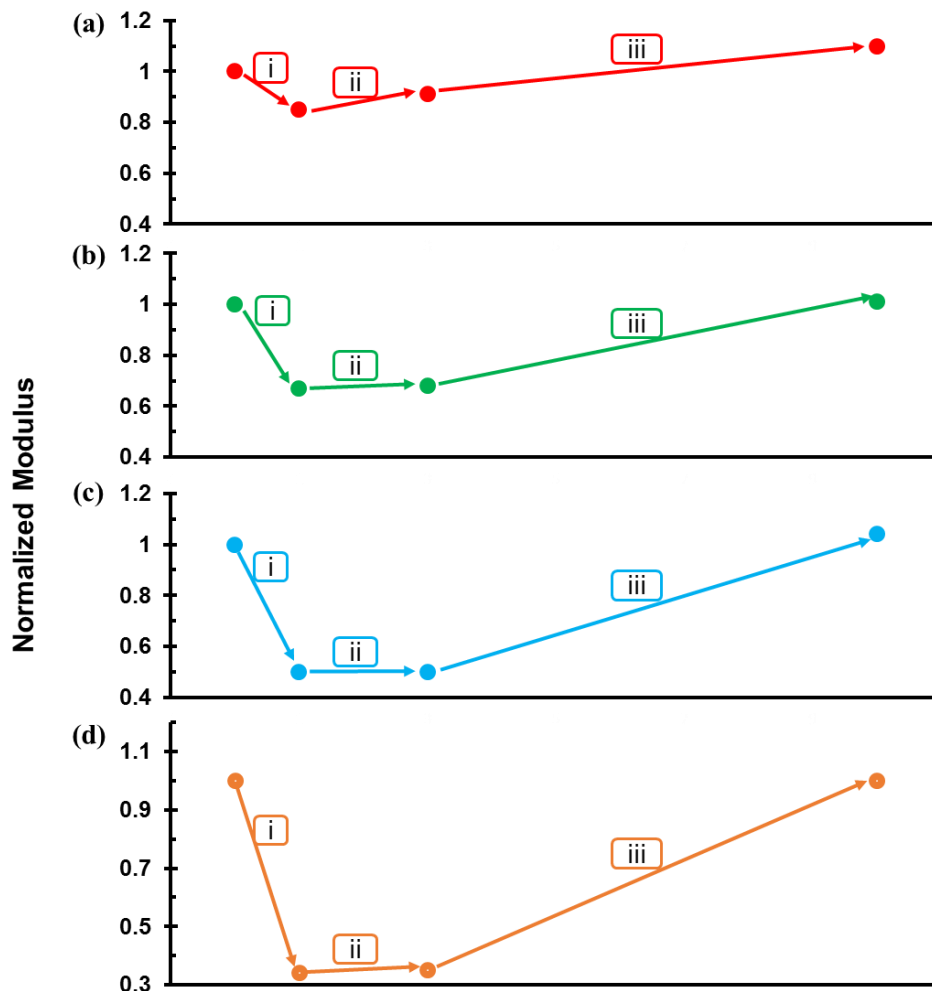


Figure 4-7. Various moduli of PADA-4 elastomers could be achieved through thermal treatments. (i) PADA-4-r samples were heated at (a) 90 °C, (b) 110 °C, (c) 130 °C and (d) 160 °C followed by a fast cooling down to room temperature to achieve PADA-4-s90, PADA-4-s110, PADA-4-s and PADA-4-s160. (ii) Samples were aged at room temperature for 2 hrs and their moduli did not show a significant change. (iii) Samples were heated at 70 °C for 24 hrs in (a), (b) and (c) and for 48 hrs in (d). Moduli were normalized as the modulus of PADA-4-r was set as 1.

To relate the change of modulus to the crosslinking density of the elastomer, PADA-4 films, including PADA-4-r, PADA-4-s90, PADA-4-s110, PADA-4-s and PADA-4-s160, were further characterized through mechanical tensile test, UV spectroscopy and swelling test.

As indicated in **Figure 4-8 (a)**, higher de-bonding temperature resulted in a softer elastomer with larger elongation at rupture.^[77] This can be attribute to the decrease of crosslinking density. Note

that PADA-4-s has a lower modulus than those of PADA-4-r, PADA-4-s90 and PADA-4-s110 but its strength at rupture is comparable to that of PADA-4-r. Its superior mechanical properties could be explained using elastomer's bimodal theory that in a crosslinking network, long chains contribute to the elastomer's extensibility while short chains correspond to high stress.^[78] Among all these PADA-4 elastomers, PADA-4-s might be closest to the optimal chain length distribution.

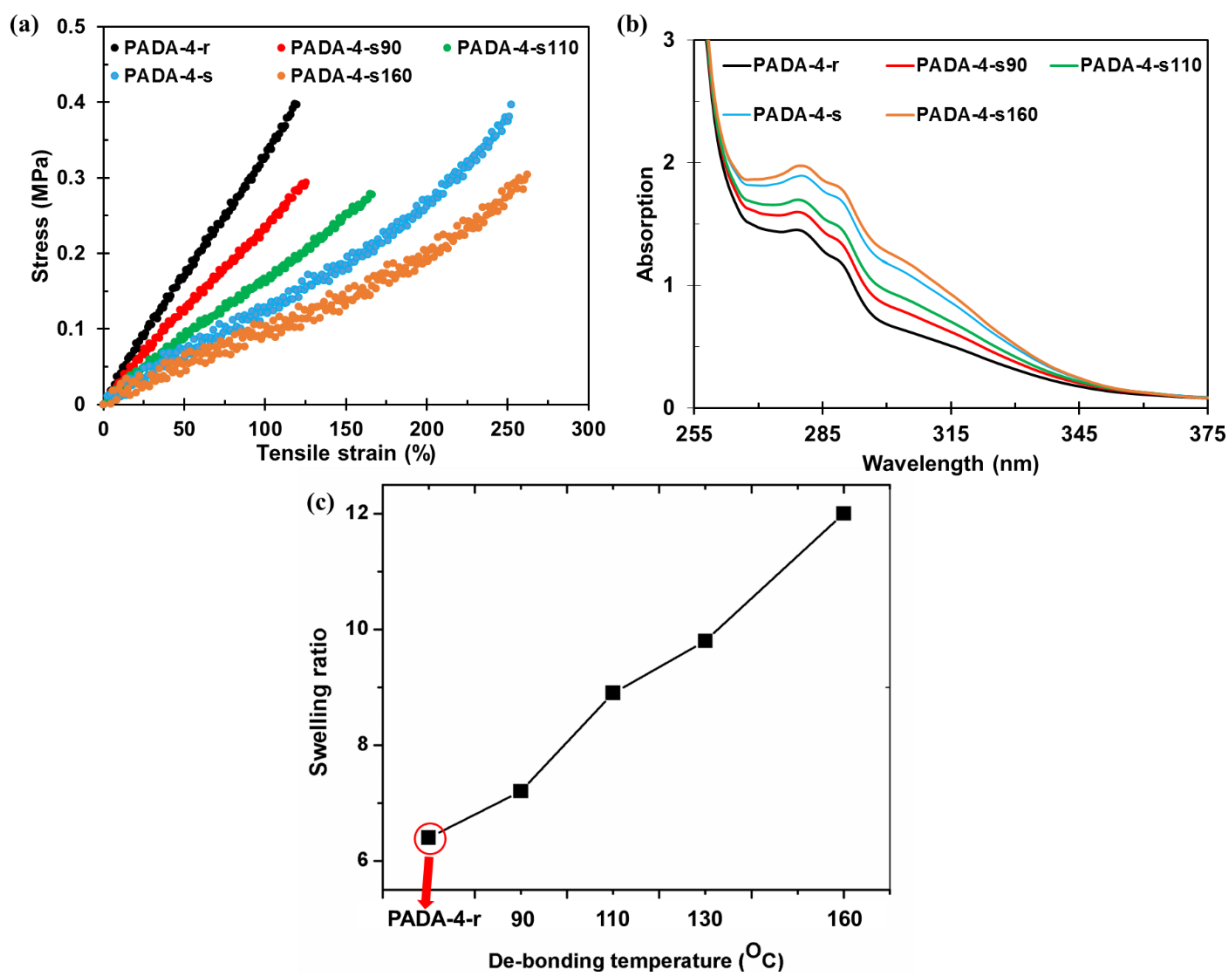


Figure 4-8. (a) Stress-strain curves of PADA-4 elastomers. A dumbbell-shaped sample was stretched to rupture at a rate of 3.33 mm/s. (b) UV spectra of PADA-4 elastomers. (c) Swelling ratios of PADA-4 elastomers in chloroform.

UV spectra (**Figure 4-8 (b)**) of PADA-4 elastomers provided a direct measurement of the progress of retro-DA reaction. The increase intensity of peak at 280 nm with elevated de-bonding

temperatures corresponded to the increased amount of conjugated O=C-C=C-C=O structure in maleimide moieties. The portions (x) of adduct of furan and maleimide pairs were calculated from the intensity of the peak at 280 nm following the method in Ref [79]^[79] and \overline{M}_C of each elastomer was related to x using Equation (25)

$$\overline{M}_C = \frac{\overline{M}_{C0}}{x} \quad (25)$$

where \overline{M}_{C0} is the average molecular weight between crosslinks in PADA-4-r.

PADA-4 films were swollen in chloroform to characterize the crosslinking density. The swelling ratio Q is defined as

$$Q = \left(\frac{a}{a_0}\right)^3 \quad (26)$$

where a and a_0 are the diameter of the plates after and before swelling, respectively. \overline{M}_C can be calculated using

$$\overline{M}_C = \frac{2\rho V_1 Q^{\frac{5}{3}}}{(1-K)} = \overline{M}_{C0} \left(\frac{Q}{Q_0}\right)^{\frac{5}{3}} \quad (27)$$

where V_1 , Q_0 and K are the molar volume of the solvent (chloroform in this case), swelling ratio of PADA-4-r in chloroform and a constant related to temperature, polymer, solvent and their interaction, respectively.^[14]

Moduli of PADA-4 elastomers were calculated using Equation (23) from \overline{M}_C values of swelling test and UV spectra and compared with the measured data. As shown in **Figure 4-9**, the measured moduli of PADA-4 elastomers with various thermal treatments matched well with the calculated moduli from both UV spectra and swelling test. This indicates that it is the crosslinking density of the elastomer that alters the modulus of PADA-4 elastomers.

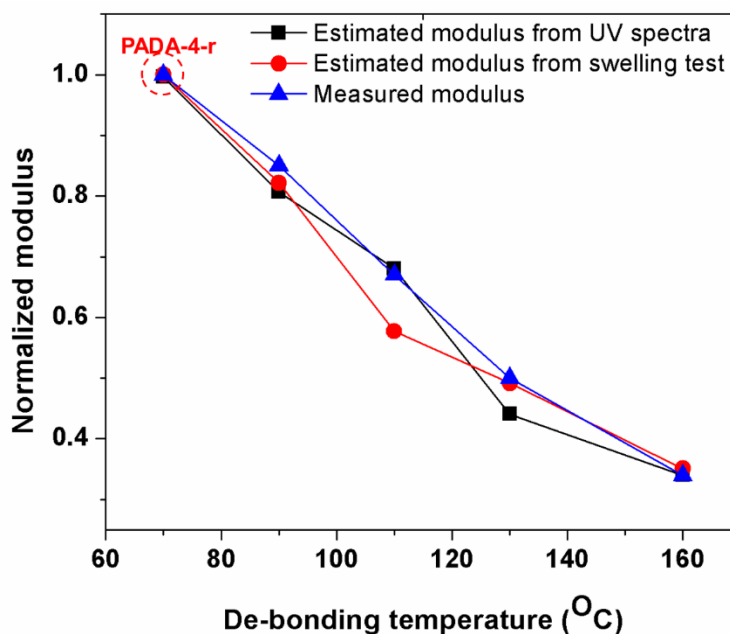


Figure 4-9. The comparison of measured moduli and estimated moduli from both UV spectra and swelling test at different de-bonding temperatures.

4.3.5. Applications as sensors and actuators

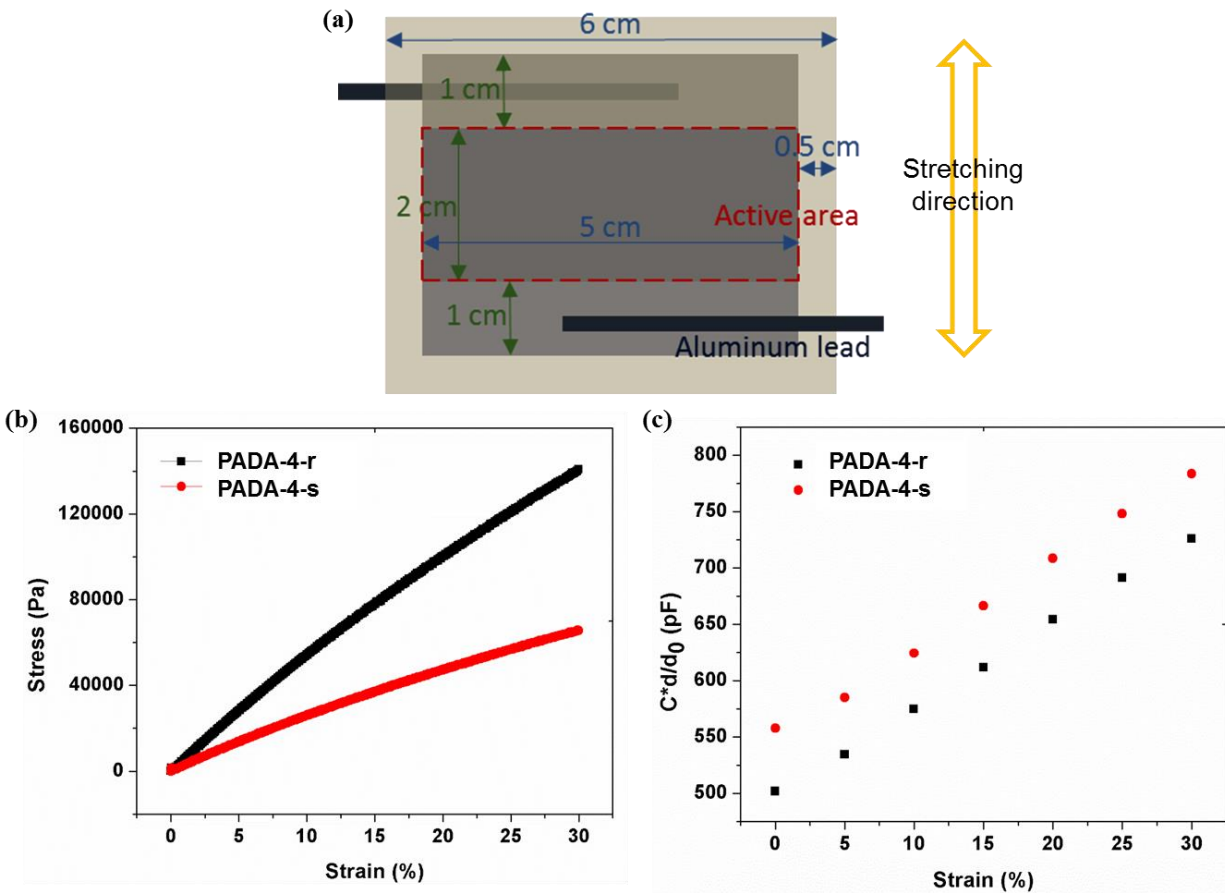
Good dielectric elastomers should be soft so that they are sensitive to small pressure changes, can detect large deformations, and exert large actuation strain and energy outputs. On the other hand, soft elastomers with low modulus could suffer from electromechanical instability.^[14,40] PADA-4 was selected to fabricate sensors and actuators thanks to its moderate moduli in both rigid and soft states. Among PADA-4 elastomers, PADA-r and PADA-s were compared.

4.3.5.1. Capacitive sensing

As indicated by the stress-strain curves of the sensors made of PADA-4-r and PADA-4-s in **Figure 4-10 (b)**, these sensors could be operated in two modes with different mechanical loadings. The sensing performance was tested with a linear stage to stretch the film at 1 mm/s and an SSU to measure the capacitance at 400 Hz. Note that in **Figure 4-10 (c) (d)**, the thickness (d) of the capacitor is normalized to 100 μm (d_0). The capacitances had a quasi-linear relationship with the

stretch strain up to 30 % linear strain, which is good for strain sensing purpose. As converted from **Figure 4-10 (b) (c)**, mechanical pressures also displayed a quasi-linear relationship with the capacitances. This sensor can potentially be integrated into more complex devices with multiple working modes.^[80] For example, knee pads with standby mode and active mode and flexible electronics with press mode and stretch mode as well.

As calculated from the measured capacitances at 0% strain, the dielectric constants (ϵ_r) of PADA-4-r and PADA-4-s are 5.7 and 6.3, respectively. The dielectric constant of the PADA-4-s is slightly higher than that of PADA-4-r, which could be attributed to the less confinement of dipoles in softer polymer network.^[81]



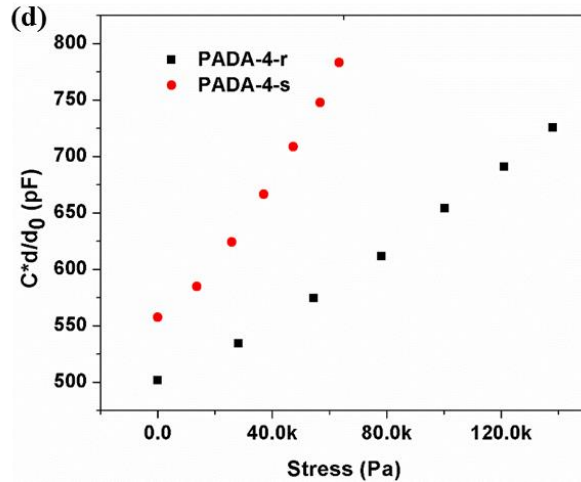


Figure 4-10. (a) The structure of a capacitive sensor. (b) The stress-strain curves of the sensors made of PADA-4-r and PADA-4-s at a stretch rate of 1 mm/s. (c) The capacitive sensing results at a stretch rate of 1 mm/s. (d) The capacitance-stress curves of the sensors. Note that in (c) and (d), the thickness of the capacitor is normalized to 100 μm (d_0).

4.3.5.2. Actuation

Actuators were fabricated with 5% by 5% biaxial prestrain to avoid wrinkling during actuation.^[39]

Carbon grease was coated on both sides of the stretched films as electrodes. Voltages were applied at each nominal 10 MV/m. The change of the actuator's active areas, defined as the overlapping area of two electrodes, were recorded by a web camera controlled by a LabView program. For both rigid and soft DA-4 films, 4 samples were tested and the average data are presented in **Figure 4-11**.

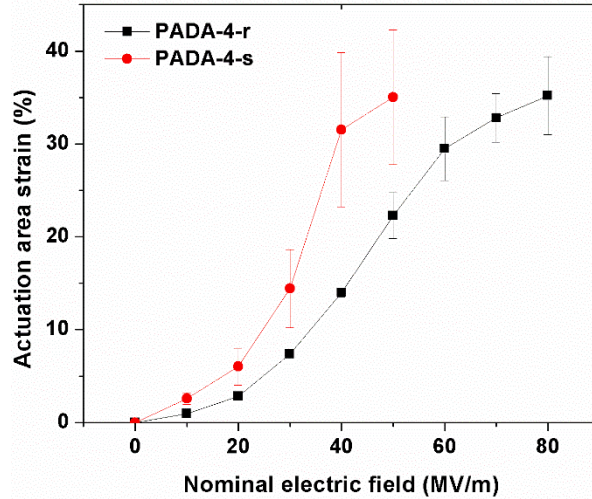


Figure 4-11. Actuation curves of PADA-4-r and PADA-4-s. Average actuation strains at each nominal 10 MV/m electric field were plotted. Both films were prestretched 5% by 5%.

As indicated in **Equation (1)**, the actuation strain is depending on the elastomer’s dielectric constant, mechanical modulus and the actuation electric field. Different from most elastomers which would show a certain actuation strain at a particular electric field, this elastomer were able to produce different actuation performances at identical electric fields. This is particularly important when constant actuation pressure and various actuation strain are needed at the same time.

Key actuation performances of the two states are listed in **Table 4-3**. The dielectric strength is calculated as the real electric field at the breakdown point. Average value of four actuators in each group is presented.

Table 4-3. Comparison of the actuation performances of PADA-4-r and PADA-4-s.

Property	$s_{a,max}$ [%]	E_b [MV/m]	p_{max} [MPa]	$u_{e,max}$ [kJ/m ³]
PADA-4-r	35±4	104±10	0.55	83
PADA-4-s	35±7	65±7	0.24	36

PADA-4 films had comparable energy densities with other dielectric elastomers with low prestrain ratios. PADA-4-r had an overall better performance than PADA-4-s did since it had a higher dielectric strength. This could be attributed to a higher modulus of the rigid film which can help prevent electromechanical instability. Additionally, some mobile Xlinker molecules inside the PADA-4-s network might result in a leakage current increase which would assist dielectric breakdown.^[14] Therefore, PADA-4-r is more suitable to be used in applications needing higher force output and energy density. However, at certain electric fields, PADA-4-s had a larger strain than PADA-4-r had, which made it useful for applications requiring higher strain at reduced operation voltages.

4.4. Conclusion

Dielectric elastomers with variable moduli were synthesized and characterized. The stiffness change of these elastomers were achieved by thermal treatments at moderate temperatures. The elastomers' moduli at their rigid states were three times of those at the corresponding soft states. The change of modulus had good reversibility as well.

The elastomers were further fabricated into capacitive sensors which could work in both high/low mechanical loading modes and actuators which could work in high strain or high force output modes. These devices could be integrated into more complex electromechanical systems with variable work conditions.

5. Summary and Future Researches

5.1. Summary of the dissertation

This dissertation focuses on the design and synthesis of new dielectric elastomer materials from molecular level.

In the first part, a series of polymer acrylate elastomers were synthesized and characterized. These formulations, with n-butyl acrylate as the based monomer, have various amount of acrylic acid. The addition of acrylic acid has increased the dielectric constant and mechanical stiffness of the resulted polymer. Actuation performances of these formulations were studied and compared. The actuation performances of the formulation with optimal amount of acrylic acid were investigated at various prestrain ratios and a threshold prestrain ratio to overcome the electromechanical instability was determined. The best actuator demonstrated a strain of 186 % in area, a dielectric strength of 222 MV/m and an energy density of 1.4 MJ/m³.

The second part of this dissertation is the development of a dielectric elastomer with high dielectric constant. To achieve that, a metallic nanofiller, aluminum nanoparticle, was modified and dispersed in a polyacrylate formulation. With methacrylate moieties bonded on the surface these nanoparticles, uniform nanocomposites were achieved. The nanocomposite containing 4 vol% aluminum nanoparticles shows a high dielectric constant of 8.4, with large elongation at rupture, high dielectric strength and low leakage current. It demonstrates an area actuation strain of 56 % which is much higher than reported values of other dielectric elastomers with comparable dielectric constants.

The third part of this dissertation is the innovation of a novel dielectric elastomer with tunable stiffness. The elastomer contains furan-maleimide Diels-Alder adduct moieties which administer the crosslinking density of the elastomeric network through reversible Diels-Alder/retro-Diels-

Alder reactions, resulting in the changes in the elastomer's stiffness. The moduli of the elastomer can be controlled between 0.17 MPa to 0.52 MPa incrementally and reversibly. The dielectric elastomer was further fabricated into capacitive sensors which could be operated in high sensitivity/low stress mode and low sensitivity/high stress mode. Also actuators fabricated with this elastomer can be operated in both high strain mode and high force output mode.

To summarize, in this dissertation, three new dielectric elastomer materials are developed focusing on different aspects to improve the actuation performances of dielectric elastomer actuators. This work will broaden the choices of materials of dielectric elastomer devices. The bottom-up synthesis from molecular level also provide convenience of device fabrication. Additionally, this dissertation provides information for more fundamental study on elastomer materials.

5.2. Future researches

Although some commercial elastomers designed for other applications have demonstrated excellent actuation performances, a great interest is on design and synthesize polymers as dielectric elastomers for actuation purposes.

To formulate dielectric elastomers with high dielectric constants will still be a focus. While conductive/dielectric composites would have an infinitely high dielectric constant approaching the percolation point, the increased loading would possibly bring in loss in compliancy, filler aggregates which future renders a low dielectric strength and a high leakage current. New techniques of synthesizing nanocomposite monolith such as polymerization from filler particles' surfaces could be adopted to achieve a uniform nanocomposite. When it comes to the mechanical properties of nanocomposites, the incorporation of rigid fillers usually give rise to a stiffness increase in the resulted polymer which may lower the actuation strain. However, these materials

are suitable to be used as energy generators in which stiffer elastomers would be able to absorb more mechanical energy.

Smart/adaptive elastomers will be another topic since they can behave like natural muscles which are able to adapt to changing working conditions. The use of dynamic bonding can administer the mechanical properties of elastomers as demonstrated in Chapter 4. Furthermore, the dielectric elastomer materials as described in Chapter 4 can be integrated into more complex electromechanical transduction devices with heating and cooling systems. Chemistries other than furan-maleimide Diels-Alder adduct are worth to explore to see if a more complete bonding/de-bonding reaction can be obtained, thus the contrast of stiffness change would be improved. This concept can be further extended to the field of shape memory polymers which is another actuation technology.

References

1. O'Halloran, A., O'Malley, F. & McHugh, P. A review on dielectric elastomer actuators, technology, applications, and challenges. *J. Appl. Phys.* **104**, 071101 (2008).
2. Anderson, I. A., Gisby, T. A., McKay, T. G., O'Brien, B. M. & Calius, E. P. Multi-functional dielectric elastomer artificial muscles for soft and smart machines. *J. Appl. Phys.* **041101**, 041101 (2012).
3. Brochu, P. & Pei, Q. Advances in dielectric elastomers for actuators and artificial muscles. *Macromol. Rapid Commun.* **31**, 10–36 (2010).
4. Pelrine, R., Kornbluh, R., Joseph, J., Heydt, R., Pei, Q. & Chiba, S. High-field deformation of elastomeric dielectrics for actuators. *Mater. Sci. Eng. C* **11**, 89–100 (2000).
5. Pelrine, R., Kornbluh, R., Pei, Q. & Joseph, J. High-speed electrically actuated elastomers with strain greater than 100%. *Science* **287**, 836–839 (2000).
6. Madden, J. D. W. in *Dielectr. elastomers as electromechanical transducers* (Carpi, F., De Rossi, D., Kornbluh, R., Pelrine, R. & Sommer-Larsen, P.) 13–21 (Elsevier Ltd, 2008).
7. Brochu, P., Stoyanov, H., Niu, X. & Pei, Q. All-silicone prestrain-locked interpenetrating polymer network elastomers: free-standing silicone artificial muscles with improved performance and robustness. *Smart Mater. Struct.* **22**, 055022 (2013).
8. Keplinger, C., Li, T., Baumgartner, R., Suo, Z. & Bauer, S. Harnessing snap-through instability in soft dielectrics to achieve giant voltage-triggered deformation. *Soft Matter* **8**, 285–288 (2012).
9. Petit, L., Guiffard, B., Seveyrat, L. & Guyomar, D. Actuating abilities of electroactive carbon nanopowder/polyurethane composite films. *Sensors Actuators, A Phys.* **148**, 105–110 (2008).
10. Shankar, R., Ghosh, T. K. & Spontak, R. J. Electromechanical response of nanostructured polymer systems with no mechanical pre-strain. *Macromol. Rapid Commun.* **28**, 1142–1147 (2007).
11. Jang, Y. & Hirai, T. A control method for triblock copolymer actuators by nano-lamellar pattern. *Soft Matter* **7**, 10818 (2011).
12. Ha, S. M., Yuan, W., Pei, Q., Pelrine, R. & Stanford, S. Interpenetrating polymer networks for high-performance electroelastomer artificial muscles. *Adv. Mater.* **18**, 887–891 (2006).

13. Zhang, H., Düring, L., Kovacs, G., Yuan, W., Niu, X. & Pei, Q. Interpenetrating polymer networks based on acrylic elastomers and plasticizers with improved actuation temperature range. *Polym. Int.* **59**, 384–390 (2010).
14. Niu, X., Stoyanov, H., Hu, W., Leo, R., Brochu, P. & Pei, Q. Synthesizing a new dielectric elastomer exhibiting large actuation strain and suppressed electromechanical instability without prestretching. *J. Polym. Sci. Part B Polym. Phys.* **51**, 197–206 (2013).
15. Biggs, J., Danielmeier, K., Hitzbleck, J., Krause, J., Kridl, T., Nowak, S., Orselli, E., Quan, X., Schapeler, D., Sutherland, W. & Wagner, J. Electroactive polymers: developments of and perspectives for dielectric elastomers. *Angew. Chemie - Int. Ed.* **52**, 9409–9421 (2013).
16. Yang, D., Tian, M., Kang, H., Dong, Y., Liu, H., Yu, Y. & Zhang, L. New polyester dielectric elastomer with large actuated strain at low electric field. *Mater. Lett.* **76**, 229–232 (2012).
17. Kornbluh, R., Pelrine, R., Joseph, J., Heydt, R., Pei Q. & Chiba, S. High-field electrostriction of elastomeric polymer dielectrics for actuation. *Proc. SPIE* **3669**, 149–161 (1999).
18. NuSil Silicone Technology CF19-2186 Product Profile. (2011).
19. Dow Corning HSIII Technical Data Sheet.
20. Zhang, X., Löwe, C., Wissler, M., Jähne, B. & Kovacs, G. Dielectric elastomers in actuator technology. *Adv. Eng. Mater.* **7**, 361–367 (2005).
21. Dow Corning 730 Technical Data Sheet.
22. Vargantwar, P. H., Özçam, A. E., Ghosh, T. K. & Spontak, R. J. Prestrain-free dielectric elastomers based on acrylic thermoplastic elastomer gels: a morphological and (electro)mechanical property study. *Adv. Funct. Mater.* **22**, 2100–2113 (2012).
23. Jung, K., Lee, J., Cho, M., Koo, J. C., Nam, J.-D., Lee, Y. & Choi, H. R. Development of enhanced synthetic elastomer for energy-efficient polymer actuators. *Smart Mater. Struct.* **16**, S288–S294 (2007).
24. Kohl, P. A. Low-Dielectric Constant Insulators for Future Integrated Circuits and Packages. *Annu. Rev. Chem. Biomol. Eng.* **2**, 379–401 (2011).
25. Ieda, M. Dielectric Breakdown Process of Polymers. *IEEE Trans. Electr. Insul.* **EI-15**, 206–224 (1980).
26. Gisby, T. A., Xie, S. Q., Calius, E. P. & Anderson, I. A. Leakage current as a predictor of failure in Dielectric Elastomer Actuators. *Electroact. Polym. Actuators Devices* **7642**, 764213–764213–11 (2010).

27. Yuan, W., Brochu, P., Ha, S. M. & Pei, Q. Dielectric oil coated single-walled carbon nanotube electrodes for stable, large-strain actuation with dielectric elastomers. *Sensors Actuators, A Phys.* **155**, 278–284 (2009).
28. Di Lillo, L., Schmidt, A., Carnelli, D. A., Ermanni, P., Kovacs, G., Mazza, E. & Bergamini, A. Measurement of insulating and dielectric properties of acrylic elastomer membranes at high electric fields. *J. Appl. Phys.* **111**, 1–8 (2012).
29. Pelrine, R. & Kornbluh, R. in *Dielectric elastomers as electromechanical transducers* (Carpi, F., De Rossi, D., Kornbluh, R., Pelrine, R. & Sommer-Larsen, P.) 33–42 (Elsevier, 2008).
30. Sheng, J., Chen, H., Qiang, J., Li, B. & Wang, Y. Thermal, mechanical, and dielectric properties of a dielectric elastomer for actuator applications. *J. Macromol. Sci. Part B* **51**, 2093–2104 (2012).
31. Lotz, P., Matysek, M. & Schlaak, H. F. Fabrication and application of miniaturized dielectric elastomer stack actuators. *IEEE/ASME Trans. Mechatronics* **16**, 58–66 (2011).
32. Lee, H. S., Phung, H., Lee, D.-H., Kim, U. K., Nguyen, C. T., Moon, H., Koo, J. C., Nam, J.-D. & Choi, H. R. Design analysis and fabrication of arrayed tactile display based on dielectric elastomer actuator. *Sensors Actuators, A Phys.* **205**, 191–198 (2014).
33. Pei, Q., Rosenthal, M. A., Pelrine, R., Stanford, S. & Kornbluh, R. D. Multifunctional electroelastomer roll actuators and their application for biomimetic walking robots. *Proc. SPIE.* **4698**, 281–290 (2003).
34. Carpi, F., Frediani, G., Turco, S. & De Rossi, D. Bioinspired tunable lens with muscle-like electroactive elastomers. *Adv. Funct. Mater.* **21**, 4152–4158 (2011).
35. See webside: <http://stretchsense.com/home/>
36. See webside: <http://www.optotune.com/index.php/products/focus-tunable-lenses>
37. See website: <http://www.tomshardware.com/news/vivitouch-vibration-feedback-headphones-eap,25691.html>
38. See website: <http://www.polymerprocessing.com/polymers/PBA.html>
39. Kofod, G., Sommer-Larsen, P., Kornbluh, R. & Pelrine, R. Actuation Response of Polyacrylate Dielectric Elastomers. *J. Intell. Mater. Syst. Struct.* **14**, 787–793 (2003).
40. Zhao, X. & Suo, Z. Theory of dielectric elastomers capable of giant deformation of actuation. *Phys. Rev. Lett.* **104**, 178302 (2010).

41. Stoyanov, H., Kollosche, M., Risse, S., McCarthy, D. N. & Kofod, G. Elastic block copolymer nanocomposites with controlled interfacial interactions for artificial muscles with direct voltage control. *Soft Matter* **7**, 194–202 (2011).
42. Stoyanov, H., Brochu, P., Niu, X., Della Gaspera, E. & Pei, Q. Dielectric elastomer transducers with enhanced force output and work density. *Appl. Phys. Lett.* **100**, 1–3 (2012).
43. Molberg, M., Crespy, D., Rupper, P., Nüesch, F., Månson, J.-A. E., Löwe, C. & Opris, D. M. High breakdown field dielectric elastomer actuators using encapsulated polyaniline as high dielectric constant filler. *Adv. Funct. Mater.* **20**, 3280–3291 (2010).
44. Galantini, F., Bianchi, S., Castelvetro, V. & Gallone, G. Functionalized carbon nanotubes as a filler for dielectric elastomer composites with improved actuation performance. *Smart Mater. Struct.* **22**, 055025 (2013).
45. Carpi, F., Gallone, G., Galantini, F. & De Rossi, D. Silicone-poly(hexylthiophene) blends as elastomers with enhanced electromechanical transduction properties. *Adv. Funct. Mater.* **18**, 235–241 (2008).
46. Kussmaul, B., Risse, S., Kofod, G., Waché, R., Wegnener, M., McCarthy, D. N., Krüger, H. & Gerhard, R. Enhancement of dielectric permittivity and electromechanical response in silicone elastomers: molecular grafting of organic dipoles to the macromolecular network. *Adv. Funct. Mater.* **21**, 4589–4594 (2011).
47. Madsen, F. B., Dimitrov, I., Daugaard, A. E., Hvilsted, S. & Skov, A. L. Novel cross-linkers for PDMS networks for controlled and well distributed grafting of functionalities by click chemistry. *Polym. Chem.* **4**, 1700–1707 (2013).
48. Sihvola, A. in *Thermal microwave radiation: applications for remote sensing* (Mätzler, C.) 464–474. (The Institution of Engineering and Technology, 2006).
49. Dang, Z.-M., Yuan, J.-K., Zha, J.-W., Zhou, T., Li, S.-T. & Hu, G.-H. Fundamentals, processes and applications of high-permittivity polymer-matrix composites. *Prog. Mater. Sci.* **57**, 660–723 (2012).
50. Lu, J. & Wong, C. P. in *Nanopackaging Nanotechnologies Electron. Packag.* (Morris, J. E.) 121–137 (Springer, 2008).
51. Carpi, F., Gallone, G., Galantini, F. & De Rossi, D. Silicone–poly (hexylthiophene) blends as elastomers with enhanced electromechanical transduction properties. *Adv. Funct. Mater.* **18**, 235–241 (2008).
52. Fredin, L. A., Li, Z., Lanagan, M. T., Ratner, M. A. & Marks, T. J. Substantial recoverable energy storage in percolative metallic aluminum-polypropylene nanocomposites. *Adv. Funct. Mater.* **23**, 3560–3569 (2013).

53. Crouse, C. A., Pierce, C. J. & Spowart, J. E. Influencing solvent miscibility and aqueous stability of aluminum nanoparticles through surface functionalization with acrylic monomers. *ACS Appl. Mater. Interfaces* **2**, 2560–2569 (2010).
54. Adiga, S. P., Zapol, P. & Curtiss, L. A. Structure and morphology of hydroxylated amorphous alumina surfaces. *J. Phys. Chem. C* **111**, 7422–7429 (2007).
55. Cai, W., Chen, Q., Cherepy, N., Dooraghi, A., Kishpaugh, D., Chatziioannou, A., Payne, S., Xiang, W. & Pei, Q. Synthesis of bulk-size transparent gadolinium oxide–polymer nanocomposites for gamma ray spectroscopy. *J. Mater. Chem. C* **1**, 1970 (2013).
56. Rong, Y., Chen, H.-Z., Wu, G. & Wang, M. Preparation and characterization of titanium dioxide nanoparticle/polystyrene composites via radical polymerization. *Mater. Chem. Phys.* **91**, 370–374 (2005).
57. Jonscher, A. K. The ‘universal’ dielectric response. *Nature* **267**, 673–678 (1977).
58. Xu, J. & Wong, C. P. Effects of the low loss polymers on the dielectric behavior of novel aluminum-filled high-k nano-composites. *Electro. Comp. & Techno. Conf., Proc. 54th*. 496–506 (2004).
59. Xu, J. & Wong, C. P. High-k nanocomposites with core-shell structured nanoparticles for decoupling applications. *Electro. Comp. & Techno. Conf., Proc. 55th*. 1234–1240 (2005).
60. Gallone, G., Carpi, F., De Rossi, D., Levita, G. & Marchetti, A. Dielectric constant enhancement in a silicone elastomer filled with lead magnesium niobate-lead titanate. *Mater. Sci. Eng. C* **27**, 110–116 (2007).
61. Brown, E., Rodenberg, N., Amend, J., Mozeika, A., Steltz, E., Zakin, M. R., Lipson, H. & Jeager, H. M. Universal robotic gripper based on the jamming of granular material. *Proc. Natl. Acad. Sci.* **107**, 18809–18814 (2010).
62. Araromi, O. A., Gavrilovich, I., Shintake, J., Rosset, S., Richard, M., Gass, V. & Shea, H. R. Rollable multisegment dielectric elastomer minimum energy structures for a deployable microsatellite gripper. *IEEE/ASME Trans. Mechatronics* **20**, 438–446 (2014).
63. Murray, C., McCoul, D., Sollier, E., Ruggiero, T., Niu, X., Pei, Q. & Di Carlo, D. Electro-adaptive microfluidics for active tuning of channel geometry using polymer actuators. *Microfluid. Nanofluidics* **14**, 345–358 (2013).
64. Verploegen, E., Soulages, J., Kozberg, M., Zhang, T., McKinley, G. & Hammond, P. Reversible switching of the shear modulus of photoresponsive liquid- crystalline polymers. *Angew. Chemie - Int. Ed.* **48**, 3494–3498 (2009).

65. Ren, Z., Niu, X., Chen, D., Hu, W. & Pei, Q. A new bistable electroactive polymer for prolonged cycle lifetime of refreshable Braille displays. *Proc. SPIE* **9056**, 905621–1–9 (2014).
66. Mitsumata, T. & Ohori, S. Magnetic polyurethane elastomers with wide range modulation of elasticity. *Polym. Chem.* **2**, 1063 (2011).
67. Shanmuganathan, K., Capadona, J. R., Rowan, S. J. & Weder, C. Biomimetic mechanically adaptive nanocomposites. *Prog. Polym. Sci.* **35**, 212–222 (2010).
68. Capadona, J. R., Shanmuganathan, K., Tyler, D. J., Rowan, S. J. & Weder, C. Stimuli-responsive polymer nanocomposites inspired by the sea cucumber dermis. *Science* **319**, 1370–1374 (2008).
69. Rosen, S. L. in *Fundam. Princ. Polym. Mater.* (Rosen, S. L.) 233–242 (John Wiley & Sons, Inc, 1993).
70. Liu, Y.-L. & Chuo, T.-W. Self-healing polymers based on thermally reversible Diels–Alder chemistry. *Polym. Chem.* **4**, 2194 (2013).
71. Gong, C., Liang, J., Hu, W., Niu, X., Ma, S., Hahn, H. T. & Pei, Q. A healable, semitransparent silver nanowire-polymer composite conductor. *Adv. Mater.* **25**, 4186–4191 (2013).
72. Chen, X., Dam, M. A., Ono, K., Mal, A., Shen, H., Nutt, S. R. Sheran, K. & Wudl, F. A thermally re-mendable cross-linked polymeric material. *Science* **295**, 1698–1702 (2002).
73. Gandini, A. The furan/maleimide Diels-Alder reaction: a versatile click-unclick tool in macromolecular synthesis. *Prog. Polym. Sci.* **38**, 1–29 (2013).
74. Yu, S., Zhang, R., Wu, Q., Chen, T. & Sun, P. Bio-inspired high-performance and recyclable cross-linked polymers. *Adv. Mater.* **25**, 4912–4917 (2013).
75. Morel, F., Decker, C., Jönsson, S., Clark, S. C. & Hoyle, C. E. Kinetic study of the photo-induced copolymerization of N-substituted maleimides with electron donor monomers. *Polymer*. **40**, 2447–2454 (1999).
76. Liu, Y. L., Hsieh, C. Y. & Chen, Y. W. Thermally reversible cross-linked polyamides and thermo-responsive gels by means of Diels-Alder reaction. *Polymer*. **47**, 2581–2586 (2006).
77. González, L., Rodríguez, A., Valentín, J. L., Marcos-Fernández, A., Posadas, P. & Madrid. Conventional and efficient crosslinking of natural rubber. *Elastom. Und Kunststoffe* **58**, 638–643 (2005).
78. Mark, J. E. Elastomeric networks with bimodal chain-length distributions. *Acc. Chem. Res.* **27**, 271–278 (1994).

79. Imai, Y., Itoh, H., Naka, K. & Chujo, Y. Thermally reversible IPN organic - inorganic polymer hybrids utilizing the Diels - Alder reaction. *Macromolecules* **33**, 4343–4346 (2000).
80. Lipomi, D. J., Vosgueritchian, M., Tee, B. C.-K., Hellstrom, S. L., Lee, J. A., Fox, C. H. & Bao, Z. Skin-like pressure and strain sensors based on transparent elastic films of carbon nanotubes. *Nat. Nanotechnol.* **6**, 788–792 (2011).
81. Zhang, Q. M., Su, J., Kim, C. H., Ting, R. & Capps, R. An experimental investigation of electromechanical responses in a polyurethane elastomer. *J. Appl. Phys.* **81**, 2770–2776 (1997).